



PROCESS SIMULATION OF THE GRAZ POWER CYCLE

Thesis submitted at the Graz University of Technology
in partial fulfilment of the requirements for
the Master's Degree Programme Mechanical Engineering and Business Economics

by

Benjamin Mitterrutzner

Supervisor: Wolfgang Sanz

Institute of Thermal Turbomachinery and Machine Dynamics (TU Graz)

Co-Supervisor: Lars O. Nord

Department of Energy and Process Engineering (NTNU)

January, 2020

EPT-M-2015-107

MASTER THESIS

for

Student Benjamin Mitterrutzner

Spring 2015

Process simulation of the Graz power cycle

Background and objective

To meet the ambitious goals set by the European Commission towards 2050, with greenhouse gas emissions reductions in the range of 80–95% from 1990 levels, CCS could be an essential technology for the fossil-fuel based thermal power plants. Also, for the future energy system in Europe, an increase in intermittent renewable energy, such as wind and solar power, is expected. A critical aspect for future thermal power plants will be the need to balance the intermittent renewable power to meet the demand and allow for a stable electrical grid. This means that part load operation and transient operation (load changes and start-up) will be growing in importance for thermal power plants.

The Graz cycle, a zero emission power plant for CCS, is an oxy-combustion concept developed at the Graz University of Technology. The concept was developed in the 80s and different configurations and analyses have been published since then. The technology has the potential to meet the requirements of the future energy system in Europe. An important aspect is to investigate the part load and dynamic behavior of the cycle by process simulation. No such analysis and results have been published to date in the scientific literature.

The overall objective of the Master's thesis is to develop a part load model, a control strategy and investigate some dynamic aspects of the Graz cycle and subsequently simulate the process and generate results such as load change behavior. The software to be used is IPSEpro.

The following tasks are to be considered:

1. Literature study on oxy-combustion CO₂ capture including the Graz cycle, as well as process simulation of power cycles.
2. Evaluation and decision of Graz cycle configuration to be studied.
3. Model and simulate a full load (design point) model of the selected Graz cycle.
4. Develop a control strategy for the cycle.
5. Model and simulate a part load model (off-design) of the selected Graz cycle.
6. Investigate some initial dynamic aspects of the Graz cycle.

Within 14 days of receiving the written text on the master thesis, the candidate shall submit a research plan for his project to the department.

When the thesis is evaluated, emphasis is put on processing of the results, and that they are presented in tabular and/or graphic form in a clear manner, and that they are analyzed carefully.

The thesis should be formulated as a research report in English with summary, conclusion, literature references, table of contents etc. During the preparation of the text, the candidate should make an effort to produce a well-structured and easily readable report. In order to ease the evaluation of the thesis, it is important that the cross-references are correct. In the making of the report, strong emphasis should be placed on both a thorough discussion of the results and an orderly presentation.

The candidate is requested to initiate and keep close contact with his/her academic supervisor(s) throughout the working period. The candidate must follow the rules and regulations of NTNU as well as passive directions given by the Department of Energy and Process Engineering.

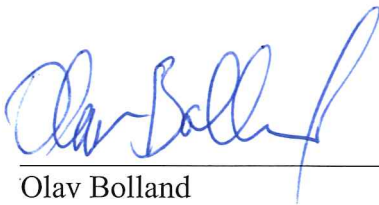
Risk assessment of the candidate's work shall be carried out according to the department's procedures. The risk assessment must be documented and included as part of the final report. Events related to the candidate's work adversely affecting the health, safety or security, must be documented and included as part of the final report. If the documentation on risk assessment represents a large number of pages, the full version is to be submitted electronically to the supervisor and an excerpt is included in the report.

Pursuant to "Regulations concerning the supplementary provisions to the technology study program/Master of Science" at NTNU §20, the Department reserves the permission to utilize all the results and data for teaching and research purposes as well as in future publications.

The final report is to be submitted digitally in DAIM. Based on an agreement with the supervisor, the final report and other material and documents may be given to the supervisor in digital format.

- Work to be done in lab (Water power lab, Fluids engineering lab, Thermal engineering lab)
- Field work

Department of Energy and Process Engineering, 3. February 2015



Olav Bolland
Department Head



Lars Nord
Academic Supervisor

Research Advisor:
Professor Wolfgang Sanz, Graz University of Technology

Statutory Declaration

I declare that I have authored this thesis independently, that I have not used other than the declared sources/resources, and that I have explicitly marked all material which has been quoted either literally or by content from the used sources.

Name: Benjamin Mitterutzner



Date: 28.01.2020

Preface

This Master thesis is submitted as a partial fulfillment of the requirements for a M.Sc. in Energy Technology and Business Economics at Graz University of Technology.

This project began 2015 at the Institute of Thermal Turbomachinery and Machine Dynamics (TU Graz) with Ao.Univ.-Prof. Wolfgang Sanz as supervisor and during my stay in Norway at the Department of Energy and Process Engineering (NTNU) with Associate Professor Lars Olof Nord, respectively, as co-supervisor.

After a break it was accomplished 2020 at Graz University of Technology. I would like to thank my two supervisors.

Acknowledgements

I would like to thank my two supervisors Wolfgang Sanz and Lars Olof Nord for their advice and guidance in the course of this thesis. I say thank you to Professor Sanz because of his unlimited patience which he had with me during these whole years and the big work he has done together with me especially at the beginning of this thesis. A big thank you also to Professor Lars O. Nord for his warm welcome he offered me in Trondheim, back in 2015, and all the things he taught me which I will never forget. Thanks to Rubén Mocholí Montañés and Rohan Dutta for their sociability and all the coffee breaks we spent together at NTNU talking about technical and non technical things.

I want to express special gratitude to all the people who helped me in the past years (and there are a lot!), which have been the most difficult years in my entire lifetime.

The most intimate thanks to my family who have supported me graciously during my time of studies and also suffering together with me. Especially I want to thank my brother Samuel, who supported me always and kept me on the ground with his looseness. I am very happy that this work is now completed.

Abstract

Carbon dioxide Capture and Storage (CCS) is an important weapon to combat the threatening climate warming climax and to achieve the ambitious goals set within the United Nations Convention on Climate Change in 2016, named Paris Agreement. The Graz Cycle, a zero emission oxy-combustion power plant concept, is one of the most promising representatives of CCS systems and constitutes the pièce de résistance of following work.

The main focus was set on the simulation of the power cycle and on the evolution of the underlying modeling of CCS components. Individual cycle components were explicitly programmed for this thesis in order to cover all simulation application stages and to achieve optimum performances and operating efficiencies by means of the assumptions given at the simulation itself. Furthermore different control structures were elaborated which distinguish this work from previous. The process simulation is composed of a design point simulation (full-load), off-design (part-load) and dynamic (transient) simulation of above-mentioned cycle. In order to do this the simulation software tool IPSEpro were used. The Graz Cycle operating at nominal design conditions gave excellent performances with a net plant efficiency of 53%. The part-load simulation generated results down to 40% load by operating with three different control strategies. For the dynamic simulation the heat recovery steam generator was selected as critical component of the cycle and therefore a dynamic simulation of a GC heat exchanger (economizer) were performed.

The off-design simulation investigations of the Graz Cycle can be seen as concluded with this work since different operating points were evaluated. The GC power plant dynamic simulation shows promise for further development in order to simulate transient load changes including start-ups and shutdowns.

Nomenclature

CC	Combustion control
CPU	Carbon dioxide compression and purification unit
ASU	Air separation unit
EEX	European Energy Exchange
GHG	Greenhouse gas
HPT	High pressure turbine
HRSG	Heat recovery steam generator
HTT	High temperature turbine
TIT	Turbine inlet temperature
DOF	Degree of freedom
ECBM	Enhanced Coal Bed Methane
EGR	Enhanced Gas Recovery
FFC	Ratio control
GC	Graz cycle
GWP	Global Warming Potential
HHV	Higher heating value
KAR	Overall load control
LHV	Lower heating value
LPST	Low pressure steam turbine
LPT	Low pressure turbine

MP Middle pressure

OTSG Once through steam generator

RES Renewable energy sources

ST Steam Turbine

Contents

Preface	i
Acknowledgements	ii
Abstract	iii
Nomenclature	iv
List of Figures	viii
List of Tables	xi
1 Introduction	1
1.1 Background and motivation	1
1.2 Objectives	3
1.3 Contribution	3
1.4 Outline	3
2 Carbon Capture and Storage	5
2.1 Energy Systems Analysis and CCS	5
2.1.1 The European electricity market	6
2.1.2 The electrical grid	7
2.1.3 Energy scenario	9
2.1.4 Economic importance of CCS	11
2.2 CCS technologies and chain	12
2.2.1 Air Separation Unit	13
2.2.2 Carbon Dioxide Compression and Purification Unit	14
2.2.3 CO ₂ - Storage	15
2.2.4 CO ₂ - Utilization	16
2.3 Oxy-combustion cycles with natural gas	17
2.3.1 Overview and classification	17
2.3.2 Semi-closed oxy-combustion combined cycle (SCOC-CC)	18

2.3.3	MATIANT cycle	19
2.3.4	NET Power Cycle	20
2.3.5	CES cycle	21
2.3.6	AZEP cycle	21
2.3.7	ZEITMOP cycle	22
3	Graz Cycle Power Plant	24
3.1	Basic Graz cycle	24
3.1.1	Cycle configuration	24
3.1.2	Design concepts	26
3.2	Modified Graz cycle	27
4	Thermodynamic cycle modelling	29
4.1	General definitions	29
4.1.1	Brayton cycle	29
4.1.2	Clausius-Rankine cycle	31
4.1.3	Combustion of fuel	32
4.1.4	Efficiency calculations	33
4.2	Control theory	34
4.2.1	Closed loop control	35
4.2.2	Load control of a gas turbine	35
4.2.3	Frequency control	36
4.2.4	Control of a steam turbine	36
4.2.5	Control of a boiler	38
4.2.6	Orifice plate	39
4.2.7	Importance of control strategy for the simulation	40
4.3	Steady-state Design Point Analysis	40
4.3.1	Gas turbine	40
4.3.2	Cooled gas turbine	41
4.3.3	Steam turbine	43
4.3.4	Compressor	44
4.3.5	Heat recovery steam generator	44
4.4	Steady-state Off-design Analysis	46
4.4.1	Steam turbine	47
4.4.2	Gas turbine	47
4.4.3	Compressor	49
4.4.4	HRSR	50
4.4.5	Condenser	51
4.5	Dynamic Analysis	51

4.5.1	The case study	52
4.5.2	Heat exchanger	53
4.5.3	Finding the heat transfer coefficient for the heat exchanger	54
4.5.4	Shell and tube fluid velocities	55
5	Process Simulation	56
5.1	Simulation tool IPSEpro	56
5.2	Methods	58
5.3	Assumptions	61
5.3.1	General assumptions	62
5.3.2	Turbomachinery	63
5.3.3	Dynamic simulation	64
5.4	Limitations	65
6	Results and Discussion	66
6.1	Full-load performance	66
6.2	Control Strategy	73
6.3	Part-load performance	82
6.4	Dynamic simulation	86
6.4.1	Design of the heat exchangers	87
6.4.2	Dynamic results	88
7	Conclusion	94
7.1	Final remarks	94
7.2	Further work	95
	Bibliography	96
A	Basic Thermodynamics	102
A.1	The conservation law of mass	102
A.2	The first law of Thermodynamics	103
A.3	The second law of thermodynamics	104
A.4	Ideal gas and polytropic process	105
A.4.1	Ideal gas model	105
A.4.2	Mixture of ideal gases	105
A.4.3	Enthalpy and specific heats	106
A.4.4	Polytropic process	107
A.4.5	Real gas model	108
B	Process stream data	110

List of Figures

1.1	Relation between Global Temperature and Carbon Dioxide Concentration in the atmosphere	1
1.2	EU decarbonisation scenarios by 2030 and 2050 (consumptions in %)	2
2.1	The electricity supply chain	7
2.2	Global natural gas prices in British thermal unit	9
2.3	Global overall energy demand by fuel	10
2.4	Global electricity production by primary energy supply	11
2.5	CO ₂ Mitigation costs out of a technology portfolio variation (in the time-frame 2015-2100)	12
2.6	Operating principles of the three main CO ₂ Capture technologies	13
2.7	Energy consumption versus oxygen purity in a cryogenic ASU	14
2.8	Overview of methods for storing CO ₂ in deep underground geological formations	15
2.9	Schematic diagram of a storage site and a core sample of injected CO ₂	16
2.10	Classification of oxy-combustion methods and Cycle proposals	18
2.11	Simplified flow diagram of Semi-Closed Oxy-Combustion Combined Cycle	18
2.12	Cycle configuration of the MATIANT cycle	19
2.13	Simplified flow diagram of the NET Power cycle	20
2.14	Cycle configuration of the CES cycle	21
2.15	Process diagram of the AZEP cycle with MCM reactor	22
2.16	Cycle configuration of the ZEITMOP cycle	23
3.1	Process flow of the Basic Graz cycle	25
3.2	T-s diagram of the Basic Graz cycle	26
3.3	Turbomachinery arrangement for the Basic Graz cycle	27
3.4	Process flow of Modified Graz cycle	28
4.1	Principal diagram of a Brayton cycle and corresponding T,s -diagram with pressure losses	30
4.2	Schematic of a steam turbine cycle with appendant T,s -diagram	31

4.3	Schematic diagram of losses and efficiencies in the Graz power cycle	33
4.4	Closed-loop control system	35
4.5	Different steam turbine control methods in the h,s -diagram	38
4.6	Control strategy for sliding pressure operation	38
4.7	Schema of a thermal power unit with once-through boiler	39
4.8	Definition of the angle β_2 and velocity w_2	42
4.9	Two structures of industrial turbines	43
4.10	T-Q diagram of a HRSG, single-pressure	45
4.11	Example of a horizontal once-through steam generator	46
4.12	Steam turbine efficiency characteristics with throttling control	48
4.13	Chocked nozzle characteristics of a turbine	49
4.14	Compressor characteristic with reduced flow rate	49
4.15	Characteristic of a water-cooled condenser	51
4.16	Heat transition curve of a boiler over time	52
4.17	Schematic diagram of the tube-side control volume	53
5.1	Principle sketch of a simple model in PSE	57
5.2	Modelling scheme of a power cycle	57
5.3	Simplified overview of the process simulation approach	60
5.4	Isentropic efficiency relation of the compressor in part-load operation	64
6.1	Thermodynamic cycle configuration and data of a Graz Cycle power plant	67
6.2	GC modifications for this study with the additional condenser marked with an asterisk (*)	70
6.3	TQ-diagram for the HRSG operating at full-load	73
6.4	Structure of the load control system of the Graz power cycle	75
6.5	Closed control loops for the operation mode S1 of the Graz power cycle	79
6.6	Closed control loops for the operation mode S2 of the Graz power cycle	80
6.7	Closed control loops for the operation mode S3 of the Graz power cycle	81
6.8	Optimal steady-state GC net efficiencies for the three different control strate- gies at part-load operation	82
6.9	Comparison of the GC net efficiencies between S1 and S3 when operating at part load	83
6.10	Heat release in the condenser for strategy S1 and S3	84
6.11	Compression and turbine power at part-load conditions for strategy S1 and S3	84
6.12	Important process parameters of the Graz Cycle at part-load operation of the control strategy S3	85

6.13	T-Q diagram for the OTSG for control strategy S3 when operating at 40% base load	86
6.14	Process simulation of the ECO1 at design point conditions	89
6.15	Process simulation of the ECO1 at design point conditions for the case study of load reduction from nominal load to 80% load	91
6.16	Time-temperature diagram of the dynamic simulation of ECO1 at full load operation	92
6.17	Time-temperature diagram of the cold-side of ECO1 for load reduction from 100% to 80% of baseload	92
6.18	Time-temperature diagram of the hot-side of ECO1 for load reduction from 100% to 80% of baseload	93
A.1	Difference between real gas and ideal gas	108
A.2	The compressibility factor of air	109

List of Tables

2.1	Global warming potential (GWP) relative to CO ₂	6
4.1	Variables of the cooled gas turbine model	42
4.2	Recommended velocities of the fluids	55
5.1	Performance comparison between the two Graz cycles	61
5.2	Component assumptions and efficiencies used in the thermodynamic simulation	62
5.3	Composition of the NG	63
5.4	Composition of the oxygen carrier	63
5.5	Parameter of the cooled gas turbine	64
5.6	Specific data of the OTSG established through literature study	65
6.1	Stream table for the Graz Cycle in nominal-load conditions	68
6.2	Key parameters of the Graz cycle power plant at design point conditions	70
6.3	Graz cycle power balance at design point conditions	71
6.4	Comparison of cycle efficiencies between ASME 05 and actual work	72
6.5	Example of manipulated and controlled variables for the particular control strategy S1	77
6.6	Control strategies of the Graz cycle	77
6.7	Gas purity at the exhaust gas drain of control strategy S3 when operating at part load	86
6.8	Calculation of heat exchanger parameter specifications	87
6.9	Geometry data employed for the dynamic model of the OTSG	88
6.10	Validation results of the ECO1 at design point operation	90
6.11	Data of the dynamic investigation of ECO1	90
6.12	Off-design results of the ECO1 for load reduction from 100% to 80% of baseload	91
A.1	Different changes of state of polytropic processes	108

Chapter 1

Introduction

1.1 Background and motivation

Many factors of the global climate are changing and the global average surface temperature is further increasing every year. The primary drivers of that global warming are human activities. Natural influences and variability cannot explain the recent observed changes, quite the contrary, they would have led, according to model simulations made by the U.S. Global Change Research Program, to a slight cooling [1]. Thus the majority of the global warming can only be explained by the emissions from burning fossil fuels, like coal, oil and natural gas. Figure 1.1 shows how the global annual average temperature is related to the increasing heat-trapping gases in the atmosphere such as carbon dioxide.

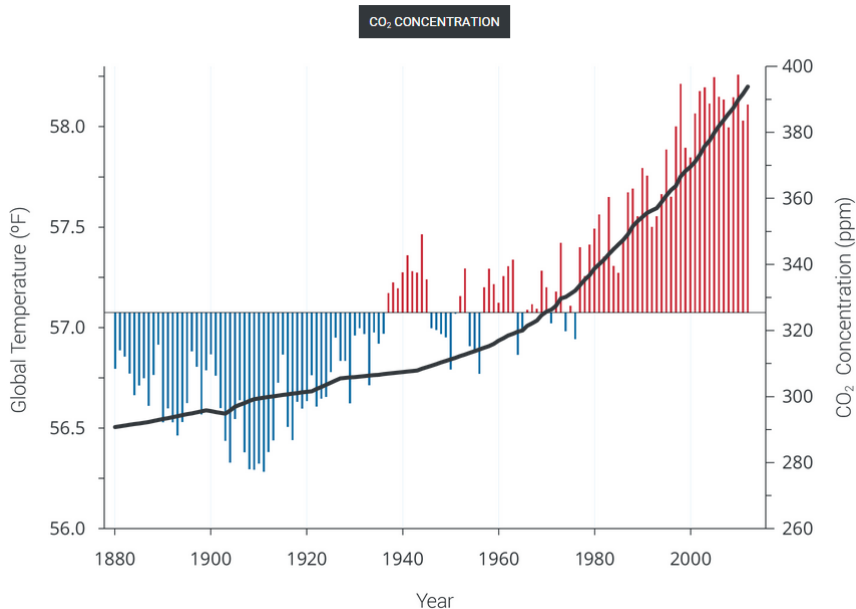


Figure 1.1: Relation between Global Temperature and Carbon Dioxide Concentration in the atmosphere [2]

For this reason the European Union has set the ambitious goal to reduce greenhouse gas emissions in the range of 80-95% below 1990 levels by 2050 [3]. This is going to be a structural and social challenge which consists in reducing the emissions while keeping a competitive and safe energy supply. These changes will primarily concern the energy sector, which produces the greatest part of man-made greenhouse gas emissions [3]. Besides strong support measures for renewable energy sources the European Union has confirmed that Europe cannot be decarbonised cost-efficiently without a significant support of Carbon Capture and Storage (CCS) [4]. CCS is a key technology for fossil fuel-based power generation, which reduces direct emissions at large scale and provides base load and balancing capacity in the power supply system [5]. Thus a generation mix of fossil fuels, like coal, lignite, oil and gas combined with CCS technologies and with renewable energy sources (RES) is the most cost-efficient and secure way to reduce carbon emissions by 80% till 2050 [4]. According to this, Figure 1.2 shows for the EU decarbonisation scenarios for 2030 and 2050 the fuel shares in primary energy consumption in comparison with the 2005 levels developed by the European Commission as “Energy roadmap 2050” [3].

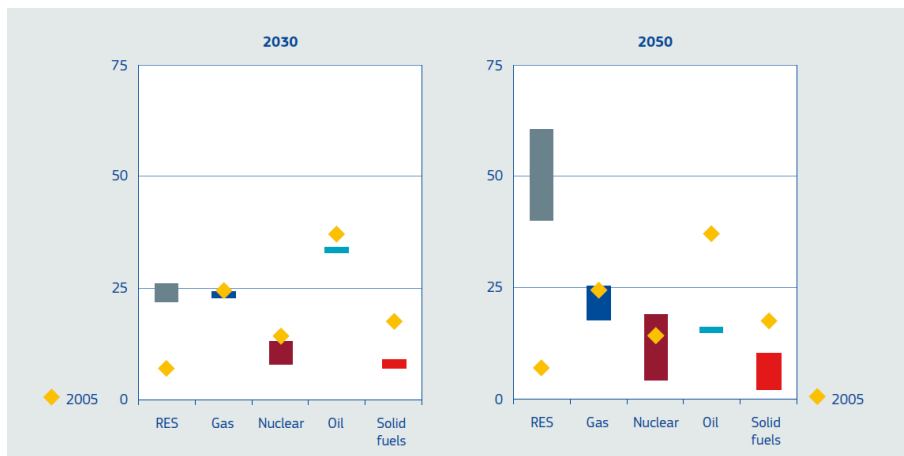


Figure 1.2: EU decarbonisation scenarios by 2030 and 2050 (consumptions in %) [3]

However, in these scenarios CCS technology will play a significant role because it has to operate in a system with large amounts of intermittent renewable power generation. Integrating fluctuating renewables in a power grid to provide sustainable electricity supply is complex, because supply and demand are linked physically and an increase or decrease of one part has to be balanced instantaneously by the other [6]. Thus the whole system has to operate dynamically and demands high flexibility of power plants including CO₂ capture in order to perform transient operation (load changes and start-up) and part-load operation [7].

1.2 Objectives

At first a literature study on oxy-combustion CO₂ capture including the Graz cycle, as well as on process simulation of power cycles (i.e. thermodynamic modelling of the power plant components plus a general description of the process simulation tool) should be carried out.

The thesis and its process simulations should give an overall view about the Graz cycle and all its components, control strategies, technologies and behaviors.

For this purpose an evaluation of the Graz power cycle, in order to find the most proper configuration, and latterly an attempt to further optimize the process during part-load operation was carried out. The set-up of the process modelling and simulation is divided into following steps:

1. Steady-state design (full-load)
2. Steady-state off-design (part-load)
3. Dynamic (transient) operation

The simulation and power cycle modelling tool used for this purpose is IPSEpro. For the specific requirements of this project a new library with convenient models and equations was built up.

The overall objective of the thesis is the development of the part-load models, control strategies and a first approach towards dynamic process modelling of the Graz cycle and subsequently the simulation of the power cycle in order to generate results such as load change behavior.

1.3 Contribution

To the author's best knowledge this work is the first dynamic process simulation and the first evolution of control strategies of the Graz Cycle. No such analysis and results have been published to date in scientific literature. It is rare to find dynamic simulation investigations of combined cycles and very rare to find something about this topic related to oxy-combustion CO₂ capture plants. After Miller et al. [8], Sanz et al. [9] and Wimmer [10] it is the fourth part-load operation analysis of a Graz Cycle; back in 2015 - when work has been initially started - it was the second one of its kind.

1.4 Outline

The first part of the thesis consists of a literature study of the CCS background and of the oxy-combustion power plants including the Graz cycle, as well as of the power cycle

modelling, which is the basis for the process simulation of power cycles. The second part contains the methodology and the results of the simulations itself. A model validation substantiates those results.

The thesis includes seven chapters and two appendices. The technical background is given in Chapter 2, where the importance of CCS and its technologies, with the main focus on oxy-combustion fuel cycles, is described. Chapter 3 gives an introduction and description of the Graz cycle, the process which is examined here. Subsequently in Chapter 4 the thermodynamic description of the GC components and the modelling are presented. In Chapter 5 the process simulation tools and the methods are described. In this chapter the different methodologies and assumptions are mentioned, too. In Chapter 6 the actual results of the Graz Cycle simulations are explicated and discussed. Ultimately, in Chapter 7, the conclusion of the thesis is presented. The two appendices are in order of appearance: Basic Thermodynamics and Process stream data.

Chapter 2

Carbon Capture and Storage

This chapter presents the world's energy scenario and the technical background of the Carbon Capture and Storage chain and technologies related to it for a basic understanding of the Graz cycle and consequently of its simulation. An important focus has been set on the oxy-combustion cycles and different cycle constellations which are state of the art and basis for research and further development.

2.1 Energy Systems Analysis and CCS

“Climate” is the long-term averaged weather and expresses environmental trends, which are developing very slowly in nature. The climate has experienced in the last decades dramatic changes, leading to a situation where the sensitive natural systems and human beings get in danger. The drastic environmental changes since the industrial revolution is due to human activity, which means that the emission of anthropogenic greenhouse gases (GHG) peaks year by year. This reality has already been discussed in Section 1.1. The main driver of the greenhouse effect is carbon dioxide (CO_2). Most of the anthropogenic GHG emissions are due to combustion of fossil fuels, which account for 78% of the total GHG emission increase in the time period from 1970 to 2010. [11]

The CO_2 emissions from the combustion of fossil fuels are like an injection into the atmosphere. Therefore the climatic trend on our earth's surface is that the temperatures are rising and generally a warming process never seen before is taking place. If temperatures are rising, the water evaporation rate and moisture content in the air is also increasing. This fact contributes to an onward temperature rise, because H_2O is also a greenhouse gas. Consequently, the water temperatures are rising too, that means that the possibility of water to absorb CO_2 becomes less and less. This so called “engine effect” gets accelerated by thawing of the permafrost soil, which as a result emits methane into the atmosphere, another important greenhouse gas. [12]

The GWP over a 100 years timeframe of CH_4 and others is shown in Table 2.1. [13]

Table 2.1: Global warming potential (GWP) relative to CO₂ [13]

Gas	Chemical formula	Atmospheric lifetime [years]	GWP [100 years]
Carbon dioxide	CO ₂	100	1
Methane	CH ₄	12	25
Nitrous oxide	N ₂ O	114	298
Sulphur hexafluoride	SF ₆	3200	22.800

2.1.1 The European electricity market

In view of this hazardous situation, the *United Nations Framework Convention on Climate Change* (UNFCCC) acceded the Kyoto Protocol in 1998. In this treaty the members pledged themselves to fight global warming and to reduce the GHG emissions.

Because the second period of the Kyoto commitment ends in 2020, a new convention was launched in 2015 by the State Parties of the UNFCCC, called by origin “Paris Agreement”. This convention in Paris brought for the first time all nations into a common cause, to wit to invest in renewable technologies and to take determined efforts to combat climate change. Developing countries have got assurance from the participants for assistance to achieve the ambitious climate goals. Those have been set to keep the global average temperature rise below 2 °C in comparison to pre-industrial conditions and to pursue any effort to achieve the climate goal of keeping temperatures below 1.5 °C. If this objective gets accomplished, a significant reduction of environmental risks and global warming effects can be achieved. [14]

To finally obtain climate neutrality the European Union has decided to introduce a EU policy, so called EU emission trading system (EU ETS). Set up in 2005, the EU ETS represents the first worldwide trading system of carbon dioxide emissions and it gets traded on the European Emission Allowances Auction (EUA) primary market [15]. On this platform European companies can buy and sell allowances to emit carbon dioxide in the atmosphere. The price at the European Energy Exchange (EEX) platform has changed from April to September 2019 from 21.06 to 25.40 €/ton CO₂; in April 2017 the rate was at 4.63 €/ton CO₂. Since carbon intensive power plants, first of all coal power plants, are discharging a lot of greenhouse gases, power suppliers are forced to invest much more in CO₂ emission licenses as a consequence; this shall shift the energy production more and more to renewable energies. On the other hand this leads to a balancing problem of the current electrical grid and the fundamental importance of thermal power plants and CCS, see Subsection 2.1.2. [16]

The liberalisation and deregulation of the electricity market is an important factor, which has to be taken into account. It means that the electricity supply is no longer a monopoly-based framework but it is an open market and customers are free to change the electricity supplier [17]. Private investors have started to built their own power plants and

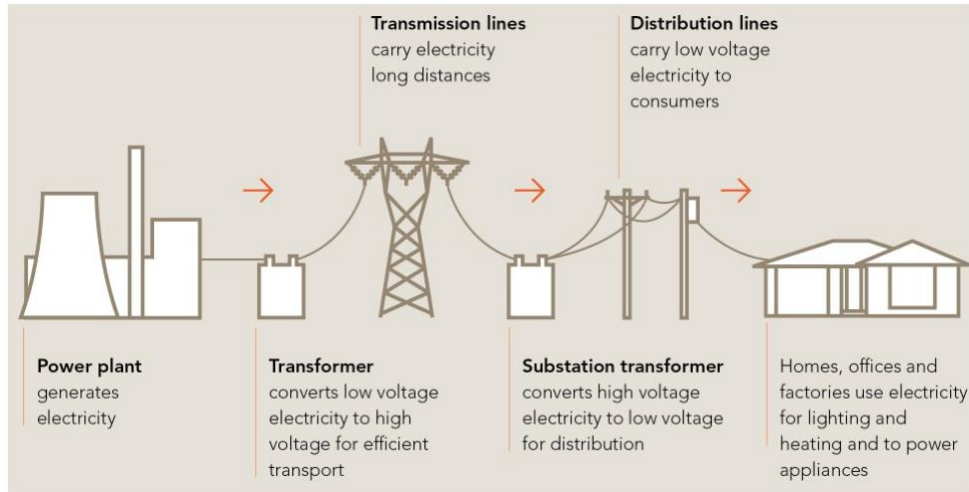


Figure 2.1: The electricity supply chain [20]

the overall production cost of electricity became fundamental. These so-called merchant plants have to bring a good return on investment and have to be competitive on an economic level. Combined cycle power plants benefit from this transition because of their low specific investment costs and construction time. [18]

In this context lays the ulterior importance of this project work and gets further analysed in the following subsections.

2.1.2 The electrical grid

The electrical grid, as Figure 2.1 shows, is fundamental in the power supply chain. It is not dependent on the type of energy source, whether it be a nuclear power plant or a renewable energy source. Power plants are often located near fuel sources or renewable energies and most of the time far away from densely populated areas and metropolises. The electrical energy of the power generation site has to be converted into high voltage in order to transfer the electricity through a high voltage long range transmission line. High voltage systems are used to reduce transmission losses. Commonly, for energy transmission over long distances, overhead power lines are used. But electric power can also be transmitted by underground cables, which are less visible and not influenced by bad weather. However, overhead constructions are by far dominant because “undergrounding” has the higher costs. At the end of the overhead power line, substation transformers are converting high voltage electricity to low voltage, in this way electricity is carried over distribution lines to the end consumer. The line frequency in Europe is set at 50 Hz, whilst in North America a 60 Hz frequency is common. [19, 20]

The future grid system will have to transport bi-directional power flows, it has to be flexible, reliable and sustainable in response to changing requirements of the liberalised electricity market. The European electricity framework is subject to market forces, which

regulate generators, and grid control centers take an overall supervisory role, which guarantee voltage stability and power balancing [17]. The balancing problem of the electrical grid is a fundamental issue for the electrical network system. The main difference between electricity and other commodities is that electricity cannot be stored in an efficient practical manner on a large scale because storing directly by batteries is expensive and advisable only for small quantities [18]. In addition electrochemical storages have following disadvantages: [21]

- the need for raw materials is very high (e.g. lithium, cobalt, coltan etc.);
- massive energy input for production of battery cells;
- recycling of batteries is still problematic;

and the hydrogen storage infrastructure as an alternative to battery storage has not yet had his fundamental breakthrough. Other indirect storage technologies, for example storage through pump storage plants or compressed air storage, is in the most cases not economic and they depend on the topography. Because of this, immediate supply of electricity is necessary when customers need it. Large fluctuations in demand and volatile renewable energies require quick reactions of power plants in real time in order to keep the balance between supply and demand. At this point lies the fundamental importance of gas turbine and combined-cycle power plants and in the future CCS power plants. They ensure quick start-ups and load changes and have relatively low investment costs and high efficiency in comparison to coal-fired power stations or nuclear plants. Especially gas turbine power plants and hydro power stations can react rapidly on load changes. In the timeframe of 15 minutes they can start-up and reach the full load, while a combined cycle power plant in the same time reaches only half of its installed capacity. In comparison coal and nuclear power plants are ramping very slow, since they take somewhat like 36 hours to reach their full load. [6, 18]

CCS will contribute to the power stability by providing decarbonised flexible back-up capacities and bringing diversification in the energy supply framework. It will also support the increasing penetration of renewables in the electrical grid in Europe. [22]

On the other hand - since fuel cost is the biggest contribution to electricity cost - natural gas power stations burn an expensive fuel compared to the others. As the electricity market became deregulated, the gas prices are volatile and are dependent on the regional context, as shown in Figure 2.2. [18]

Uranium, the primary energy carrier for nuclear power plants, and coal, the main fuel for steam power plants, have stable prices at low costs, e.g. the averaged coal price in October 2019 was at 1.96 US\$/MMBtu (6 €/MWh) [23]. The cost of Uranium is even lower than this value [18]. The gas price in Japan is equal to the average LNG import

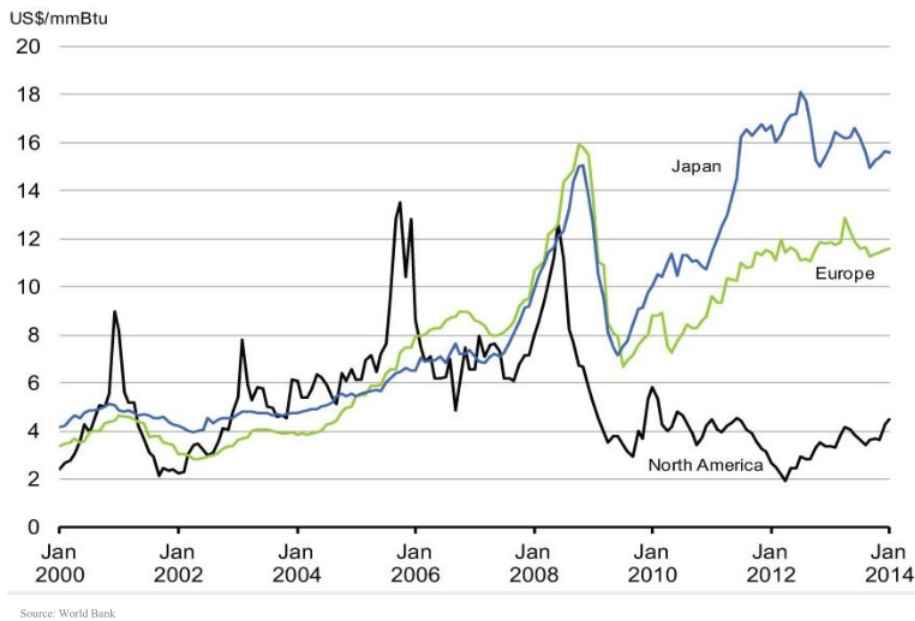


Figure 2.2: Global natural gas prices in British thermal unit [25]

price [18], meanwhile the prices in Europe are coupled with the crude oil price. That was priorily also the case with the North American gas (based on the Henry Hub index), but with the massive increase of unconventional oil and gas production, also called fracking, the price got uncoupled from the conventional oil prize and is now trending towards coal prices (in July 2019 the Henry Hub gas price was rated at 2.36 US\$/MMBtu) [24].

When spot market gas prices go up, owners of gas-fired power plants are often forced to reduce the load because of rentability; or they switch to the back-up fuel and sell natural gas on the gas market. In the worst case they are forced to close the plant or to enforce long downtimes. [18]

2.1.3 Energy scenario

Because of an increasing world population (in 2100 it is estimated to reach almost 12 billion people [26]) and the need of electricity and fast economic growth of the emerging countries the global energy demand is further rising. This scenario is presented in Figure 2.3 in which the world consumption of primary energy carrier is shown. The demand is increasing for all forms of energies with natural gas growing most rapidly [25]. In the year 2018 the share of natural gas in energy consumption rised around 45%, while the energy demand had the fastest pace of growth this decade, to wit 2.3% in the year 2017-2018 [27].

Since the energy demand is rising and on the other hand the GHG emissions have to decrease versus zero, the importance of Carbon Capture and Storage and Utilisation is evident, especially for coal and gas. Both of these fuels are going to be the highest ranked primary energy by demand together with crude oil. In order to achieve climate goals

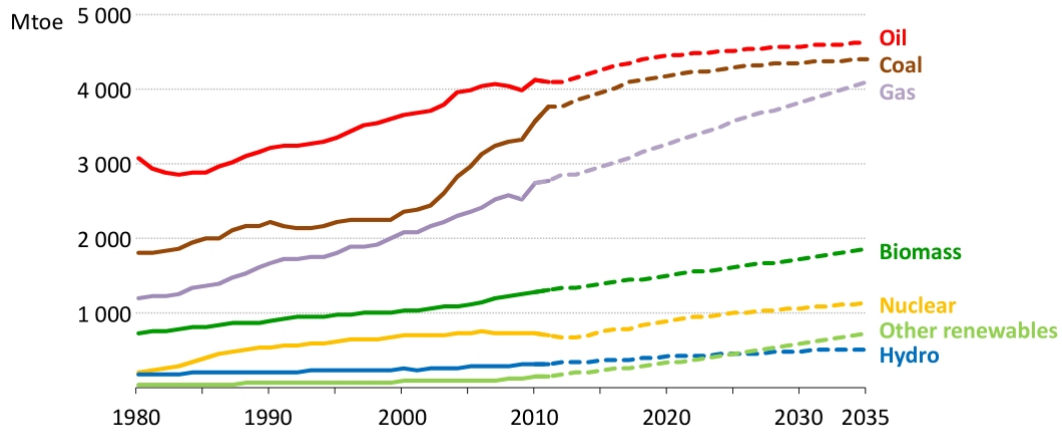


Figure 2.3: Global overall energy demand by fuel [25]

it will be necessary to invest not only in renewable energies but also in CCS combined with sustainable bioenergy (Bio-CCS). More than 50% of renewable energy consumption in Europe is currently coming from biomass energy. CCS in combination with bioenergy is the only large-scale technology that can remove CO₂ from the atmosphere. According to the International Panel on Climate Change (IPCC) this technology pair will be crucial to avoid irreversible climate change and maybe it is a necessary technology for saving this planet from climate warming. [26, 22]

In Figure 2.4 the specific energy mix of the electricity production in the year 2010 and for two different future energy scenarios by 2050 is presented. In the scenario “Jazz” coal is expected to remain dominant, whilst the share of gas increases (especially in North America) and CCS as technology plays a minor role. The nuclear energy part shown in Figure 2.4 find use mainly in non-OECD countries (in the year 2018 the growth of nuclear energies was 3.3% - by bringing global production back to pre-Fukushima levels [27]). Hydro and wind electricity are competitive and renewables account for roughly 30% of total electricity generation by 2050. [25]

The scenario “symphony” shows a different picture of primary energy supply in which the coal share drops and CCS becomes increasingly necessary. On the other hand the share of renewable and nuclear energies are increasing by ensuring a quicker transition. Renewables undergo a rapid development, accounting for almost 50% of total electricity generation in 2050 (in comparison in 2010 the renewable energies accounted only for 20%). This scenario should lead to a world with less GHG emissions but enforced by a critical ramp of nuclears. [25]

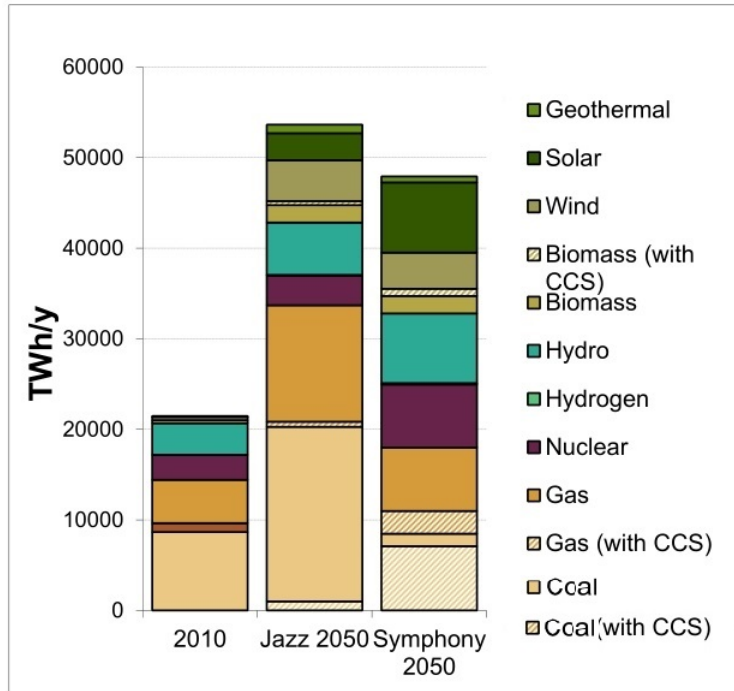


Figure 2.4: Global electricity production by primary energy supply [25]

2.1.4 Economic importance of CCS

Carbon Capture and Storage is a complete end to end supply chain system from the capturing of the CO_2 in large power sources, for instance power plants, to the transport (e.g. in pipelines) to the storage in deep geological formations and the application of monitoring methods in order to guarantee long-term safe keeping. Adding CCS technologies to power plants or industry processes makes investments necessary and accordingly the cost of electricity will increase significantly. It is in fact a resource intensive technology and the cost of capturing and storing carbon dioxide is estimated to be around \$60-65 per metric ton. This means that there is a need for policies, economic incentives and a global societal will for implementation of Carbon Capture and Storage into the current electricity mix. But on the other hand, to involve CCS in the technology portfolio for preventing climate change is necessary from an economic perspective because the long-term overall mitigation costs will be brought down (see Figure 2.5). There are several pilot scale power plants with CCS worldwide in operation and some are planned for the future. “All the individual components of an integrated CCS chain are in use in various parts of the fossil energy chain” [28]. [28]

The transportation sector’s responsibility for GHG emissions will shift it in the future more and more into the electricity supply chain since electric vehicles are gaining importance.

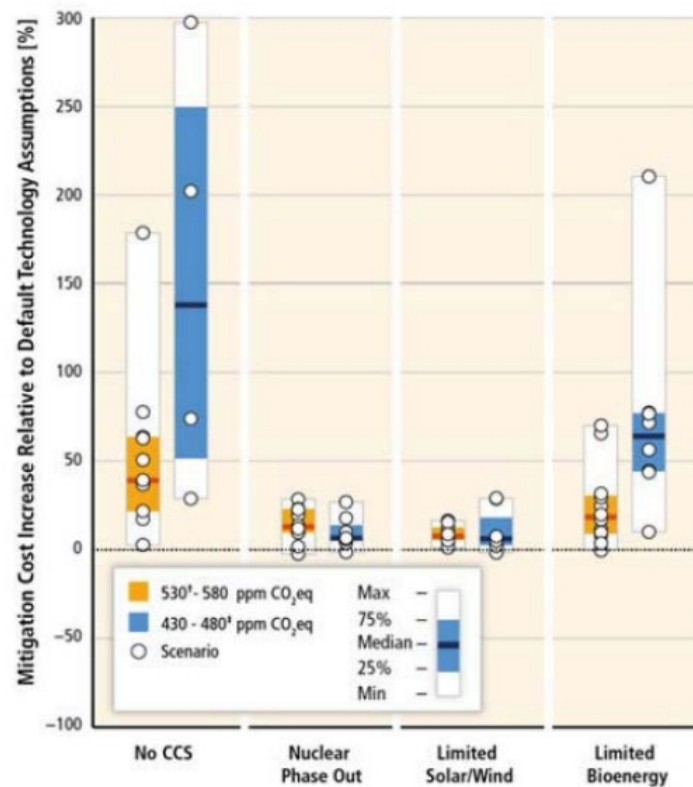


Figure 2.5: CO₂ Mitigation costs out of a technology portfolio variation (in the timeframe 2015-2100) [29]

2.2 CCS technologies and chain

Power generation by combustion of fossil fuels causes greenhouse gases and predominantly CO₂. There are several possibilities to reduce those emissions: [30]

- Improving efficiency of power plant
- Introduction of combined cycles for high thermal efficiencies
- Replacement of hydrocarbon fuels with renewable resources
- Substitution of coal and lignite with gas due to lower carbon content
- CO₂ Capture and Storage

The first four options can achieve an incremental reduction of greenhouse gases but Carbon Capture and Storage is the only technology which allows the usage of fossil fuels with almost zero emissions.

CCS involves more technologies used in industrial operations today, first to separate the CO₂ from the gaseous products at the capture facility and to compress it to a high

density, then to transport it to suitable storage sites like depleted oil and gas reservoirs, deep saline aquifers or coal beds and finally to store it there for a long time period.[31] The captured CO_2 could also be used for EOR (Enhanced Oil Recovery), which works most commonly by injection of the gas into the reservoir whereupon it expands and pushes thus additional oil to the well.

The methodology of the three main approaches to capture CO_2 is shown in Figure 2.6.

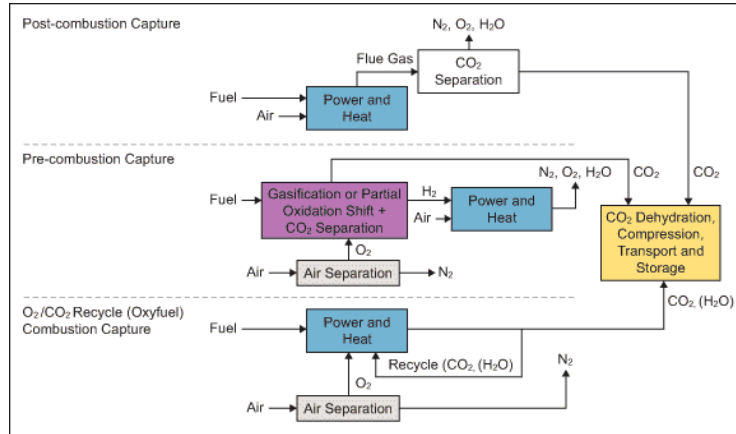


Figure 2.6: Operating principles of the three main CO_2 Capture technologies [32]

Post-combustion technology separates the containing CO_2 from the flue gas, produced by the combustion of primary fuels. The most advanced methods use aqueous amine solution to capture the small fraction of CO_2 (between 3-15% of the volume) present in the waste gas in which nitrogen is the main component [31]. Pre-combustion systems, the second method, gasify the fossil fuels using steam and oxygen to obtain a mixture of predominantly CO and H_2 (“synthesis gas”). Additional steam is hereupon added to start up the “water-gas shift” reaction to obtain a resulting mixture of hydrogen and CO_2 [33]. Using a physical solvent, the CO_2 can be separated, leaving a carbon-free fuel gas, which can be combusted to produce power and heat. Oxyfuel combustion systems, like the Graz cycle, use oxygen (with a purity of 95-99%), produced in an ASU, instead of air for the combustion. The result is a waste gas mixture of mainly CO_2 and water vapor, which can be separated in the next step by cooling and compressing the gas stream. Further treatment may be needed to remove nitrogen and other pollutants before the gas is ready to be stored [31].

2.2.1 Air Separation Unit

There are different technologies for separating oxygen from air, like polymeric membranes, cryogenic distillation and adsorption techniques. But the only commercially available technology today to produce cost-effectively large quantities of O_2 with high purity is cryogenic distillation.[34]

Air Separation Units (ASU) using cryogenic distillation are based on the different boiling points of oxygen and nitrogen. The boiling point temperature of nitrogen at atmospheric pressure is $-195.8\text{ }^{\circ}\text{C}$, of argon $-185.9\text{ }^{\circ}\text{C}$ and of oxygen $-182.9\text{ }^{\circ}\text{C}$. The water vapour and the CO_2 have much higher boiling points; water freezes at $0\text{ }^{\circ}\text{C}$ and CO_2 sublimates at $-78.46\text{ }^{\circ}\text{C}$ [13]. To remove the water and CO_2 , the compressed air gets first cooled using cooling water. This is necessary for further cooling down the air by a refrigeration process within an insulated enclosure (cold box), in order to get liquefied nitrogen, oxygen and argon. However, oxygen is the least volatile component of those three and it is collected at the bottom of the distillation column, whereas argon and nitrogen are collected at the top. As the boiling point of oxygen and argon is very close, it is difficult to separate them from each other. It means a large number of trays or a large height of packing in a column [13].

As a result air separation can be cost-intensive and is a continuous trade-off between energy consumption and capital costs on the one hand and oxygen purity on the other. Figure 2.7 shows this dilemma.

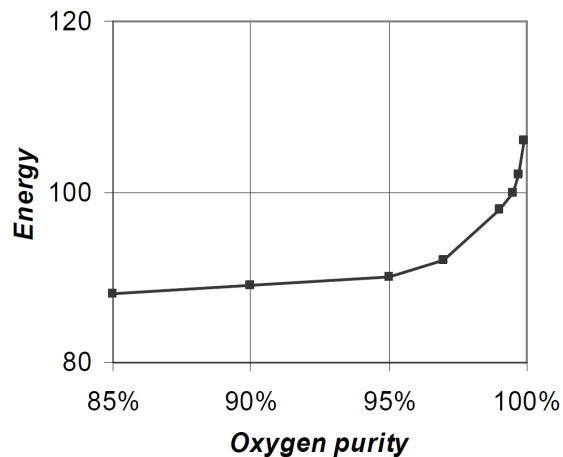


Figure 2.7: Energy consumption versus oxygen purity in a cryogenic ASU [34]

The air separation cycles for the production of oxygen at 95% purity, developed at the beginning of the 1990s, represent a good compromise between energy consumption (respectively cost expenditure) and oxygen purity and thus are commonly used for oxy-combustion power plant processes.

2.2.2 Carbon Dioxide Compression and Purification Unit

The task of a Carbon Dioxide Compression and Purification Unit is to capture the CO_2 from the flue gas and subsequently to purify and compress it to the required specifications. Therefore the composition of the flue gas has a high impact on the design and capital costs of a CO_2 CPU.[34] Today there is no common CO_2 product specification but the final

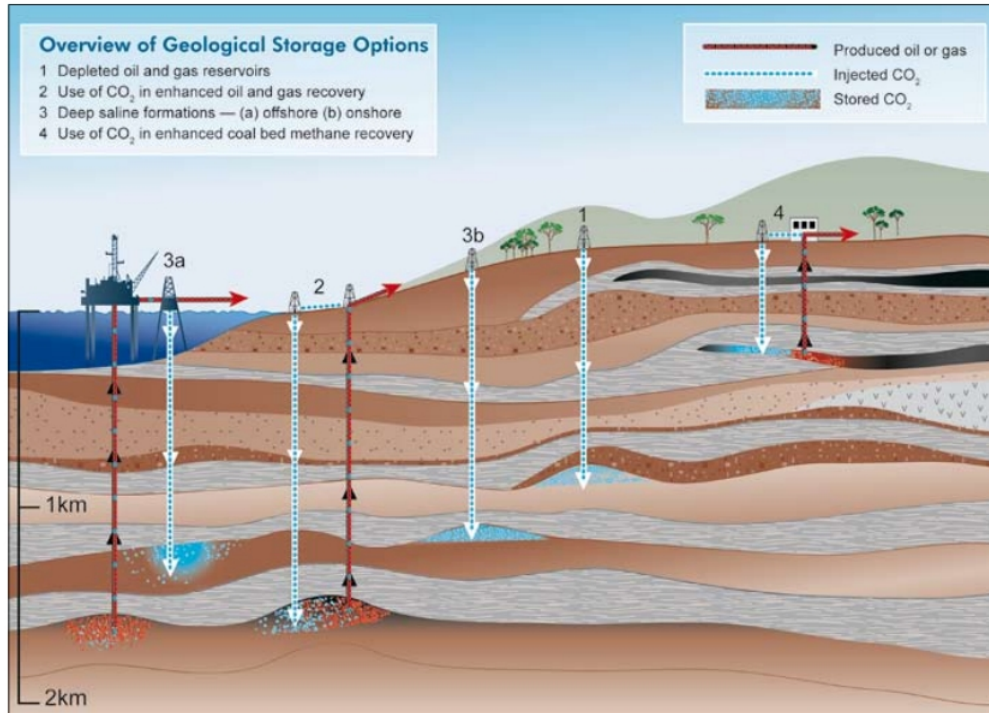


Figure 2.8: Overview of methods for storing CO₂ in deep underground geological formations [31]

compression up to 110 bar is often used.[35]

The basic steps for processing combustion flue gas to get pure CO₂ are the following:[34]

1. Compression of the wet flue gas
2. Drying of the wet flue gas
3. Purification of the flue gas by auto-refrigerated inerts removal
4. Final compression of the condensed product

2.2.3 CO₂ - Storage

In order to prevent the emission of carbon dioxide into the atmosphere, it is possible to store the captured CO₂ in geological formations for a sufficiently long period. The different options for storing CO₂ are shown in Figure 2.8. The underground structures comprise depleted oil and gas reservoirs, saline formations (porous reservoir rocks saturated with brackish water or brine) and coal formations. Further the CO₂ can be stored and used to enhance production of oil (EOR), natural gas (EGR) and methane through enhanced coal bed recovery (ECBM).

The captured carbon dioxide has to remain at least 10,000 years in deep formations in order to help preventing climate warming. A research team led by Cambridge University has found out that “natural accumulations of carbon dioxide that have been trapped

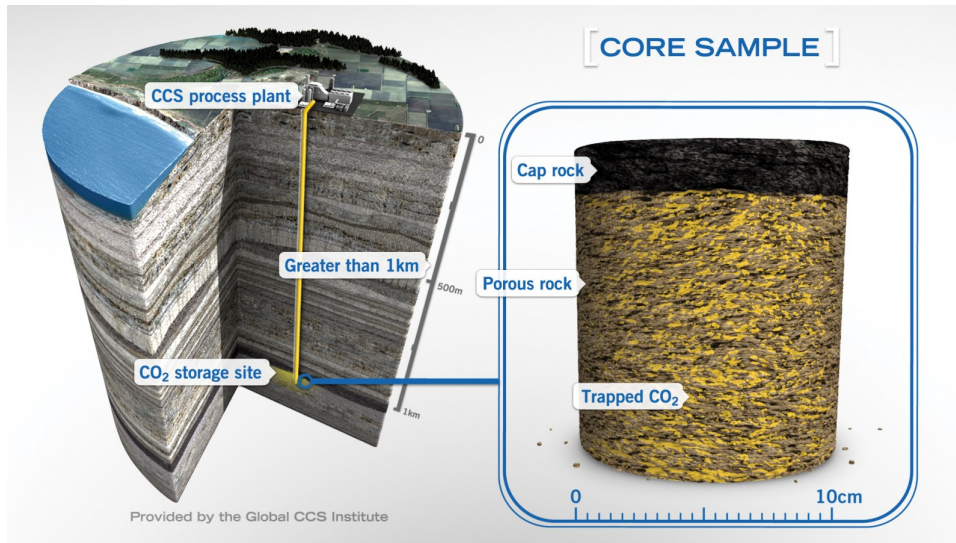


Figure 2.9: Schematic diagram of a storage site and a core sample of injected CO₂ [36]

underground for around 100,000 years have not significantly corroded the rocks above, suggesting that storing CO₂ in reservoirs deep underground is much safer and more predictable over long periods of time than previously thought” [36]. In Figure 2.9 the key element for storing CO₂ underground, which is the cap rock (an impermeable rock barrier) lied over the porous rock is depicted. The CO₂ is stored in the pores of the porous rock formation, also called reservoir. Although the carbon dioxide is a relatively dense fluid when it gets injected, it is still less dense than the brine which originally lies in the pores of the sandstone, and it rises till it reaches the impermeable cap rocks. Previously the most important concern was that the carbon dioxide dissolves, forming an acidic, carbonated solution, which then corrodes the cap rock by diffusing upwards. But the corrosion layer is very thin and remains solid, so that burying CO₂ underground is safer than emitting it directly to the atmosphere. [36]

2.2.4 CO₂ - Utilization

An alternative option to the storage of carbon dioxide is the usage or utilisation of CO₂. In the year 2011 approximately 110 Mt CO₂ is used industrially, excluding the use for EOR. About two thirds of the total amount is consumed in urea, which is an anorganic compound of carbon, nitrogen, oxygen and hydrogen, and is used for fertilisers and other products. [13]

Following are the fields of application: [13]

- Chemicals and petroleum: as already mentioned large quantities of CO₂ are used for the production of urea and methanol
- Metals: CO₂ is used on a large scale as shield gas in Metal Inert Gas (MIG) welding

or Metal Active Gas (MAG) welding and is also used in the manufacture of casting molds to enhance their hardness

- Manufacturing and construction, e.g. dry ice pellets are used to replace sandblasting for removing the painting from surfaces
- Health care, e.g. as an additive to oxygen as a respiration stimulant
- Electronics, e.g. in the waste water treatment
- Food and beverages
- Refrigerant
- CO₂ laser

2.3 Oxy-combustion cycles with natural gas

Since the focus in this thesis has been set on oxy-combustion cycles, in this chapter different processes of this type working with the fuel natural gas are presented.

2.3.1 Overview and classification

The first zero emission power plant using the oxy-combustion method dated in 1967 and was built with the main purpose of producing liquid CO₂ [13]. Today the fundamental idea of an oxy-combustion power plant is producing clean energy by avoiding the dilution of combustion products with nitrogen. In order to achieve that, the combustion takes place with pure or almost pure oxygen, producing a flue gas which consists mainly out of CO₂ and H₂O. To attain a high efficiency a big part of the exhaust gases are recycled to the combustion chamber.

The pure oxygen is provided by an external Air Separation Unit (ASU) or is done internally by using for example a metal oxide as an oxygen carrier.

Hence Figure 2.10 shows how oxy-combustion cycles can be classified, dividing the different cycles into Brayton and Rankine cycles on the second level. In the Brayton cycle, well known as gas turbine cycles, the working fluid of the cycle is in a gaseous state for the whole process. The Rankine cycle, as used in steam power cycles, works most of the time with H₂O as a working fluid, switching between gaseous and liquid state.

On the third level the different cycle concepts are differentiated by the composition of the working fluid. The working fluid of the cycles differs between the internally fired power cycles, where the flue gas is used as a working fluid in the power cycle, and the externally fired power cycle, where the combustion heat is used to heat a separate working fluid, like in a steam power plant.[13]

Some of the different cycle proposals are discussed in Chapter 2.3 and 3.

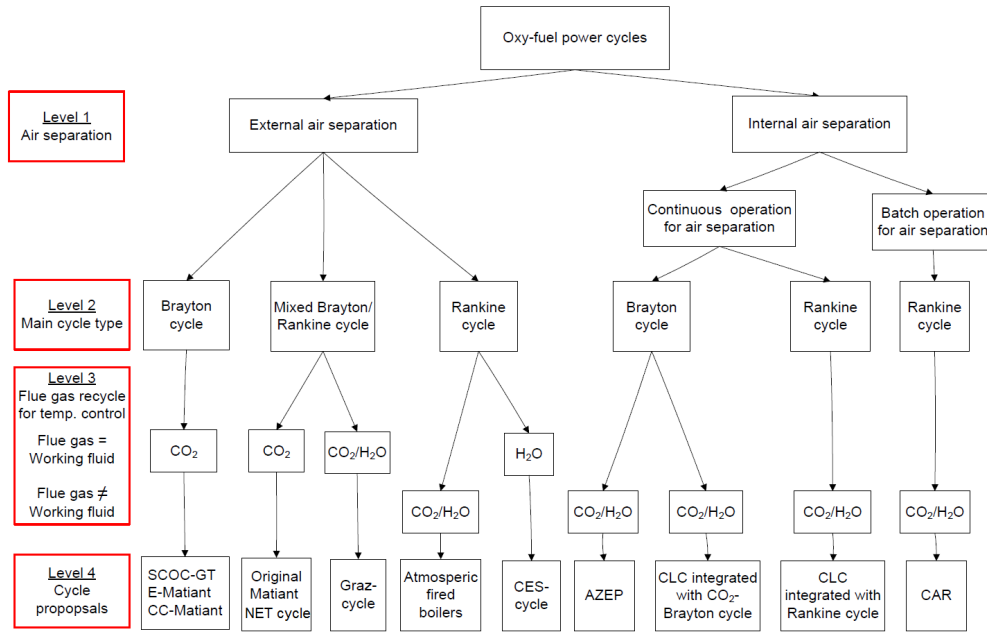


Figure 2.10: Classification of oxy-combustion methods and Cycle proposals [13]

2.3.2 Semi-closed oxy-combustion combined cycle (SCOC-CC)

The SCOC-CC, shown in Figure 2.11, reminds a lot on a common air-based combined cycle and has one of the the simplest arrangements among all cycle proposals. In the combustor a near-to-stoichiometric combustion with oxygen instead of air takes place, producing an exhaust gas which consists mainly of CO_2 (83%) and H_2O (15%) [37]. The combustion products are expanded in the gas turbine and then cooled down in the heat recovery steam generator (HRSG), providing the heat for the bottoming cycle, which operates the steam turbine.

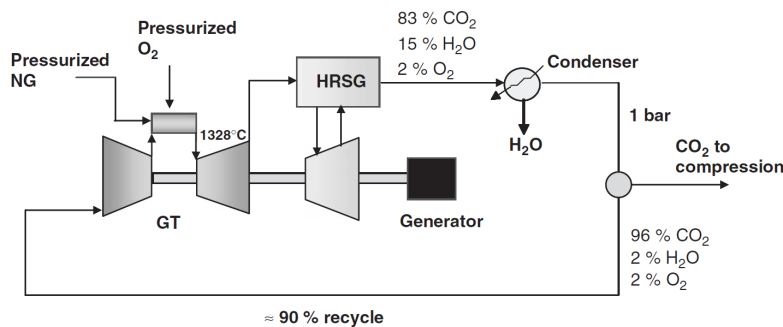


Figure 2.11: Simplified flow diagram of Semi-Closed Oxy-Combustion Combined Cycle [37]

Most of the water content gets extracted in a flue gas cooler by condensing at nearly ambient temperatures. A large fraction (almost 90%) of the CO_2 is recycled back to the compressor inlet of the Brayton cycle in order to maintain a constant turbine inlet

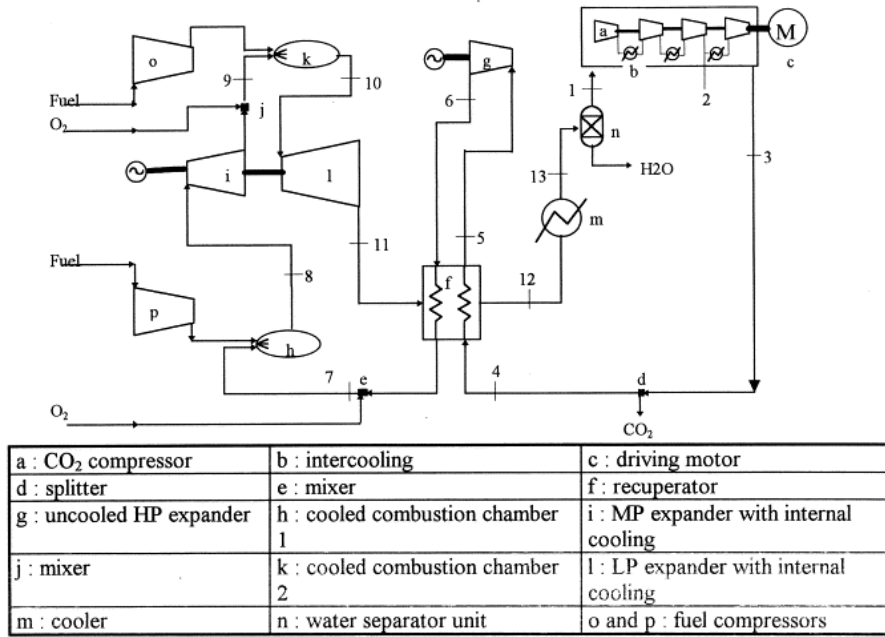


Figure 2.12: Cycle configuration of the MATIANT cycle [38]

temperature in the gas turbine. The rest, containing the combustion generated CO₂ is sent to the purification and compression unit for long term storage.[35]

The net efficiency of natural gas-fired SCOC-CC power plants with combustion temperatures in the range of 1300-1400 °C and pressure ratios between 30 and 45 is reported in the literature to be around 45-48% [35].

2.3.3 MATIANT cycle

The MATIANT cycle uses a CO₂-based mixture as working fluid. [13]

Carbon dioxide is compressed to a very high pressure (300 bar) using intercoolers between the compression stages (see component “a-b” in Figure 2.12), before getting heated up to 700 °C in a heat exchanger (“f”) [35]. At this stage the CO₂, generated at the combustion process, is already extracted (compare “d”).

The following uncooled turbine (“g”) is expanding the working fluid to 40 bar and after the gas is heated up again in the recuperator, it gets injected in the combustion chamber (“h”) to fix the turbine inlet temperature at 1300 °C. The hot CO₂ mixture is led to the MP cooled turbine (“i”), reheated in a second oxy-fuel combustor (“k”) and finally expanded in the LP cooled turbine (“l”) to atmospheric pressure. CO₂ released from the LP turbine represents the hot side of the heat exchanger (“f”). In the cooler (“m”) the working fluid gets further cooled down and the H₂O, produced in the combustions, is condensed and extracted, as indicated in Figure 2.12 by the water separator unit (“n”). [35]

The original MATIANT cycle has been assessed 1999 by Mathieu and Nihart [38]. Fur-

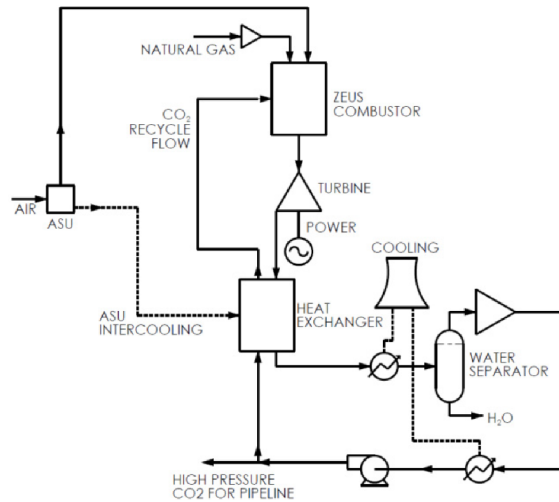


Figure 2.13: Simplified flow diagram of the NET Power cycle [39]

ther enhancements have been achieved since then by a second version, named E-MATIANT, and a third version called CC-MATIANT cycle.[35]

The E-MATIANT cycle is an Ericsson-like cycle, representing a simplification of the original cycle and reducing critical components [35]. An optimal efficiency of 47% has been achieved for the E-MATIANT.

2.3.4 NET Power Cycle

A simplified configuration of the NET Power Cycle, which is developed by a consortium established by NET Power LLC, Exelon Corporation, Toshiba Corporation and the Shaw Power Group, is shown in Figure 2.13 [35]. The cycle is a supercritical CO₂ cycle.

CO₂ gets compressed in an intercooled compressor and a pump up to 200-400 bar. The gas is then preheated in a heat exchanger up to 700-750 °C by the hot exhaust gas from the turbine. The intercooling heat of the ASU compressors is forwarded as well to the heat exchanger and provides CO₂ preheating at low temperatures. After the regenerator the CO₂ is sent to the oxy-combustion chamber, where it gets heated up to temperatures in the range of 1100-1200 °C, and subsequently to the cooled turbine. The turbine inlet temperature is regulated by the flow rate of the recycled CO₂ stream directed to the combustor (supposing a fixed natural gas mass flow rate). The resulting working fluid consists out of 90% of CO₂. After the expansion in the turbine to 20-30 bar, the hot CO₂ stream passes the regenerator, where it gets cooled down and afterwards purified in a water separator. [35]

This plant configuration obtains an overall cycle efficiency of 53.9% [39].

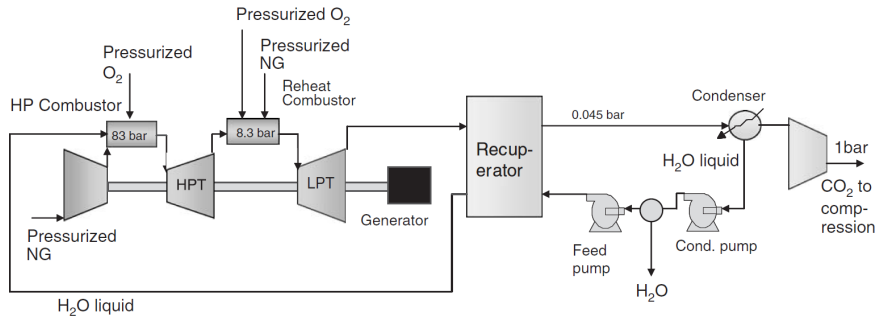


Figure 2.14: Cycle configuration of the CES cycle [35]

2.3.5 CES cycle

The “CES cycle” or “water cycle” was developed by Clean Energy Systems around 2000, using water as principle medium [13]. There are several versions of the CES cycle, the one shown in 2.14 was proposed in the year 2008 for large power plants [40].

In the combustion chamber, or so called “gas generator”, the fuel gets burned with almost pure oxygen at pressures around 80-100 bar. Preheated water is working as a temperature moderator to keep the turbine inlet temperature at constant levels (760°C). The flue gas gets then expanded in an uncooled HP steam turbine and subsequently reheated to very high temperatures (about 1760°C) by a second oxy-fuel combustor and ultimately expanded in an IP turbine and in a LP turbine to the condensing pressure (see 2.14). A heat exchanger at the LP turbine outlet recovers the heat of the hot flue gas by preheating the high pressure recycle water. The carbon dioxide gets extracted in the vacuum condenser and compressed subsequently to the final pressure level needed for storage. [35]

Regarding to Kvamsdal et al. the efficiency of the CES cycle is 44.6%, considering a HPT and HTT inlet temperature of 900°C and 1328°C , respectively, and a condensing pressure of 0.045 bar, as shown in Figure 2.14. [37]

2.3.6 AZEP cycle

The AZEP (Advanced Zero Emission Power Plant) cycle is based on a combined cycle using a mixed conductive membrane (MCM) reactor, as shown in 2.15 [37].

Ambient air leaving the compressor of the gas turbine is sent to the membrane reactor, where oxygen is separated from air with an oxygen transport membrane (OTM) and the oxygen depleted air is consequently heated up to about $700\text{-}900^{\circ}\text{C}$. The necessary heat for the process is supplied by a high-temperature recycle stream consisting of CO_2 and H_2O , produced by a near-to-stoichiometric combustion of fuel with oxygen. Part of the hot flue gas leaves the recycle stream, enabling thereby the oxygen permeation, and is subsequently cooled down with a fraction of air from the gas turbine compressor and in the HRSG before sent to the cooling, separation and compression section. As Figure

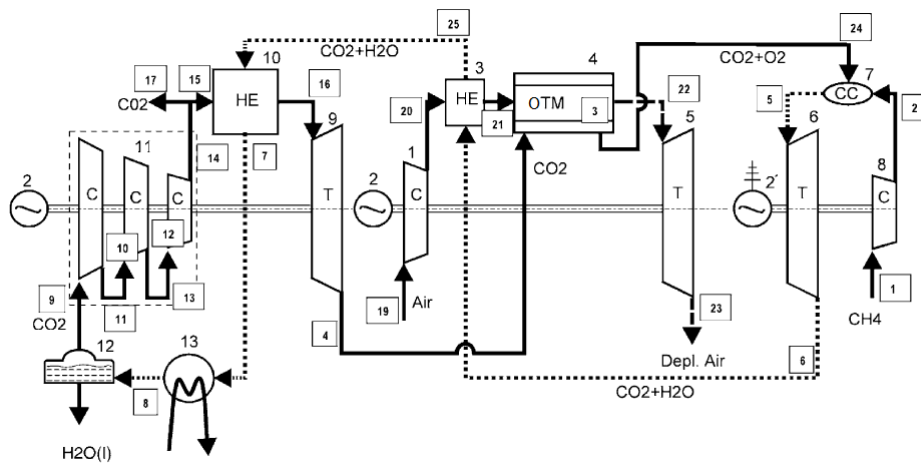


Figure 2.16: Cycle configuration of the ZEITMOP cycle [42]

Chapter 3

Graz Cycle Power Plant

The origin of the so-called Graz cycle goes back to 1985 and has been developed and presented by H. Jericha at the CIMAC conference in Oslo, Norway [43]. This cycle was originally created for solar generated oxygen-hydrogen fuel and in 1995 was changed to fossil fuels [44].

Since then several improvements have been presented and there are different cycle layouts and modifications existing. Chapter 3.1 and 3.2 discuss the Basic cycle configuration, which has been presented at the ASME Turbo Expo 2005 in Reno-Tahoe (Nevada, USA), and the modified cycle configuration with working fluid condensation at 1 bar, presented at the ASME Turbo Expo 2006 in Barcelona (Spain). Both cycle configurations are also known as S-Graz cycle (i.e. “high steam content” Graz cycle) using steam and not CO₂ as temperature moderator, like previous versions of the Graz cycle did. [35]

3.1 Basic Graz cycle

The Basic Graz cycle is the reference cycle for this thesis and is presented in this subsection. Further on the ASME paper 2005 [45] is the basic reference for the development of the process simulation and assumptions are built on that.

3.1.1 Cycle configuration

At first the cycle configuration is discussed. Figure 3.1 shows the configuration of the Basic Graz cycle power plant with the main components and cycle data.

The natural gas gets burned by the almost pure oxygen at a pressure of 40 bar. Steam and a recycled CO₂/H₂O mixture keep the TIT at constant levels (1400 °C) and cool the burners and the liner of the combustion chamber. The exhaust gas consisting of water steam and CO₂ is then led to the high temperature turbine, which expands the fluid to a pressure of 1,053 bar and 579 °C. The cooling of the HTT is performed splitting steam after the HPT, leading to a working fluid composition of 77% H₂O and 23% CO₂ at the

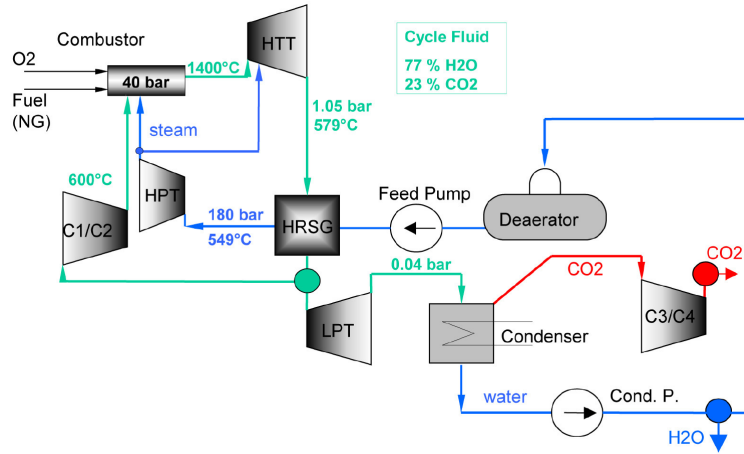


Figure 3.1: Process flow of the Basic Graz cycle [45]

HTT exit. After the turbine the gas is cooled down in the HRSG for evaporizing and superheating steam for the HPT. Around 45% of the cycle mass flow gets subsequently forwarded to the LPT and expanded to the condenser pressure of 0,04 bar into the wet steam area by passing the water saturation line (see Figure 3.2). The condenser is supplied with cooling water at an average temperature of 10 °C, separating the liquid water content from the gaseous phase [46]. Following, the gas is compressed by the compressors C3/C4 with an intermediate cooler for further extraction of condensed water. The CO₂ at the outlet has a purity of 86% at atmosphere pressure level.

After separation of liquid water in the condenser, the H₂O is forwarded to the deaerator, whose heat is provided by a split stream of the hot flue gas after the HRSG. From there on the liquid H₂O is preheated in the following economizer, evaporated and finally superheated by the C1/C2 intercooler and the HRSG superheater to the HPT pressure of 180 bar and 549 °C (see the blue line in Figure 3.2). As Figure 3.1 shows, the steam after the expansion is used for cooling the combustor and the HTT stages. [45]

The major part of the working fluid is recycled to the combustor after being compressed by an intercooled compressor C1/C2. The maximum temperature of the recycled stream is 600 °C.

The net cycle efficiency of the Basic Graz cycle is 52.2%, including the energy consumption of oxygen supply and compression in the ASU and CO₂ compression to storage conditions. In comparison to other cycle proposals, the Graz cycle offers a few advantages, consisting in a very high temperature heat input and an expansion to almost vacuum conditions, conceding an optimum thermal efficiency according to Carnot. Furthermore less than the half of the water steam of the working fluid releases its heat of vaporization in the condenser, but the majority is recycled in the gaseous phase so taking the high heat content back to the combustor. [45]

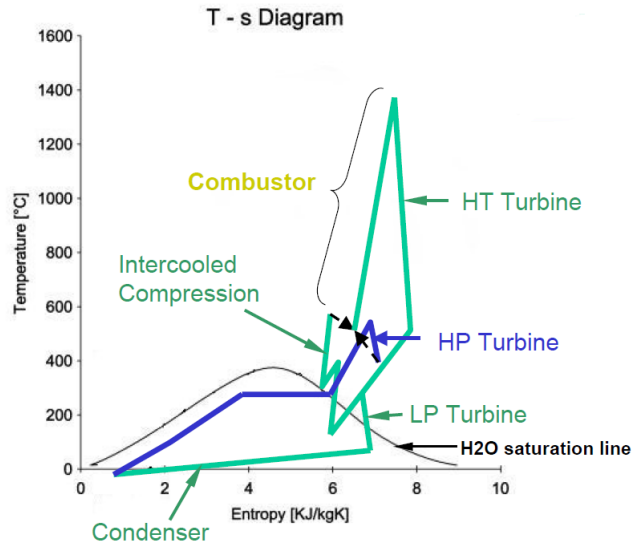


Figure 3.2: T-s diagram of the Basic Graz cycle [45]

3.1.2 Design concepts

Due to the unusual working fluid consisting approximately of three-quarter H_2O and one quarter CO_2 , several components of the Graz cycle are not standard. Nevertheless, the high temperature turbine (HTT) is very similar to a conventional air-breathing gas turbine, but the working fluid has a higher enthalpy drop at given pressure ratio and a different behavior on high-temperature materials [46]. Since CO_2 and H_2O steam is very compressible, the different turbine and compressor stages have to handle with high changes in volume flow and require a multi-shaft arrangement connected by gears (see Figure 3.3), which was presented for the first time at the ASME 2004 conference for the Basic Graz cycle. [47]

The first shaft consists of all four compressors, the HPT and the first stage of the HTT. The two latter are driving the working fluid compressors C1 and C2 and in normal performance also the CO_2 compressors C3 and C4, whereby there is a clutch placed between the compressor 4 and compressor 1 (cf. Figure 3.3). The three remaining stages of the HTT are run at 12.000 rpm and deliver power to the generator using a gear box. As Figure 3.3 indicates, the generator is driven on the other side by the LPT in a way very similar to large steam turbines. [45]

The combustion chamber must burn natural gas with a nearly stoichiometric amount of oxygen and in an environment consisting of CO_2 and steam. Scientific investigations have shown that the concept of oxy-fuel combustion using steam cooling is viable and is not more difficult to operate than any other standard combustor. [48]

Other critical components are the HRSG and the condenser, which have to cope with the unusual flue gas. The presence of a non-condensable gas in the condenser is a big

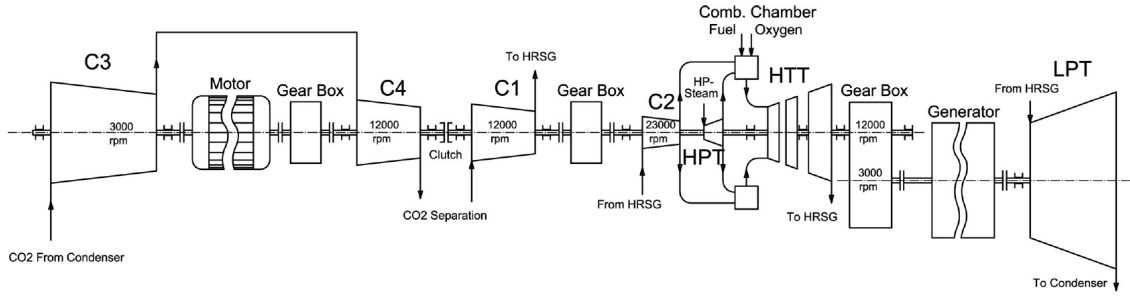


Figure 3.3: Turbomachinery arrangement for the Basic Graz cycle [47]

challenge because it reduces the heat transfer [46]. Furthermore the combination of CO_2 and water increase the risk of corrosion by the possible formation of carbonic acid.

3.2 Modified Graz cycle

The Modified Graz cycle consists of a high-temperature and a bottoming low-temperature cycle as shown in Figure 3.4. The high temperature part of the cycle is composed of HTT, HRSG, C1/C2 compressors and HPT; the low temperature part of the LPST. As the process scheme of the high temperature cycle is the same as for the Basic cycle configuration described in Figure 3.1.1, the following description focuses on the low temperature part.

The main difference to the Basic Graz cycle is that the condensation of the working fluid takes place at atmospheric pressure and not at vacuum conditions [45]. Basic for the modification was the suggestion in the Austrian patent of the Graz cycle [49] to condense a fluid consisting of water steam and CO_2 at atmosphere pressure range due to the formation of a heat transfer detaining layer of CO_2 in order to avoid a excessive large condenser surface and related high costs at vacuum conditions [44].

The working fluid of the bottoming cycle is pure steam with extensively cleaned feed water, which gets evaporized by the condensation heat of the high-temperature fluid at a pressure of 0,75 bar and subsequently expanded in the LPST and condensed. Very low cooling temperatures of Northern Europe, as assumed in the work presented at the ASME IGTI conference 2006 in Barcelona [44], allow a low condenser pressure at 0,021 bar. Each of the two heat exchangers for re-evaporation of the bottoming cycle are following a compressor stage for an increase of the pressure of the water content. In addition the compressors C3 and C4 work ahead of the final compression to storage conditions. At the first pressure level of 1.27 bar around 63% of the water fraction can be segregated; at the second of 1.95 bar further 25% of the original water content is removed. For low pressure water preheating further cooling of the working fluid takes place, causing an additional water removal of 11% and a final water content of 1% of the delivered CO_2 stream.

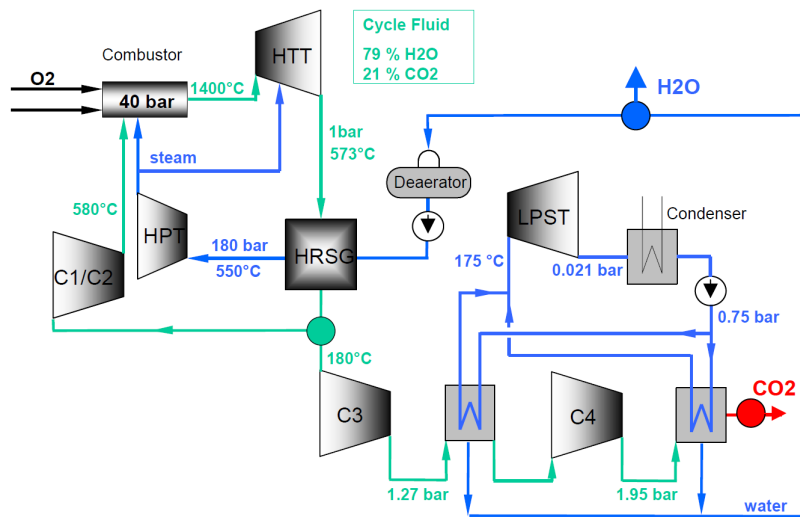


Figure 3.4: Process flow of Modified Graz cycle [44]

Chapter 4

Thermodynamic cycle modelling

In this chapter the technical background and the modelling of the power cycle components are presented. The equations depicted here are used later on in the process simulation modelling software package. The modelling part consists of the steady-state design point (or full-load) analysis, the steady-state off-design (or part-load) analysis and the dynamic modelling analysis. Beyond that the control theory is presented by describing different aspects and how the single components of a power cycle are controlled.

This chapter is introduced by general definitions of the power cycle, which are fundamental for understanding the following process simulation of the thesis.

4.1 General definitions

In this section are presented thermodynamic arrangements and calculations. The calculations comprises the heat (fuel) input formulas, as well as the efficiency calculations. The Graz power cycle differs from common combined cycles. It is a mixed Brayton and Rankine cycle, as described in Subsection 2.3.1.

4.1.1 Brayton cycle

The Brayton cycle is a simple gas turbine process, whose diagram is presented in Figure 4.1. It consists basically of a compressor, a combustor, a turbine and a generator, which is connected with the compressor and the turbine by a shaft. Atmospheric air flows through the compressor and is compressed to a pressure range of 10-35 bar. The pressurized air is forwarded to the combustion chamber where fuel (commonly natural gas) is injected and combusted. The flue gas can reach a temperature up to 1500 °C and is thereupon expanded in the turbine to almost atmospheric pressure. The energy contained in the working fluid is transformed by the turbine stages in a rotatory motion, which is ultimately used by the generator to produce energy. Each stage is composed of a stator, which is attached to the casing, and a moving blade row (called rotor), which is part of the shaft. [13]

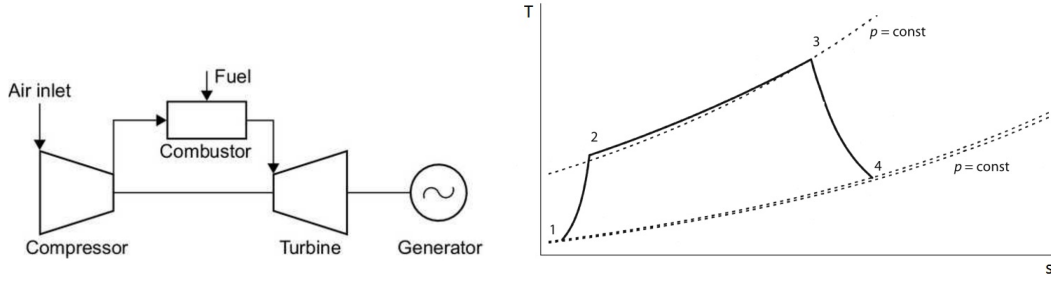


Figure 4.1: Principal diagram of a Brayton cycle and corresponding T,s -diagram with pressure losses [50, 51]

The temperature-entropy diagram of the open Brayton cycle in Figure 4.1 shows the three process steps compression (point 1 to point 2), combustion (point 2 to point 3) and expansion (point 3 to point 4) of the working fluid. For compression of the air power is necessary. This power comes from the rotating turbine when expanding the hot gas to atmospheric pressure and a temperature range of 450-650 °C and is typically about two-thirds of the generated power by the turbine [13]. For a closed Brayton cycle it is necessary to recycle the flue gas from point 4 to point 1 in the T - s -diagram so that a heat exchange (cooling) has to take place. In an idealized isentropic compression and expansion, the connecting lines from one point to the other would be vertical. The pressure losses at the inlet of the gas turbine and at the combustor basically mean a higher demand of compression work [51].

The turbine inlet temperature is preferably as high as possible with respect to cycle efficiency and Carnot process, which represents the ideal of energy transformation. The thermal efficiency, which is valid for every cycle process, is presented by equation 4.1: [52]

$$\eta_{th} = \frac{\text{output}}{\text{input}} = \frac{\text{benefit}}{\text{cost}} = \frac{|q_{in} - q_{out}|}{q_{in}} = 1 - \frac{|q_{out}|}{q_{in}} \quad (4.1)$$

The thermal efficiency is the ratio between the useful output of the power system and the input, which has to be put up in energy terms.

For the Brayton cycle the thermal efficiency η_{th} can be expressed most generally as follows: [53, 13]

$$\eta_{th} = \frac{\dot{W}}{\dot{Q}_{in}} = \frac{\dot{W}_{shaft} \eta_g}{\dot{m}_f \bar{h}_{rp}} \quad (4.2)$$

The electric power output of this system is presented by the numerator in Eq. 4.2, where \dot{W}_{shaft} denotes the power generated by the gas turbine system and transferred through a shaft to the generator with the efficiency η_g . The denominator denotes the heat input \dot{Q}_{in} , where \dot{m}_f is the fuel flow rate and \bar{h}_{rp} the lower heating value (LHV) of the fuel. Latter is explained more in detail in Subsection 4.1.3.

If the first law of thermodynamics (see Eq. A.2) is applied on the Brayton cycle with

the assumption of an ideal gas cycle, following equation is the result: [20]

$$\dot{Q} = \dot{m}_{in}(h_{out} - h_{in}) + \dot{W} \quad (4.3)$$

4.1.2 Clausius-Rankine cycle

The steam turbine is only a part of a sophisticated process, where the working fluid is circulating in a closed cycle by changing its properties continuously. The idealized type of cycle is called Clausius-Rankine cycle.

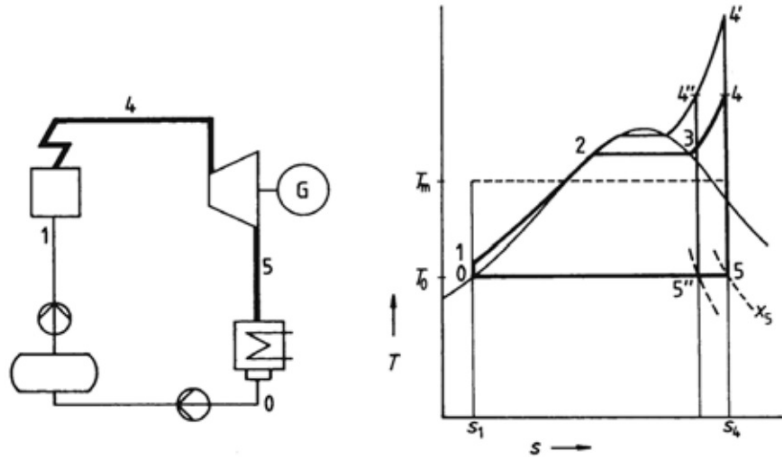


Figure 4.2: Schematic of a steam turbine cycle with appendant T,s -diagram [52]

In Figure 4.2 the simple schematic diagram of the steam turbine cycle is presented. Water with the condition 0 is pumped through the deaerator to the steam boiler, to wit to point 1 (compare with the T - s -diagram of Figure 4.2). The maximum pressure of the fluid is nowadays 350 bar for a supercritical cycle and 120 bar for a subcritical cycle. At this point the fluid is heated up till it reaches point 2 at the boiling curve (where the gaseous mass fraction x is equal to zero). Subsequently the water is evaporated at constant pressure and after becoming saturated steam (point 3; $x = 1$), it is superheated to point 4 (live steam temperature: $t_{ls} \sim 550$ °C). The vapor then enters the turbine, where it is expanded to the pressure level at point 5, depending on the cooling temperature. In the Clausius-Rankine cycle, like in the Carnot process, heat is extracted at constant temperature (assuming point 5 is in the wet steam area) to initial point 0.[52, 19]

The temperature-entropy-diagram in Figure 4.2 illustrates the idealized case of expansion in a turbine for an isentropic process. In reality the entropy in the turbine expansion increases. T_m shows the middle temperature of the heat input $q_{zu} = h_4 - h_1$ in the T - s -diagram and is illustrated by a rectangle area: [52]

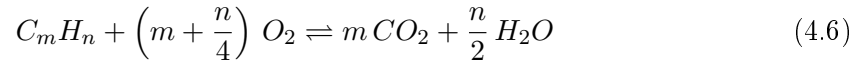
$$T_m = \frac{h_4 - h_1}{s_4 - s_1} \quad (4.4)$$

Thus the thermal efficiency, by application of equation 4.1, is following: [52]

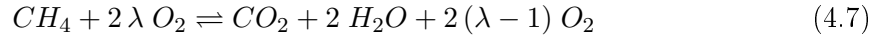
$$\eta_{th} = 1 - \frac{T_0 (s_5 - s_0)}{T_m (s_4 - s_1)} \quad (4.5)$$

4.1.3 Combustion of fuel

Combustion is a chemical reaction between a fuel (may it be coal, oil, methan etc.) and an oxidant. The general equation for a chemical combustion of a hydrocarbon is expressed in equation 4.6: [54]



The equation for combustion of methane (CH_4) with excess air (in this case only O_2) is expressed by the parameter λ , called excess air ratio, and it is as follows: [54]

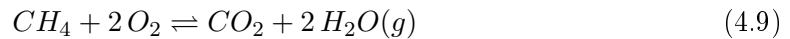


In order to understand the term heating value it is fundamental to know about the enthalpy of combustion or formation \bar{h}_{rp} . Formation here means that the reaction is in standard state, to wit the temperature assumed is usually 298 K or 25 °C. This often gets signalised by the superscript "0". The general definition is presented in equation 4.8: [53]

$$\bar{h}_{rp} = \sum_p n_o \bar{h}_o - \sum_r n_i \bar{h}_i, \quad (4.8)$$

where \bar{h}_o means the enthalpy of formation for the products and \bar{h}_i the enthalpy of formation for the educts.

Equation 4.8 can be used for any chemical reaction in order to analyse if the reaction is exothermic ("-") or endothermic ("+"). For the combustion of methane the chemical reaction is following, assuming that the water in the reaction product is in gaseous state: [13]



By taking equation 4.8 and 4.9, the calculation of the heating value in standard state is then self explaining: [13]

$$\begin{aligned} \bar{h}_{rp}^0 &= n_{CO_2} \bar{h}_{CO_2}^0 + n_{H_2O} \bar{h}_{H_2O}^0 - n_{CH_4} \bar{h}_{CH_4}^0 - n_{O_2} \bar{h}_{O_2}^0 = \\ &1 \cdot (-393.5) + 2 \cdot (-241.8) - 1 \cdot (-74.6) - 1 \cdot (0) = -802.6 [kJ/mol] = -50.03 [MJ/kg] \end{aligned} \quad (4.10)$$

The negative value from equation 4.10 is the lower heating value of methane with water

in a gaseous state. If the water of the product is in a liquid state then the result is the higher heating value (HHV); which in case of methane is 11% higher [13]. The LHV and HHV are substance-specific and can also be read from tables of thermodynamics. The very low entropy of formation of carbon dioxide explains its strong exothermic reaction if it is among the products.

4.1.4 Efficiency calculations

For the simulation of the Graz cycle different efficiency calculations have been used in order to analyse the processes and the whole CCS system chain. To keep the efficiency as high as possible is important for the overall plant economy and to maintain a low cost of electricity by saving fuel which directly depends on the plant efficiency. Figure 4.3 shows the schematic image for a net plant efficiency calculation for a general power plant. The losses and efficiencies of the Graz power cycle are the same as pictured in the above-mentioned figure.

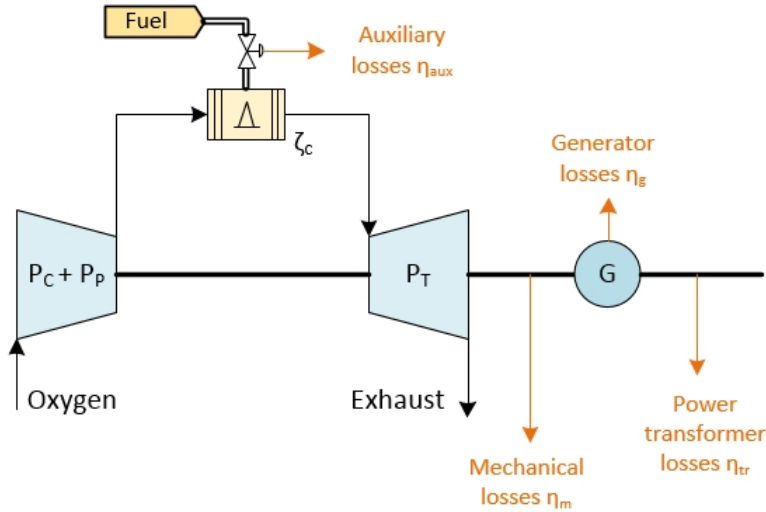


Figure 4.3: Schematic diagram of losses and efficiencies in the Graz power cycle

The thermal efficiency of the Graz cycle can be calculated according to following formula:

$$\eta_1 = \frac{\sum_1^6 P_{T,i} - \sum_1^4 P_{C,i} - \sum_1^2 P_{P,i}}{\dot{Q}_{in} (1 + \zeta_c)}, \quad (4.11)$$

where P_T is the total turbine power of the power plant from which the power of the compressors P_C and the pump power P_P is subtracted. The term \dot{Q}_{in} is explained in subsection 4.1.1, ζ_c is the combustor heat loss. The power balance of the Graz power cycle accounts for six turbines (taking into account that the high temperature turbine consists of three turbine parts, which are counted separately), four compressors and two feed water

pumps.

In equation 4.12 the net power plant efficiency η_2 for the GC power island is presented considering mechanical losses, generator losses, power transformer losses and auxiliary losses: [13]

$$\eta_2 = \frac{\left(\sum_1^6 P_{T,i} - \sum_1^4 P_{C,i} \right) \eta_m \eta_g \eta_{tr} - \frac{\sum_1^2 P_{P,i}}{\eta_m} - P_{aux}}{\dot{Q}_{in} (1 + \zeta_c)} \quad (4.12)$$

The individual efficiencies related to the cycle are illustrated in Figure 4.3. The GC auxiliary losses P_{aux} are referred to the heat input.

$$\eta_3 = \frac{\left(\sum_1^6 P_{T,i} - \sum_1^4 P_{C,i} \right) \eta_m \eta_g \eta_{tr} - \frac{\sum_1^2 P_{P,i}}{\eta_m} - P_{aux} - P_{ASU} - P_{C,ASU}}{\dot{Q}_{in} (1 + \zeta_c)} \quad (4.13)$$

The efficiency η_3 considers in addition the power for the Air Separation Unit (P_{ASU}) for the oxygen production and the power for the corresponding compressors, pressurizing the oxygen from a level of 2.38 to 42 bar.

In equation 4.14 the net efficiency η_4 of the Graz power cycle system is shown:

$$\eta_4 = \frac{\left(\sum_1^6 P_{T,i} - \sum_1^4 P_{C,i} \right) \eta_m \eta_g \eta_{tr} - \frac{\sum_1^2 P_{P,i}}{\eta_m} - P_{aux} - P_{ASU} - P_{C,ASU} - P_{CPU}}{\dot{Q}_{in} (1 + \zeta_c)}, \quad (4.14)$$

where the additional power of the CPU and its corresponding compressors, which compress the CO₂ from 1 to 100 bar, is considered.

4.2 Control theory

In this section the control theory of some basic power plant elements is explained. The explanations provide an understanding of the simulation results in the respective chapters and give insight in control strategies and functionalities of the power plant.

The control system is like the brain of the power plant and the responsibilities are supervision, control and protection of the plant, enabling hereby safe and reliable operation. The important control loops of a CCS power plant can be divided into three groups: [18]

1. The overall load control loop of the power plant
2. The secondary control loops, i.e. the control systems which maintain the important process parameters such as temperatures, pressures, drum levels etc.

- Control loops which are component specific and are important for the safe work of the individual process components, e.g. minimum and maximum flow control for a pump, pressure control of the lube oil. This third group of control systems do not affect the main plant load and are therefore not discussed here.

4.2.1 Closed loop control

One type of control in a gas-fired or combined-cycle power plant is a closed loop control. Here a controller receives the actual measured data and uses it to correct the signal to the control device in order to reach the set point of a given parameter. [18]

A feedback controller has tuning parameters to ensure closed loop stability and still provide effective control of the process. This is accomplished by a proper setting of control modes to fulfill the requirements of the process and by a satisfying tuning of those modes. Figure 4.4 presents a closed-loop control system, also known as feedback control system. The reference *feedback* means that there are one or more paths leading back from the Output $c(t)$ to the Input $R(t)$ reference signal. The aberration between the two (Error $e(t)$) is used by the controller to manipulate the process parameter to set the system error to zero [55]. In new systems computers have been used to replace analog PID controllers, e.g. by driving valves in direct digital control. [56]

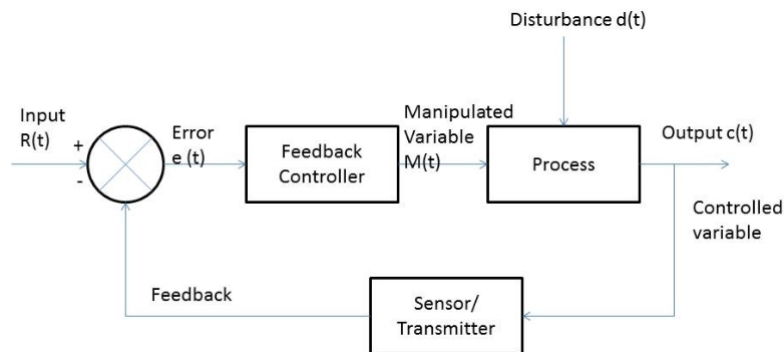


Figure 4.4: Closed-loop control system [55]

4.2.2 Load control of a gas turbine

The electrical power output in a combined cycle plant is controlled by the gas turbine whilst the steam turbine process will always follow the topping cycle whatever steam conditions are available from the HRSG [18]. In a similar way the Graz cycle works but the two processes are linked in a less clear way. There are two methods for varying the load of a gas turbine: [13]

- fuel control by activating the fuel valve to the combustor

- reduction of the air flow capacity of the compressor by setting the variable inlet guide vane (VIGV) and fuel control in the above-mentioned manner

In both cases the gas turbine inlet temperature (TIT) changes which is the most significant parameter of the gas turbine process. The second one is normally used in combined cycle systems because it ensures a higher part-load efficiency in comparison to the prior one. [13]

The gas turbines nowadays are equipped with up to three rows of VIGVs allowing a high TET down to 40% load. If the load has to be further reduced, than the TIT is decreased since the airflow reduction is linked. If the exhaust temperature decreases, automatically the steam temperature in the HRSG of a combined cycle is reduced and consequently the steam cycle efficiency (application of the Carnot theorem). Modern gas turbines react very quickly to frequency changes and they normally compensate the thermal inertia of the steam process. [13]

4.2.3 Frequency control

The power grid has to maintain the predetermined frequency of the alternating current. Thus the power generation has to be in balance with the power consumption, see equation 4.15. [57]

$$\sum P_{gen} = \sum P_{cons} \quad (4.15)$$

There is a narrow relationship between load and frequency control. If the power consumption prevails then the frequency falls. This is the case as long as the power generation is not equal to the power consumption. If there is a frequency change in the power grid, there is automatically a change of the rotational speed of the plant turbomachinery and of the power of all electricity producers of the grid. This phenomenon is called frequency response. In order to sustain a stable grid a dead band of $\pm 0.1 \text{ Hz}$ is introduced. Within this limits the power plants do not respond; outside there is a droop setting in which the power system reacts. Generally, gas turbine and combined cycle power plants, respectively CCS plants, can react very quickly to load changes. [57, 13]

4.2.4 Control of a steam turbine

Here three techniques of regulation for a steam turbine plant are presented, which are: [52]

- floating pressure operation
- throttle control
- sliding pressure operation

Floating pressure operation means fully open valves and the fluid runs freely towards turbine inlet without restrictions in order to minimize throttling losses. The live steam pressure is left uncontrolled. The negative side of this operation strategy is that the time response to load changes is slow. [58]

The throttle governing is a simple control method where a throttle, positioned in front of the turbine, acts as correcting element. The control strategy is presented in Figure 4.5a. In order to reach a part-load, the inlet pressure $p_{\alpha N}$ is diminished to $p_{\alpha T}$ so that the enthalpy difference Δh is less, but the entropy of the process increases. That is due to the fact that the throttling speed is transformed to heat. If the first law of thermodynamics is applied on the open adiabatic throttling process, following is resulting:

$$w_{12} + q_{12} = h_2 - h_1 + \frac{c_2^2 - c_1^2}{2} + g(z_2 - z_1) \quad (4.16)$$

$$\implies h_2 = h_1 \quad (4.17)$$

In equation 4.16 the velocities are the same before and after the throttle and the height difference is negligible. Hereby, a line in the h,s -diagram results indicating equation 4.17. Due to the reduced cross section the flow rate decreases automatically. The advantage of the throttle governing is the simplicity of the hardware and the good controllability down to 10% part load. [59, 52]

In case of the sliding pressure operation the performance is, according to Zotica et al. [58], adjusted online and it is commonly controlled by the steam generator or gas turbine system and not at the turbine inlet section. The load is changed by the feed pressure of the feedwater pump and the fuel flow rate of the steam boiler for the heat regulation. The live steam temperature at the inlet of the turbine remains constant, see Figure 4.5b. Thereby thermal stresses in the different components of the turbine are avoided. Like the throttle governing the thermal efficiency is reduced by the system. Due to the high specific heat capacity of the steam generator load variations cannot be achieved quickly. [59, 52]

In a modern combined cycle plant the gas turbine power output accounts for approximately two thirds of the total power output, meanwhile the steam turbine process generates one third. For this reason a control strategy without regulation of the steam process is preferred. That is also supported by the fact that gas turbine systems react extremely quick to load and frequency changes in the grid. The steam cycle is operated with fully open valves or sliding pressure operation mode down to approximately 50% load, see Figure 4.6. This mode of operation ensures best part-load efficiencies. Below 50% load the live steam pressure is kept constant. [18]

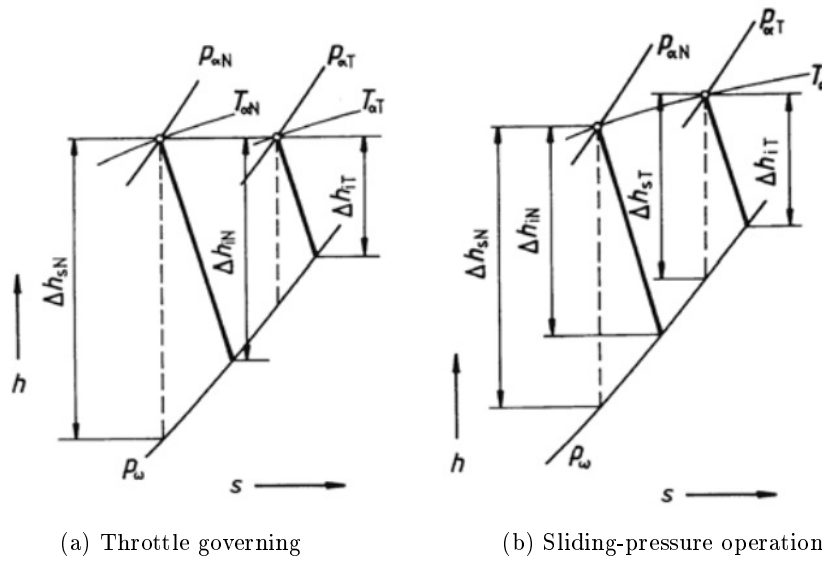


Figure 4.5: Different steam turbine control methods in the h,s -diagram [52]

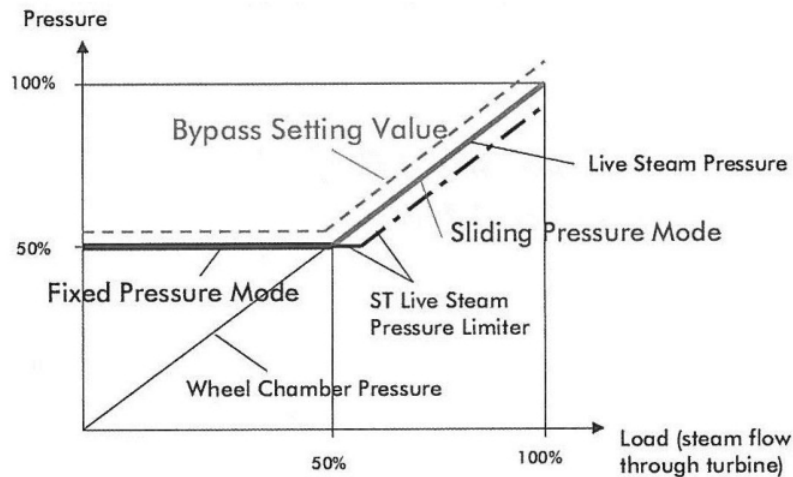


Figure 4.6: Control strategy for sliding pressure operation [60]

4.2.5 Control of a boiler

The boiler in a combined cycle plant is usually controlled by the waste heat of the gas turbine system (fuel-controlled gas turbine) or by an additional firing unit. To improve the controllability of a power generation plant the water flow rate can be reduced, whereby the steam tapping of the steam turbine reduces automatically [57].

In a once-through steam generator, the evaporation point moves locally depending on the load attained from the power system. At a certain point of the boiler the enthalpy is determined by use of the measured variables pressure and temperature and subsequently compared to the desired value of the specific load level. The controlled variable in this case

is the feed water regulator which either reduces the water flow (so the enthalpy is rising) or vice versa.

In Figure 4.7 an example of a block-unit power station with a once-through boiler and its control strategy are presented. The turbine uses an upstream pressure control in the base load operation and other than that a rotational speed control for part-load operation. The fuel input is regulated by the load-frequency control of the power unit. The once-through boiler is the critical component of the system because it has to follow immediately the power demand of the controlled turbine. The accumulation of heat occurs in the fuel deposit F , in the once-through boiler B inclusively the piping and in the reheater R . All those heat storage capacities are mentioned in yellow in the Figure 4.7. The dynamic behavior and how those heat storage capacities influence the whole power unit behavior is described also in subsection 4.5.1. [57]

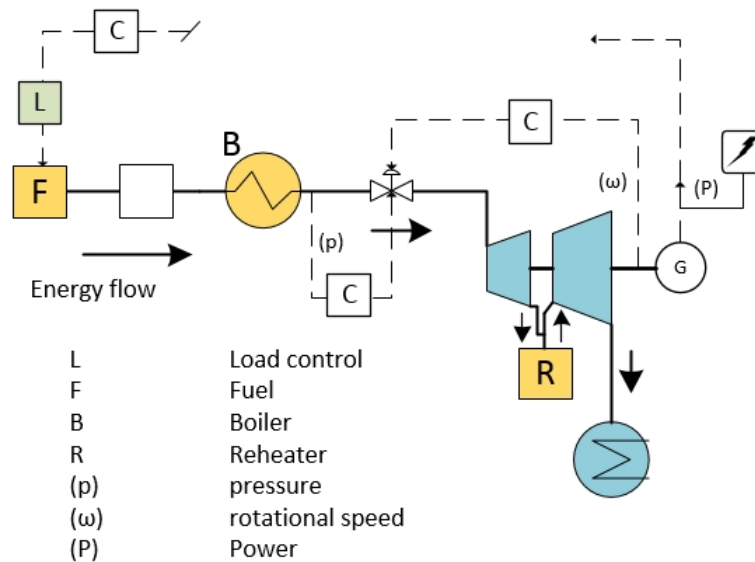


Figure 4.7: Schema of a thermal power unit with once-through boiler [57]

4.2.6 Orifice plate

An orifice plate is a metal disc with a hole in it and is placed into the piping in order to either measure the flow rate or restrict the flow to a constant volumetric flow rate. Orifice plates are very simple and inexpensive and therefore widely used. A problem can be the inaccuracy (the error can be of $\pm 5\%$) and the permanent pressure loss. For the calculation of the properties of the fluid restricted by the orifice plate, the Bernoulli's principle is applicable, which states the relationship between velocity and pressure of the fluid. [61]

Orifice plates are used - and so it is in the Graz power cycle for this investigation - for setting split-ratios between two streams.

4.2.7 Importance of control strategy for the simulation

In order to make a dynamic or off-design simulation of a power plant process, control strategies and operation modes have to be identified and incorporated in the simulation. That is due to the fact that different control modes change results of the simulation. This is proved by this investigation and the results of the different control modes are presented in Section 6.3.

In a combined-cycle plant the operation mode is very good analyzed in standard literatures. For the gas-fired CCS cycles this is not the case since they have very different and often interlaced cycle schemes. This is also the case with the Graz cycle power plant, where cycle fluid compositions change and the whole thermodynamic cycle design is much more complex than in a combined-cycle power plant.

4.3 Steady-state Design Point Analysis

The operating concept of a power plant decides at which operating point the plant has to have its best efficiency. This operating point is called design point and is of major importance when it comes to overall plant efficiencies. [13]

4.3.1 Gas turbine

Turbines are generally designed either radially or axially, whereby axial turbines are better suited for large-scale power generation plants. Gas turbines for power generation can be divided into two groups: [13]

- aeroderivative gas turbines, which are modified for industrial duty and are modified jet engines
- heavy duty industrial gas turbines, which originally come from steam turbine technology

The principles of energy transfer in a turbine are complex but can be characterised by the equation of state, the first law of thermodynamics, the momentum equation and the energy equation. The isentropic efficiency - generally discussed in subsection A.4.4 - for a turbine can be seen in eq. 4.18 as the ratio between the real and isentropic (ideal) performance. [62]

$$\eta_{is,t} = \frac{\text{real work}}{\text{isentropic work}} = \frac{\dot{W}_{cv}/\dot{m}}{\left(\dot{W}_{cv}/\dot{m}\right)_{is}} \quad (4.18)$$

Typical values for the isentropic efficiency of a turbine are in the range of 0.7 to 0.9. The polytropic efficiency for a turbine can be written as follows: [20]

$$\eta_{p,t} = \frac{n-1}{n} \frac{\kappa}{\kappa-1} \quad (4.19)$$

Thinking of the Carnot efficiency definition, the thermal efficiency of a power generation system is the higher the turbine inlet temperature is. A limiting factor for very high temperatures in a gas turbine is the limitation of the materials used for the blades. In order to achieve maximum inlet temperatures in a gas turbine, the blades are cooled by a layer of air which is released through holes in the blade. [62]

4.3.2 Cooled gas turbine

The cooled gas turbine model used here was developed at the Institute of Thermal Turbomachinery and Machine Dynamics (TU Graz) and is built on a simple stage-by-stage methodology similar to the work presented by Jordal et al. [63]. Profound information are found in [64]. [45]

The model calculates the necessary cooling mass flow rate per stage. The model assumes that half of the cooling mass is injected to the turbine at the inlet and the rest at the outlet [45]. The turbine blade surface has a prescribed maximum metallic temperature (T_{metal}), which is not allowed to be exceeded. The turbine blades are cooled as described above; a minimum temperature difference of 150 °C between the surface temperature of the blade and the cooling medium at the outlet of the blade holes is assumed. [10]

The mass flow rate of the cooling medium is calculated by application of equation 4.20, 4.21 and 4.22: [10]

$$\dot{m}_c = \dot{m}_1 \frac{(h_1 - h_{2a}) \left(\frac{T_1 + T_{2a}}{2} - T_{metal} \right)}{\vartheta \left(h_{k(T_{metal} - \Delta T_{cooling})} - h_{k(T_k)} \right)} \quad (4.20)$$

$$\vartheta = \frac{T_1 - T_{2a}}{f_A n_{st} St \frac{1}{\sin(\beta_2)}} \quad (4.21)$$

$$St = \frac{h\nu}{c_p w_2} \quad (4.22)$$

$$f_{power} = \frac{k_{stat} - 1 + \frac{(n_{st}+1)(4n_{st}-1)}{6n_{st}}}{n_{st}} \quad (4.23)$$

The above-mentioned variables are described in Table 4.1. [10]

Table 4.1: Variables of the cooled gas turbine model

Symbols	Description
\dot{m}_1	inlet mass flow rate of the turbine
h_1	specific enthalpy of the inlet mass flow
h_{2a}	specific enthalpy of the outlet mass flow, uncooled
T_1	temperature of the inlet mass flow
T_{2a}	temperature of the outlet mass flow, uncooled
$h_{k(T_{metal}-\Delta T_{cooling})}$	specific enthalpy of the cooling medium at the outlet of the cooling holes
$h_{k(T_k)}$	specific enthalpy of the cooling medium at the inlet
f_A	ratio of blade surface area to axial passage area
n_{st}	number of stages of the turbine
St	Stanton number
β_2, w_2	angle and velocity, defined in Figure 4.8
k_{stat}	cooling mass flow rate of the stator
$\Delta T_{cooling}$	temperature difference at the blade outlet holes between metal and cooling medium
T_{metal}	Metal temperature of the blade

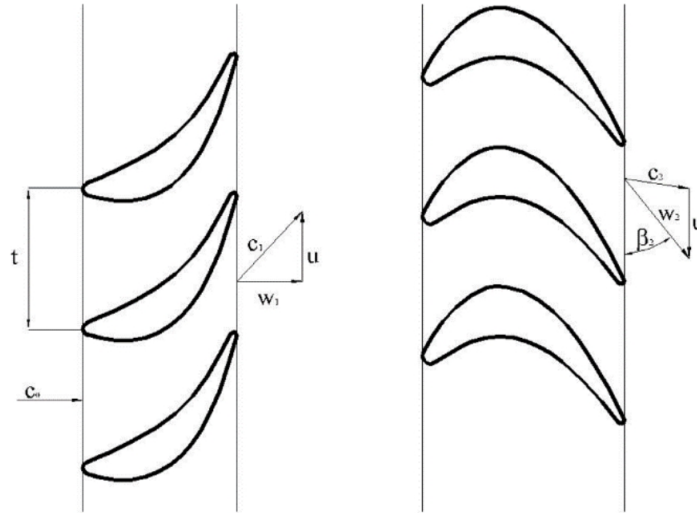


Figure 4.8: Definition of the angle β_2 and velocity w_2 [10]

The cooling steam, once it left the turbine blade, also expands with the main flow and produces power. Therefore, it is assumed that the cooling medium leaving the stator blades, is subsequently expanded in the rotor. The rest of the stage cooling medium, which gleaves the rotor blades, produces power in the following stages of the turbine. [10]

Hence, the ratio of the additional power of the cooling medium mass flow can be found as described by equation 4.23. [10]

4.3.3 Steam turbine

The steam turbine utilizes the high live steam temperatures (up to 520-565°C) and the live steam pressure (on a level of 100-160 bar)¹ for an expansion process in order to produce mechanical energy [18]. Each turbine stage consists of nozzles in which the steam is accelerated and the “pressure” energy is transformed into kinetic energy, and rotor blades which convert the kinetic energy to rotational energy and power output. Depending on the number of pressure levels in the HRSG there are multiple inlets in the steam turbine and therefore the steam mass flow increases towards the outlet of the turbine. In a combined-cycle plant short start-up and shut-down times are of particular importance.

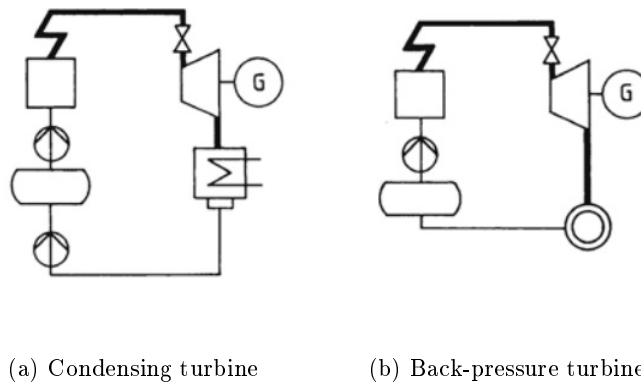


Figure 4.9: Two structures of industrial turbines [52]

Here two types of turbine set-ups are presented, which are relevant for this work: one is the condensing turbine (see Figure 4.9a), the other is the back-pressure turbine (see Figure 4.9b). The set-up of the condensing turbine is the same as in most industrial turbines with high power output. The process produces only mechanical work, if applicable with the waste heat of an other process in the case the temperature is necessarily high enough. The exhaust heat is condensed by the cooling water of the condenser at the lowest temperature possible in order to get a preferably high enthalpy drop. [52]

The back-pressure turbine set-up has a turbine bank pressure above atmospheric pressure levels. The exit temperature is therefore higher than the one of the condensing turbine and the enthalpy drop is accordingly less, because the condensing heat is transferred to a heat consumer. By this way the whole energy of the live steam is used at high efficiency. The steam mass flow follows the demand of the heat consumer. Thus, the power output cannot be controlled. [52]

¹Values are for subcritical processes; for more information see Subsection 4.1.2

4.3.4 Compressor

Like turbines, modern turbocompressors can be divided into two categories: axial or radial compressors. For large mass flows and medium to large sized power generation systems the axial turbocompressor is the best choice. In an axial compressor the air (or an other gas like pure oxygen) enters and exits the axial direction and high pressure ratios can be achieved. In equation 4.24 is presented the relation between the isentropic work and the actual work; the isentropic performance characteristics of a compressor or pump are following: [62]

$$\eta_{is,c} = \frac{\textit{isentropic work}}{\textit{real work}} = \frac{\left(-\dot{W}_{cv}/\dot{m}\right)_{is}}{\left(-\dot{W}_{cv}/\dot{m}\right)} = \frac{T_{02,is} - T_{01}}{T_{02} - T_{01}} = \frac{\frac{p_{01}}{p_{02}}^{\frac{\kappa-1}{\kappa}} - 1}{\frac{T_{02}}{T_{01}} - 1} \quad (4.24)$$

Typical values for the isentropic efficiency of a compressor are in the range of 0.75 to 0.85. The polytropic efficiency for a compressor can be written as follows: [20]

$$\eta_{p,c} = \frac{n}{n-1} \frac{\kappa-1}{\kappa} \quad (4.25)$$

Modern turbocompressors in a gas turbine system are equipped with VIGVs for control and regulation of the mass flow, see subsection 4.2.2.

4.3.5 Heat recovery steam generator

In a combined cycle process the heat recovery steam generator unit is the connection between the gas cycle and the steam cycle. That is also the case with the Graz Cycle. The function of the HRSG is to transform the water into steam by taking advantage of the exhaust gas energy of the gas turbine cycle. In an idealized heat exchanger the energy transferred per unit temperature would be the same in both streams at any point in order to prevent energy and exergy losses. The HRSG is the only component of a combined-cycle power plant, which is not standardized and therefore the hardware is different in each power plant.

In Figure 4.10 the T-Q diagram of a single-pressure HRSG is presented. The feedwater is heated up in the economizer to the approach temperature, which marks the difference between the boiling point in the drum and the water temperature at the economizer outlet. Usually this difference is between 5 to 12 K and avoids the evaporation in the economizer at off-design mode. Subsequently the water mass flow enters the drum and is evaporated in the evaporator unit at a constant pressure level. Saturated steam then leaves the drum and is superheated by the hottest turbine exhaust gas. The pinch point temperature identified in Figure 4.10 is the temperature difference between the gas at the evaporator outlet and the boiling temperature. The lower this temperature difference is the more heating

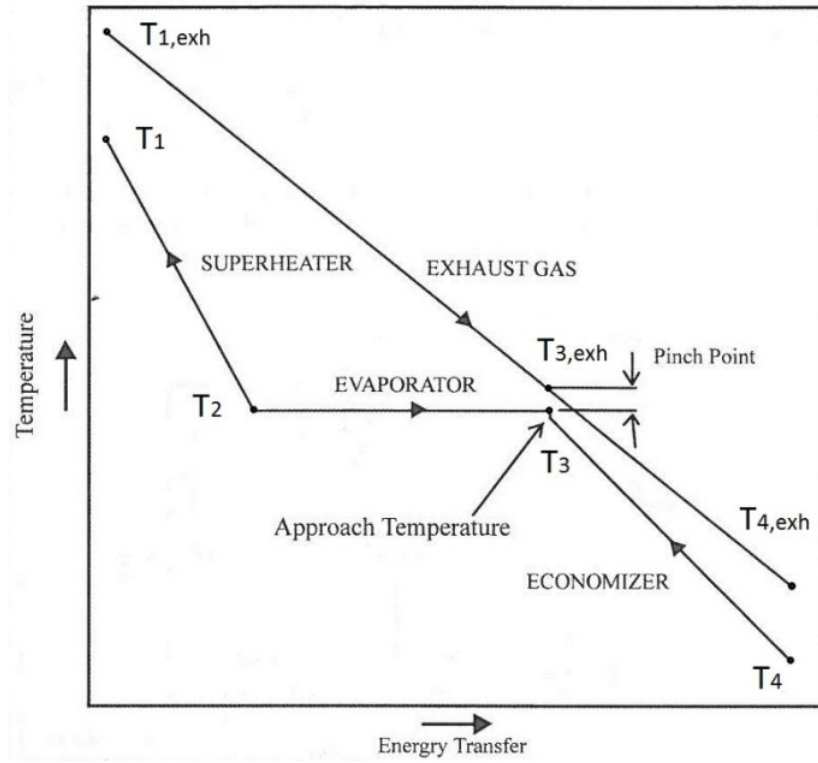


Figure 4.10: T-Q diagram of a HRSG, single-pressure [18]

surface is needed (costs are increasing in this case) and the more steam is produced by the evaporator. Depending on the economic investment the pinch point temperature is normally between 8 and 15 K. [18]

The surface area required for a heat exchange is presented in following equations: [18]

$$\dot{Q} = k \cdot A \cdot \Delta T_{LMTD} \quad (4.26)$$

$$\Rightarrow A = \frac{\dot{Q}}{k \cdot \Delta T_{LMTD}} \quad (4.27)$$

$$\Delta T_{LMTD} = \frac{\Delta T_A - \Delta T_B}{\ln\left(\frac{\Delta T_A}{\Delta T_B}\right)} \quad (4.28)$$

where k is the overall heat transfer coefficient, A the heat transfer surface area and ΔT_{LMTD} the logarithmic mean temperature difference.

The heat balance for any section of the HRSG, shown in Figure 4.10, is written in equation 4.29. [13]

$$\Delta \dot{Q} = \dot{m} c_p \Delta T \quad (4.29)$$

The total energy transfer for superheater, evaporator and economizer is following: [13]

$$\dot{m}_{steam} (h_1 - h_4) = \dot{m}_{exh} c_{p,exh} (T_{1,exh} - T_{4,exh}) \quad (4.30)$$

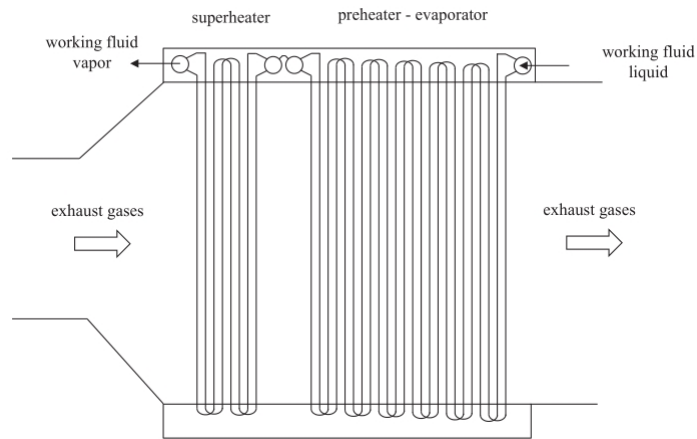


Figure 4.11: Example of a horizontal once-through steam generator [65]

For this work a once-through steam generator (OTSG) is chosen, which will be discussed in the following paragraph. The HRSG described before is a heat exchanger system with a drum. In an OTSG the economizer, evaporator and superheater is all in one tube, so that water enters at one end and leaves the tube as superheated steam. Since a HRSG is subject to many load changes, the drum-based heat exchanger with design pressures above 100 bar impose restrictions on this duty. The OTSG is hereby favorable since there is no drum which does limit start-up and load change times. This design is built in both construction versions: horizontal and vertical HRSGs. [18]

The most common OTSG, used in waste-heat recovery, coal and gas-fired power generation plants, is called Benson boiler with a partially sectioned design. In Figure 4.11 an OTSG with horizontal exhaust gas flow and vertical steam flow tubes is shown.

4.4 Steady-state Off-design Analysis

This subsection explains the modelling of the GC components in steady-state off-design conditions. Following the research questions this is a major part of the thesis.

Typically, there are many variations in ambient conditions and in the operating environment which leads (from design) to off-design conditions for a CCS power plant. The multiple parameters which have to be considered are, e.g.: [18]

- Plant load (which is the parameter that is priorily reported in this work)
- Ambient air temperature and pressure
- Cooling water temperature (typically combined-cycles are situated near rivers which can change their conditions during seasons)
- Frequency

- Fuel type

4.4.1 Steam turbine

The steam mass flow ratio for off-design conditions is calculated using the Law of Cones, with reference to Kehlhofer [18]:

$$\frac{\dot{m}_s}{\dot{m}_{s,0}} = \frac{\bar{V} \cdot p_\alpha}{\bar{V}_0 \cdot p_{\alpha,0}} \sqrt{\frac{p_{\alpha,0} \cdot v_{\alpha,0}}{p_\alpha \cdot v_\alpha}} \cdot \sqrt{\frac{1 - \left(\frac{p_\omega}{p_\alpha}\right)^{\frac{n+1}{n}}}{1 - \left(\frac{p_{\omega 0}}{p_{\alpha 0}}\right)^{\frac{n+1}{n}}}}, \quad (4.31)$$

where the indices 0 indicate the design point, s stands for steam, α for the ST inlet section and ω for the ST outlet section. The variable \bar{V} expresses the average swallowing (or absorption) capacity. The pressure ratio $\frac{p_\omega}{p_\alpha}$ is very small in the condensing turbines due to low pressure at the steam turbine outlet. The ratio of average swallowing capacities is also close to 1 and therefore the ratio can be simplified written: [18]

$$\implies \frac{\dot{m}_s}{\dot{m}_{s,0}} = \sqrt{\frac{p_{\alpha,0} \cdot v_{\alpha,0}}{p_\alpha \cdot v_\alpha}} \quad (4.32)$$

Equation 4.32 may be used for part-load in order to express the relation between the steam mass flow and the pressure of the live steam. The efficiency of the steam turbine depends on the enthalpy difference. At off-design conditions there is not a great alteration in the enthalpy drop except in the last turbine stages. Therefore the polytropic efficiency in the superheated area can be set constant [18]. This statement is valid for a ST in sliding-pressure operation.

Referring to Stodala [66], the changes of the mass flow, inlet and outlet pressures and inlet temperature of the steam in part-load (in comparison to full-load) conditions are following:

$$\dot{m}_s \cdot \sqrt{\frac{p_{\alpha,0}^2 - p_{\omega,0}^2}{T_{f,0}}} = \dot{m}_{s,0} \cdot \sqrt{\frac{p_\alpha^2 - p_\omega^2}{T_f}} \quad (4.33)$$

If the steam turbine is operated with throttle control at the turbine inlet, then the live steam expands isenthalpic in the throttle valve (point A to point B) before it further expands in the stages of the ST, see Figure 4.5a and 4.12.

4.4.2 Gas turbine

For the gas turbine the choked nozzle equation is commonly used. Choked flow means that the mass flow does not increase even if there is a further decrease in the downstream pressure. So in this case a broader pressure difference over the turbine section does not

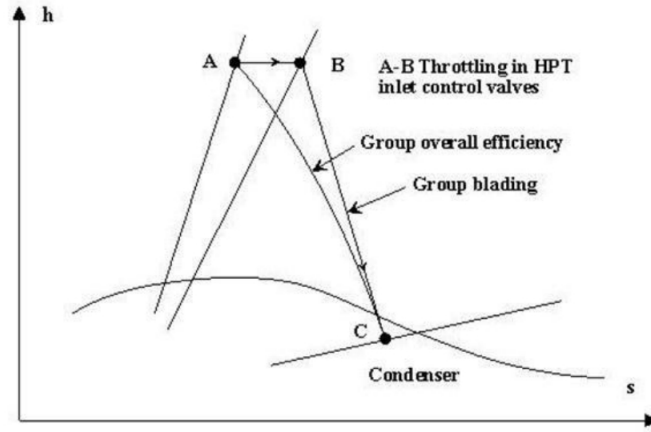


Figure 4.12: Steam turbine efficiency characteristics with throttling control [67]

involve an increase in the mass flow [13]. The choked nozzle equation can be derived by taking into account non-dimensional numbers, as shown in Figure 4.13. So for a reduced mass flow rate, viz. $\frac{\dot{m}\sqrt{T}}{p}$, and a constant rotational speed, viz. $\frac{N}{\sqrt{T}}$, the curves of the choked condition are illustrated in Figure 4.13. As the backpressure decreases and thus the pressure ratio increases, the reduced flow rate is set constant, indicated by the dashed line. The suffix 3 and 4 indicate the turbine inlet and outlet. Following equation results respectively: [13]

$$\frac{\dot{m}\sqrt{T_3}}{p_3} = \text{constant} \quad (4.34)$$

By taking into account also the molecular weight (MW), which makes sense if the working fluid molecular weight changes during the process through steam injection in the turbine, following can be stated: [13]

$$\left(\frac{\dot{m}}{p} \sqrt{\frac{T}{MW}}\right)_3 = \left(\frac{\dot{m}}{p} \sqrt{\frac{T}{MW}}\right)_{3,0} \quad (4.35)$$

$$\Rightarrow \frac{p_3}{p_{3,0}} = \frac{\dot{m}_3}{\dot{m}_{3,0}} \sqrt{\frac{T_3}{T_{3,0}} \frac{MW_{3,0}}{MW_3}} \quad (4.36)$$

The choked nozzle equation in equation 4.36 expresses that the inlet pressure ratio of the turbine is proportional to the mass flux ratio and to the square root of the temperature ratio. It is inversely proportional to the square root of the molecular weight ratio. [13]

The isentropic efficiency can be assumed constant at part-load operation. [67]

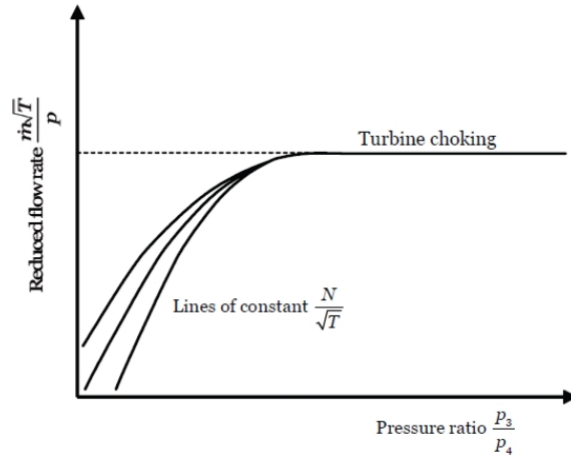


Figure 4.13: Choked nozzle characteristics of a turbine [13]

4.4.3 Compressor

Compressors are usually coupled with a gas turbine and a generator, running on a single-shaft with constant speed. In Figure 4.14 a typical compressor characteristic with the pressure ratio on the vertical axis and the reduced mass flow rate on the horizontal axis is presented. The suffix 1 and 2 stands for the compressor inlet and the compressor outlet, respectively.

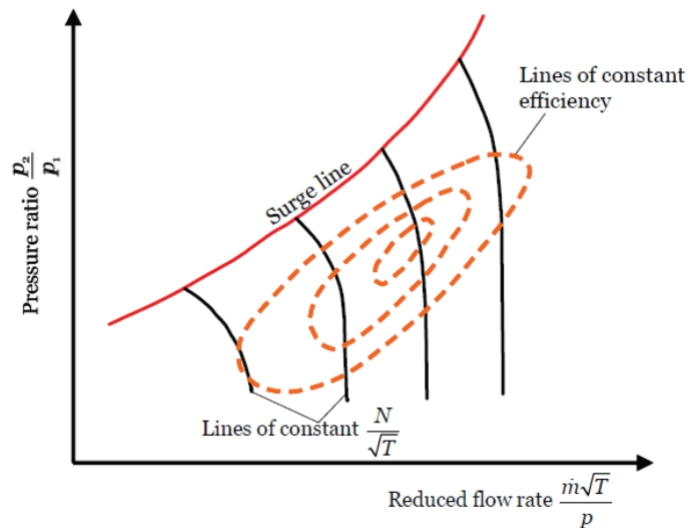


Figure 4.14: Compressor characteristic with reduced flow rate [13]

For constant speed of the compressor it can be assumed that the volumetric sucking capacity at the compressors inlet is constant. The derivation of the part-load behavior of the compressor starts with the ideal gas law (see equation 4.37) and the equation of

continuity (explained in Appendix A.1): [13]

$$pv = \frac{p}{\rho} = RT \quad (4.37)$$

$$\dot{m} = \rho u A_c = \rho \dot{V} \quad (4.38)$$

$$\implies u = \frac{\dot{m}RT}{pA_c} \quad (4.39)$$

For constant speed it can be assumed following equation, whereby the index 0 indicates the design point:

$$\left(\frac{\dot{m}RT}{pA_c} \right)_1 = \left(\frac{\dot{m}RT}{pA_c} \right)_{1,0} \quad (4.40)$$

$$\implies \frac{\dot{m}_1}{\dot{m}_{1,0}} = \frac{p_1}{p_{1,0}} \frac{R_{1,0}}{R_1} \frac{T_{1,0}}{T_1} \frac{A_{c1}}{A_{c1,0}} \quad (4.41)$$

From equation 4.41 it can be followed that if the ambient conditions are the same, the inlet mass flow (in a common gas turbine it is usually air) is proportional to the cross-sectional inlet area (A_{c1}) of the compressor. It can be considered constant, unless variable inlet guide vanes (VIGV) are used to control the flow rate. VIGVs are used for start-up and during part-load operation, whereby the flow rate can be reduced to 60-70% of the flow rate at design point. [13]

4.4.4 HRSG

The HRSG is designed based on the desired steam pressures and temperatures in order to get to know the surface areas of the heat exchanger. This is also important for the definition of the tubing and the desired flue gas pressure drop when it passes through the HRSG. When the gas turbine system runs at part-load operation the flue gas conditions change radically in comparison to the design point [67]. Since the heat exchanger surfaces are fixed, the conditions on the water/steam side and on the flue gas side within the heat exchanger change, subsequently also the overall heat transfer coefficient will change, to wit in following way: [68]

$$\frac{k \cdot A}{(k \cdot A)_0} = \left(\frac{\dot{m}_h}{\dot{m}_{h,0}} \right)^m \quad (4.42)$$

The suffix h means the hot side of the heat exchanger. The exponent m is a constant and has a value (for staggered tubes) between 0.56-0.58, depending on the geometry of the HRSG. Taking into account equation 4.26, it can be followed that the total heat transfer depends on the flue gas mass flow. A reduced flue gas mass flow will result in a lower ΔT_m , which will probably lead to a reduced pinch point in the HRSG. [68, 67]

Also the pressure drop will decrease in the HRSG at part-load conditions and is defined

in equation 4.43:

$$\frac{\Delta p}{\Delta p_0} = \left(\frac{\dot{m}}{\dot{m}_0} \right)^2 \quad (4.43)$$

4.4.5 Condenser

The purpose of the condenser is to reject the heat of condensation of the fluid at the steam turbine outlet of the power plant. The direct water cooling of the condenser is typically the first choice if the power plant is located near a river or ocean. The cooling system is a large heat exchanger with the cooling water flowing inside a large number of tubes and with the condensing fluid on the shell-side of the condenser. [13]

One option to operate the condenser in part-load is to keep the cooling water mass flow constant, regardless the decreased load. By doing that the cooling water pumps are operated at constant speed. In part-load operation less steam is produced in the HRSG and subsequently a lower mass flow rate has to be condensed.

Figure 4.15 illustrates the T-Q-diagram of the water-cooled condenser, whereby the temperature of the inlet cold mass flux is kept constant. Therefore the slope of the cooling water curve will be equal to the slope at the design point. But at the same time, as mentioned before, the steam mass flow gets less at part-load conditions and therefore the heat transfer from the steam/water side to the cooling water side is reduced. As a consequence the temperature difference at the hot side cooling water outlet increases at constant condenser pressure. The result of part-load operation might be a lower steam condensing pressure and subsequently the steam/water line in Figure 4.15 moves down. [67]

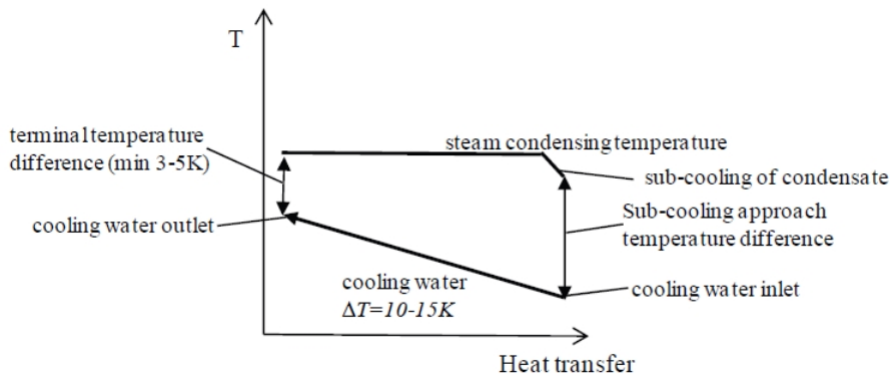


Figure 4.15: Characteristic of a water-cooled condenser [13]

4.5 Dynamic Analysis

In this section the dynamic (transient) behaviour of the CCS power plant is analyzed in order to find out which are the critical components. In order to find out the best suited

plant for design and off-design operation it is important to know not only the steady-state behavior of the cycle but also its dynamic behavior throughout the whole operation. For a calculation of the dynamic behavior it is important to know the detailed properties of the hardware of all plant components. It has to be taken into account that a dynamic response always leads to a steady-state point when the necessary time factor is respected. [18]

4.5.1 The case study

With reference to the necessary transient of a power plant with an output-controlled turbine, the boiler unit is the most critical part of the entire system. That is the case because the boiler has to follow with his steam output as fast as possible the steam demand of the turbine. In order to facilitate the boiler's task, it is necessary to take advantage of the mass and heat capacities of the other components of the process cycle. Therefore it is also important to know where in the block the heat storage occurs and how this capacity influences the cycle in case of a load change. It can be either positive or negative. A component with its heat storage capacity has a positive effect if it supports the load change with its respective behavior. The heat storage capacity of the boiler is primarily determined by the metallic masses and only in second order by the fluid content of the boiler. [57]

Even if the combustion with his power output would follow immediately the heat demand of the turbine, there would always be a delay in the steam delivery because of the heat capacities of the working fluid and the masses of the boiler as well as the live steam piping. The boiler with his inertness follows therefore the volatile combustion unit according to following relation: [57]

$$F = \frac{1}{1 + t_k \cdot s}, \quad (4.44)$$

here s is the Laplacian operator and t_k is the time constant. If this constant is small than the boiler releases heat faster. In comparison with other once-through steam generators a Benson boiler has a very high heat capacity due to its packages of collection unit and downpipe. [57]

The relation described above is shown in Figure 4.16.

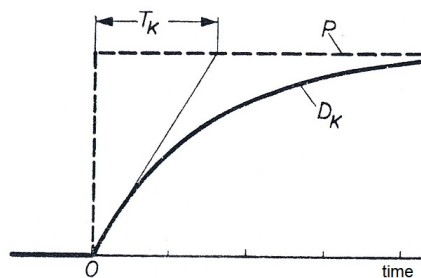


Figure 4.16: Heat transition curve of a boiler over time [57]

Since the boiler (in this study a once-through steam generator was chosen for the Graz Cycle) is the most sensitive component of the power system when it comes to dynamic behavior, in this thesis the focus was set on the heat exchangers for the transient analysis. The following subsections will amplify on this thematic.

According to a back-of-the-envelope calculation of commercial boilers the ratio between the mass of the boiler equipment to the transferred heat is around $4.3 \frac{to}{MW}$.

4.5.2 Heat exchanger

In this section a simple heat exchanger is described which is used for the dynamic process simulation. The heat exchanger model is based on a shell - tube configuration. In the tube the cold fluid (water) circulates, whereby in the shell the hot process medium flows counter-currently. Heat losses are neglected and the mass flow rates are assumed to be constant. The energy equation (see equation A.2) is the basis for the development of the model, meanwhile Figure 4.17 shows how the equation is derived for the tube section. It shows the bounding surface of the control volume of the tube with the heat transfer $Q(\tau)$ between shell and tube which is time-dependent.

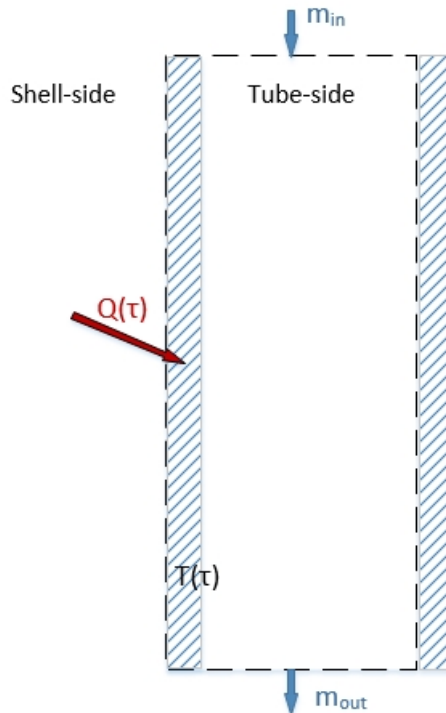


Figure 4.17: Schematic diagram of the tube-side control volume

The equation for the tube-side is following:

$$dU = \delta Q + \sum dm_i(h_i) \quad (4.45)$$

$$\rho_{tube} V_{tube} c_{p,tube} \frac{dT_{tube}}{dt_{tube}} = \rho_c \dot{V}_c c_{p,c} (T_{c,in} - T_{c,out}) + Q \quad (4.46)$$

The equation for the shell-side is shown in eq.4.47:

$$\rho_{shell} V_{shell} c_{p,shell} \frac{dT_{shell}}{dt_{shell}} = \rho_h \dot{V}_h c_{p,h} (T_{h,in} - T_{h,out}) - Q \quad (4.47)$$

Both equations are solved for given outlet temperatures at each side of the heater. The heat value Q is calculated with the aid of eq.4.26 and 4.28. How the necessary overall heat transfer coefficient k is obtained is shown in the following subsection.

4.5.3 Finding the heat transfer coefficient for the heat exchanger

When determining the operating performance of combined (or CCS) plants the data of the gas turbine usually is given and only the HRSG and steam turbine is individually designed. Since the HRSG investigations are an important part of this work, in this chapter the tools for the calculation are given.

The overall heat transfer coefficient k can be obtained by following equation: [69]

$$k = \frac{1}{\frac{1}{\alpha_h} + \frac{d_o}{2\lambda_{tube}} \cdot \ln\left(\frac{d_o}{d_i}\right) + \frac{d_o}{d_i \alpha_c}} \quad (4.48)$$

Correlations of the tube-side heat transfer coefficient used in this work are as follows:

$$Nu_{d_i} = \frac{\alpha_c d_i}{\lambda_c} \quad (4.49)$$

If $[Re = (c \cdot d_i / \nu) > 10^4]$ turbulent pipe flow:

$$Nu_{d_i,turb} = \frac{\left(\frac{\xi}{8}\right) Re_{d_i} Pr}{1 + 12.7 \sqrt{\frac{\xi}{8}} \left(Pr^{\frac{2}{3}} - 1\right)} f_1 f_2 \quad (4.50)$$

$$\xi = [1.8 \log(Re_{d_i}) - 1.5]^{-2} \quad (4.51)$$

$$f_1 = 1 + \left(\frac{d_i}{L}\right)^{\frac{2}{3}} \quad (4.52)$$

$$f_2 = \left(\frac{Pr}{Pr_w}\right)^{0.11} \dots liquid \quad (4.53)$$

$$f_2 = \left(\frac{T}{T_w}\right)^{0.45} \dots gas \quad (4.54)$$

If $[Re < 2300]$ laminar pipe flow:

$$Nu_{d_i, lam} = \sqrt[3]{3.66^3 + 0.664^3 Pr \left(Re_{d_i} \frac{d_i}{L} \right)^{\frac{3}{2}}} \quad (4.55)$$

where the index w indicates the tube wall, c is the velocity of the fluid, d is the diameter of the tube and L is the tube length. The value ν expresses the kinematic viscosity and μ the dynamic viscosity. All values in case of forced convection are calculated at mean fluid temperature.

For the shell-side of the heat exchanger, following is obtained through the application of the Kern's method: [70]

$$Re = \frac{c \cdot d_e}{\nu} \quad (4.56)$$

$$Nu_{d_e} = \frac{\alpha_h d_e}{\lambda_h} \quad (4.57)$$

$$d_e = \frac{1.27}{d_o} (p_t^2 - 0.785 d_o^2) \quad (4.58)$$

$$Nu_{d_e} = j_h Re Pr^{\frac{1}{3}} \left(\frac{\mu}{\mu_w} \right)^{0.14} \quad (4.59)$$

where d_e is the hydraulic mean diameter. According to a rule of thumb the tube pitch (p_t) is 1.25 times the outer tube diameter (d_o). j_h is the heat transfer correction factor and for this study a variation of the shell-side Reynolds numbers over the range of 15,000-50,000 is set, thus the values of j_h vary (and depreciate in values) from 0.005 to 0.0028 [70].

4.5.4 Shell and tube fluid velocities

High velocities of the fluids lead to high heat transfer coefficients but also high pressure drops. Low velocities cause lower friction losses, subsequently the pump duty decreases and the operating costs and first of all the invest costs for the pump are going down.

Nonetheless, the velocity must be high enough to prevent any deposit of solids, but not too high to cause erosion [70]. Typical design velocities are shown in Table 4.2: [70]

Table 4.2: Recommended velocities of the fluids

Condition	Tube [m/s]	Shell [m/s]
Liquid	1 to 2	0.3 to 1
Gas	20 to 40	10 to 15

Chapter 5

Process Simulation

This chapter gives a description of the methodology for the process simulation and an explanation of the associated simulation tool. The methodological approach ensures that the simulation can be reproduced and in detail understood. Furthermore, a summary of the assumptions made is given, which is essential for the parameter setting of the process simulation. Hereby, the research question about the decision of the Graz cycle configuration is answered. The limitations at the end of the chapter present the limits of following work allowing possible improvements in a future work.

As stated before, this chapter is introduced by the presentation of the simulation tool and a study of process simulations of power cycles. The first programs for calculating power cycles and for performing process simulations were developed in the 1960s. In the year 1973 was presented a procedure to calculate process cycles with the characteristic of splitting the complex cycle in single components and streams, which are numbered by indices. Hereby, the cycle is shown as a series of numbers and can be interpreted by the computer. Nowadays most of the commercial programs have the same approach for the simulation of power cycles. [71]

5.1 Simulation tool IPSEpro

The process simulation tool for the simulation of the “Graz cycle” is the software system IPSEpro. It is a powerful tool for modelling, analysing and simulation of thermodynamic processes. IPSEpro works with two principal modules, which is the process simulation environment (PSE) and the model development kit (MDK). By using a basis catalogue of components or by building them individually in the MDK package, the user is able to build up process schemes in PSE for simulation and analysis [71]. The software package gives the user the possibility to implement fluid properties and to subsequently simulate the real gas behaviour of the fluid used in the process simulation.

On the process level it is possible to arrange the components individually by building

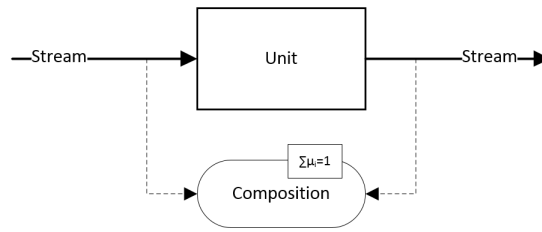


Figure 5.1: Principle sketch of a simple model in PSE [71]

up a process scheme in a form of a graph. It is possible to simulate parts of a power cycle or a whole complex system. All numerical data and the output of the simulation can be shown on the project window in the PSE module. Further, it is possible to look into the process data in detached tables or in the output protocol.

Figure 5.1 shows a principle outline of a simple model to demonstrate how the process simulation environment works. The simple model consists of a single component (unit) and two streams (inflow and outflow), which refer to the same global object (composition). This object is defined by mass fractions μ_i (see subsection A.4.2 for more detailed information about) of the different components of the stream. To avoid overdetermination of the process simulation all mass fractions despite one have to be defined, because $\sum \mu_i = 1$ is used.

In Figure 5.2 is shown a process scheme with the power cycle and the transferred process into IPSEpro, where the sketch of the modelling is displayed. Subsequently, the process is simulated and the results are shown in the project window together with a generated output log. The structure and the underlying equation of the models are the main tasks to fulfill in order to do the process simulation. [71]

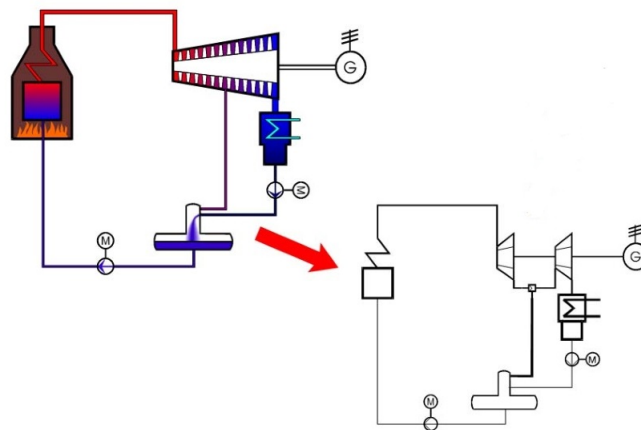


Figure 5.2: Modelling scheme of a power cycle [71]

The component level (MDK) allows to define the properties of the different components of the power cycle and to elaborate the thermodynamic cycle models. It is possible to change the models of a library individually for the process simulation. The model equa-

tions used in MDK are based on a relatively simple model language, called MDL (Model Description Language). MDL is not a sequential language, that means that the order of the equations is irrelevant because the solving procedure is implicit. A model compiler converts the equations into a binary system, ready for use in the process level. For the numerical solution of the system of equations the PSE package uses the Newton's method. [71]

5.2 Methods

This section presents the connection between the different cycle data and how the approach for the process simulation is in order to answer the research questions (see Figure 5.3).

For this work, first and foremost, a new Graz Cycle model library has been developed (with the aid of the already existing model database), which covers all the components of the power cycle. The old GC model library was not error free and has been flattened to the essential by making it more customer friendly and concrete. The thermodynamic cycle modelling and the equations used for the model library are presented in Chapter 4. On the basis of the modelling created in the software package MDK is assembled the cycle layout in PSE with the linking of the different models. Hence, the simulation process is performed and results of the design point (in this case full-load) are achieved by using the parameter settings and assumptions made in Section 5.3. The results are validated with the reference cycle, presented in ASME paper 2005 [45], in order to check the plausibility and get correct results.

Validated results are then used for parameter input for the part-load simulations based on the off-design models in MDK. The off-design equations of the cycle components are mostly functions related to the steady-state design-point results (see for this purpose Section 4.4). Once the part-load simulations of the Graz Cycle are performed eventual changes are conducted of the process cycle layout of the full-load simulation in order to achieve an optimal process scheme for part-load conditions. New results or adjustments achieved for the nominal operating conditions of the Graz cycle are subsequently used for the off-design simulation and the parameter for the off-design models are adjusted. The off-design simulation settings are linked to the respective control strategy applied. Since for the off-design operation of the Graz Cycle several process control methods are investigated; the best ones are selected and a load reduction from 100% down to at least 60% is performed in the part-load simulation. The control system design and the selection of controlled, manipulated and measured variables is carried out by following the method of Seborg [72] and Zotica [58].

Once the off-design simulation of the Graz Cycle is performed, the dynamic simulation of the critical cycle components, in this case the heat exchanger part (cf. case study in

subsection 4.5.1), is evaluated. Therefore the thermodynamic data previously obtained is used for the dimensioning of the components and is subsequently integrated in the process simulation as parameter input. The dynamic models in MDK, thus, will serve for the dynamic process simulation in the PSE environment. As a result, time-dependent thermodynamic states at the outlet of the component or component group, are obtained. These results are then ultimately validated with the part-load results in order to draw final conclusions. The dynamic model of the OTSG is a first approach by using an energy balance for a simple heat exchanger. This model can be further improved by sectionalizing the heat exchanger and by applying finite-difference approximations [72].

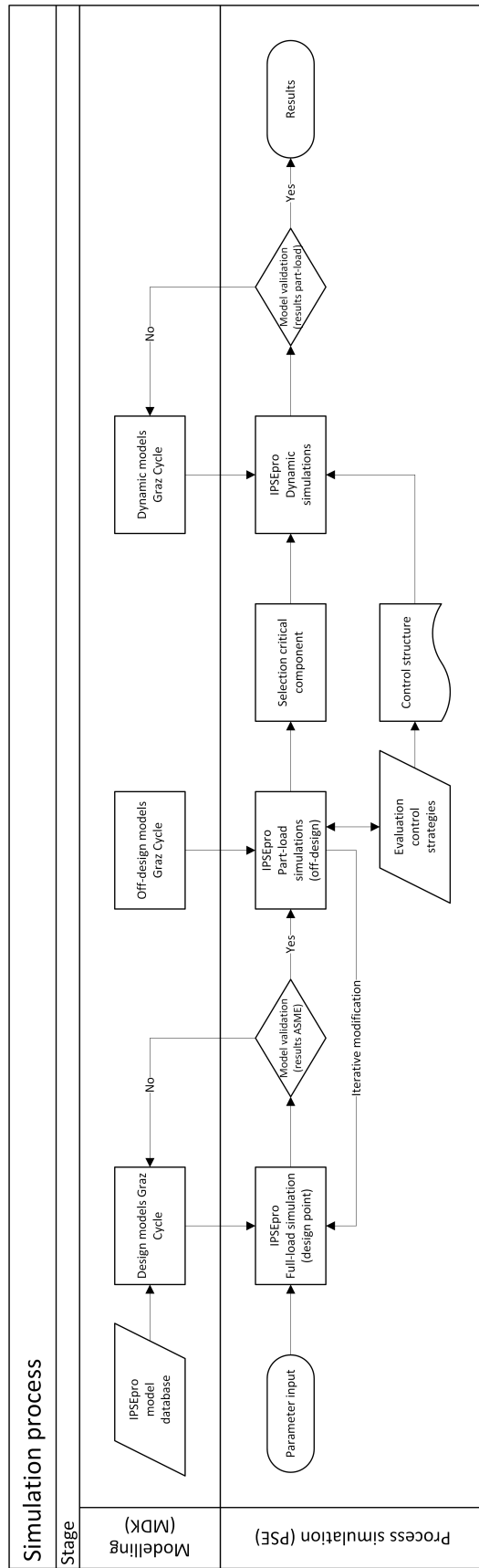


Figure 5.3: Simplified overview of the process simulation approach

5.3 Assumptions

For the application of the simulation implemented in this work, the cycle configuration of the Basic Graz cycle, presented by Sanz et al. [45] and explained in this thesis in Section 3.1, was chosen in discussions with TUG and NTNU supervisors. The power cycle is fired with natural gas and presents the most suitable option for a first demonstration plant, even if under certain conditions the syngas option (a gas mixture mainly of CO and H₂O) ensures higher thermodynamic efficiencies. The Modified Graz cycle, presented in Section 3.2, has a modified low pressure section in order to solve the problem of the very large condenser size of the Basic Graz cycle. The presence of CO₂ in the condenser leads to low heat transfer coefficients because of extra mass transfer resistance [35]. In addition the condensation takes place at vacuum pressures and therefore large heat exchange and cross-section areas are predictable. But the Modified Graz cycle is much more complex compared to the Basic Graz cycle and there is a need of a great amount of heat exchange equipment, which unveils the detailed flowsheet of the Modified Graz cycle presented at ASME Turbo Expo 2008 [73, 35]. According to the investigation about oxy-fuel cycles made by Ferrari [35], the Basic Graz cycle has an advantage in terms of efficiency compared to the Modified Graz cycle, see Table 5.1. Besides that, the evaporation at sub-atmospheric pressure taking place in the bottoming cycle of the Modified Graz cycle, leads to economically non-optimal designs of the heat exchanger since the presence of large volume flows of evaporated low pressure steam [35]. This considerations led to the decision in favour of the Basic Graz cycle, presented at ASME Turbo Expo 2005.

Table 5.1: Performance comparison between the two Graz cycles [35]

Performance	Case [35] Basic Graz	ASME 05 Basic Graz	Case [35] Modified Graz	ASME 08 Modified Graz
Gross electr. efficiency	65.4%	66.5%	64.0%	67.6%
Cycle net electr. efficiency	64.0%	64.6%	62.6%	65.7%
Plant net electr. efficiency	51.4%	52.6%	50.9%	54.1%

In the course of the evaluation of this work the paper ASME 05 [45] is taken as a baseline and the validation and verification is carried out by means of that. The methodology is thereby described for the design point simulation and assumptions are adopted from this paper. Assumptions which differ from this are indicated and named. The above listed further simulations are indirectly linked with the full-load simulation and are verified as shown in the procedure in Figure 5.3.

5.3.1 General assumptions

The GC component efficiencies used in this work are the same as in the Paper ASME 2005 [45] and are shown in Table 5.2. The simulation is proceeded under the premises stated below, whereby the exceptions, where values differ from the reference paper, are written in the column nearby. Generally these assumptions are valid for the design point operating environment, which means full-load performance. How and at which extent the assumptions and conditions are changing at part-load operation, is described in the following subsection and in the next chapter at the off-design results.

Table 5.2: Component assumptions and efficiencies used in the thermodynamic simulation [45]

Variable	ASME 05	Thesis
Fuel	Natural gas	no change
Combustion pressure	40 bar, 4% pressure loss	n.c.
Combustion heat loss ζ_c	0.25%	n.c.
Combustion temperature	1400 °C	n.c.
Oxygen excess	3%	n.c.
Turbine efficiency η_{is} HTT	90.3%	n.c.
Turbine efficiency η_{is} HPT	90%	n.c.
Turbine efficiency η_{is} LPT	88%	n.c.
Turbine efficiency η_{is} IPST	92%	n.c.
Compressor efficiency η_{is} C1+C2	88%	n.c.
Compressor efficiency η_{is} C3+C4	78%	n.c.
Pump efficiency	70%	n.c.
Pump mechanical efficiency η_m	98%	n.c.
Heat exchanger pressure loss	3%	n.c.
HRSG pressure loss: cold side	3% per heat exchanger	n.c.
HPT pipe pressure loss	5 bar	n.c.
HRSG pressure loss: hot side	4 kPa	n.c.
HRSG minimum temperature difference ECO	5 K	n.c.
HRSG minimum temperature difference SH	25 K	15 K
Condenser exit temperature	18 °C	n.c.
Condenser pressure	0.041 bar	n.c.
Cooling water inlet temperature	5 °C	10 °C
Fuel temperature after preheat	150 °C	n.c.
Oxygen temperature at combustor inlet	150 °C	n.c.
Mechanical efficiency η_m	99.6% of net power	n.c.
Generator efficiency η_{gen}	98.5%	n.c.
Transformer efficiency η_{tr}	99.65%	n.c.
Auxiliary losses P_{aux}	0.35% of heat input	n.c.
Oxygen production	0.25 kWh/kg = 900 kJ/kg	757 kJ/kg
Oxygen compression	2.38 - 42 bar: 325 kJ/kg	n.c.
CO ₂ compression	1 - 100 bar: 350 kJ/kg	300 kJ/kg

For the condenser a direct water cooling is chosen, which normally is the first choice

for cooling systems of power assets because it allows low condenser pressures and it is the most economical option. In this case the power plant has to be located nearby an ocean, a river or a cooling pond. The water cooling temperature is assumed to be 10 °C (i.e. North Europe). [13]

The new value for the oxygen production is calculated by the graph of Figure 2.7 and following the indications given in Table 5.4. The oxygen carrier of this study consists of 95% oxygen whereby the energy consumption accounts for 84% of the 900 kJ/kg of the reference paper (in that case 100% oxygen is assumed). For this study the CO₂ compression-value of 300 kJ/kg is set as a new premise since it is closer to the state of the art.

The fuel used for the combustor is natural gas and the composition in mass fractions is shown in Table 5.3.

Table 5.3: Composition of the NG [45]

Fuel composition	Value
Methan CH_4	89%
Ethan C_2H_6	8.11%
Carbon dioxide CO_2	2%
Nitrogen N_2	0.89%
Lower heating value LHV	46465 kJ/kg

The oxidant fed to the combustor consists of 95% oxygen in this study instead of the 100% purity in the reference paper. This change in value is due to techno-economical reasons explained in Subsection 2.2.1. The Table 5.4 shows the difference between both works.

Table 5.4: Composition of the oxygen carrier

Composition	Assumption ASME 05	Assumption Thesis
Oxygen	100 %	95 %
Nitrogen	0 %	1.66 %
Argon	0 %	3.33 %

5.3.2 Turbomachinery

Here the assumptions made for the turbomachinery components are presented, to wit compressors and turbines.

For the model of the cooled gas turbine the same assumptions as in the reference paper are made, which are shown in Table 5.5. The description of the variables are shown in Subsection 4.3.2, cf. Table 4.1. The HTT consists of three parts, whereby only the first two are cooled by a water stream.

Table 5.5: Parameter of the cooled gas turbine

Variable	Value
β_2	20°
k_{stat}	0.5
$\Delta T_{cooling}$	150 °C
f_A	4
n_{st}	1 (1 st part HTT), 2 (2 nd part HTT)
St	0.004
T_{metal}	750 °C

As stated in Subsection 4.4.2, the isentropic efficiency at part-load operation can be assumed constant. This is not the case for the compressors. For this purpose a simple approach is chosen, which describes the isentropic efficiency in relation to the feed mass ratio, see Figure 5.4. Referring to Sanz et al. [9] the linear spline represents the relation of isentropic efficiency to feed mass ratio; in this work a cubic spline is selected for the GC compressor model.

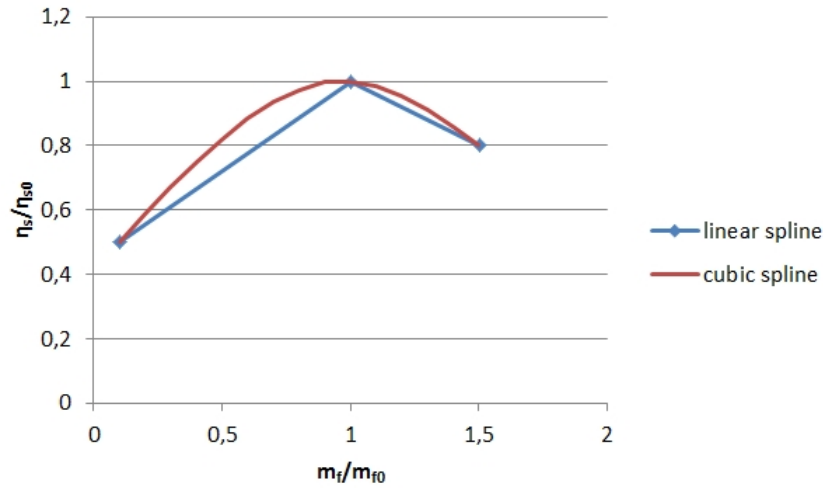


Figure 5.4: Isentropic efficiency relation of the compressor in part-load operation

5.3.3 Dynamic simulation

In this subsection some basic assumptions regarding the heat exchanger hardware for the dynamic simulation is presented. Thermodynamic properties like the specific heat capacity for the calculation of the dynamic equations are determined with the physical property tool miniREFPROP by NIST, the properties of steels are obtained from Richter [74].

The dimensions of the OTSG utilized for the dynamic modeling are shown in Table 5.6. This investigation is limited on the first element of the OTSG, which is the Economizer 1. Following units, e.g. ECO2, EVAP etc. can be calculated by means of the approach and results investigated in following work. For more specific information about the structure

Table 5.6: Specific data of the OTSG established through literature study [70]

Parameter	ECO1
Alloy steel (shell and tubes) [-]	13CrMo44
Heat conductivity of alloy steel λ [W/mK]	45
Tube arrangement [-]	Staggered
Tube inner diameter [mm]	32.8
Tube outer diameter [mm]	38
Tube pitch [mm]	$1.25 \cdot 38 = 47.5$
Tube wall thickness [mm]	2.6
Velocity tube inside [m/s]	1
Shell thickness [mm]	9.5
Velocity shell (tube outside) [m/s]	10

and dimensions of ECO1, like for example the number of tubes used in the heat exchanger, see Subsection 6.4.1.

5.4 Limitations

The following listing shows the limitations of this thesis:

- For the dynamic simulation the most critical part is chosen, that means components in which the most heat can be stored and therefore react slower to load changes. This is upmost the case in the HRSG.
- For the HRSG a once-through system is chosen. Thereby drums, circulating pumps, additional tubes and control systems are avoided.
- The natural gas and the oxygen streams enter the combustion chamber through two separate valves. For the simulation the assumption of a perfect lambda-controller is made, which controls the inflow of O_2 , such in a way that a constant excess air ratio ($\lambda-1$) is made.
- The simulation of start-up and shut-down are excluded a priori.

Chapter 6

Results and Discussion

This chapter contains the results of this thesis and their evaluation. The simulations follow the assumptions made in the previous chapter and go through the design model simulation, off-design model simulation to the final dynamic simulation, leading to an iterative adjustment between parts of it. The section containing the control strategies is from fundamental significance for the subsequent part-load simulations.

6.1 Full-load performance

The full-load performance of the Graz cycle represents the steady-state design point operating condition. The plant-operating concept is therefore built under the condition that the cycle configuration should have the best efficiencies at base load.

In Figure 6.1 the cycle configuration and the thermodynamic data of the Graz cycle are shown, which are found as the optimum design in this work. For a better understanding the different cycle mediums are coloured differently and streams are indicated by numbers. Henceforth, the process description will refer to those stream numbers. The stream table (cf. Table 6.1) shows all the process parameters like temperature, pressure, mass flow and the chemical composition of the single streams of the Graz cycle. The cycle process is described in detail in subsection 3.1.1; here the differences to the reference cycle are discussed.

The fluid leaves the combustion chamber (which is operated at 40 bar) with a mixture of 72.5% steam, 25% CO₂, 0.7% N₂, 0.5% O₂ and 1.3% Ar. At a temperature level of 1400 °C the working medium enters the HTT, which is cooled by the streams 38 and 40, coming from the HPT. The stream 38 cools the first part of the HTT (HTT1), and stream 40 cools the second part (HTT2). The ratio of cooling steam mass flow to HTT feed mass flow is 13.36%. This value is somewhat lower than the one of the reference cycle and arises from the different cycle composition and the less specific mass flow ratio (ratio of mass flow to heat input) at the inlet of the HTT. The reason is that in the process simulation of the

Table 6.1: Stream table for the Graz Cycle in nominal-load conditions

No.	T (°C)	p (bar)	\dot{m} (kg/s)	H_2O (-)	CO_2 (-)	O_2 (-)	Ar (-)	CH_4 (-)
1	150.0	41.7	2.45	-	0.02	-	-	0.89
2	150.0	41.7	10.07	-	-	0.95	0.03	-
3	1400.0	40.0	57.05	0.72	0.25	0.00	0.01	-
4	1087.8	15.0	62.13	0.74	0.23	0.00	0.01	-
5	742.4	3.0	64.68	0.75	0.22	0.00	0.01	-
6	568.8	1.05	64.68	0.75	0.22	0.00	0.01	-
7	202.9	1.01	64.68	0.75	0.22	0.00	0.01	-
8	102.4	1.01	34.69	0.75	0.22	0.00	0.01	-
9	446.0	13.7	34.69	0.75	0.22	0.00	0.01	-
10	391.3	13.3	34.69	0.75	0.22	0.00	0.01	-
11	598.1	41.7	34.69	0.75	0.22	0.00	0.01	-
12	202.9	1.01	27.59	0.75	0.22	0.00	0.01	-
13	27.2	0.04	27.59	0.75	0.22	0.00	0.01	-
14	18.0	0.04	9.49	0.30	0.64	0.01	0.03	-
15	206.5	0.25	9.49	0.30	0.64	0.01	0.03	-
16	25.0	0.24	7.10	0.06	0.86	0.02	0.04	-
17	165.2	1.0	7.10	0.06	0.86	0.02	0.04	-
18	43.8	1.0	0.61	0.04	0.87	0.02	0.04	-
19	156.2	1.0	7.71	0.06	0.86	0.02	0.04	-
19*	20*	1.0*	7.34*	0.03*	0.90*	0.02*	0.05*	-
20	202.9	1.01	2.40	0.75	0.22	0.00	0.1	-
21	18.0	0.041	18.10	1	-	-	-	-
22	25.0	0.242	2.39	1	-	-	-	-
23	18.8	0.041	20.48	1	-	-	-	-
24	18.8	1.0	20.48	1	-	-	-	-
25	18.8	1.0	4.80	1	-	-	-	-
26	18.8	1.0	15.68	1	-	-	-	-
27	94.0	1.0	15.68	1	-	-	-	-
28	43.8	1.0	1.79	1	-	-	-	-
29	88.9	1.0	17.48	1	-	-	-	-
30	92.4	213.0	17.48	1	-	-	-	-
31	174.3	209.8	17.48	1	-	-	-	-
32	368.5	206.6	17.48	1	-	-	-	-
33	366.3	201.3	17.48	1	-	-	-	-
34	372.6	195.3	17.48	1	-	-	-	-
35	549.0	179.7	17.48	1	-	-	-	-
36	330.1	41.7	17.48	1	-	-	-	-
37	330.1	41.7	2.54	1	-	-	-	-
38	210.6	15.0	2.54	1	-	-	-	-
39	330.1	41.7	14.93	1	-	-	-	-
40	330.1	41.7	5.08	1	-	-	-	-
41	330.1	41.7	9.85	1	-	-	-	-

cycle proposed by Sanz et al. [45] a slightly different fuel composition (as stated by the data) feeds the combustor and therefore the oxygen demand differs in comparison to the actual study. For the fuel composition of the actual study, see Table 5.3.

However, as a consequence the TET, which is at a level of 569 °C, is lower compared to the original cycle. This relation and all the key parameters of the two cycle configurations are compared in Table 6.2, where the column with the name “ASME 05” represents the data by Sanz et al. [45], whereas the column “thesis” represents the actual work. According to the Carnot cycle process a lower exhaust gas temperature automatically means a gain in efficiency. This context is shown in Table 6.3, where the specific HTT power, that means the ratio of turbine power to total heat input, is somewhat bigger in the actual study than in the reference cycle.

According to Table 6.3 the reference cycle has a net power output of 75.5 MW compared to the 60.5 MW of the actual study. The difference of the power output values is the reason why a presentation of the specific values is chosen in Table 6.3. Both power cycle dimensions are adequate for a first demonstration plant. The ASME 05 cycle has a total heat input of 143.4 MW, meanwhile the cycle of this study has a heat input of 113.7 MW. Due to the difference of power output a great difference in the mass flow ratios between the two cycles is resulting, see Table 6.2.

After passing the HRSG 42.6% of the fluid is further expanded to vacuum conditions in the LPT. The LPT inlet temperature is shown in Table 6.2 as one of the parameters which differs from the Sanz et al. [45] cycle configuration. This change in value is due to the prior discrepancy of the HTT exhaust gas temperature and continues till the LPT.

For each temperature of the working fluid (mainly condensable steam and non-condensable carbon dioxide) condensation starts at the corresponding partial pressure $p'_s(t)$ of the water vapour [54]. For a given condenser exit temperature the amount of condensed steam is affected by the pressure of the condenser, whereby the optimum GC condenser pressure was reported by Sanz et al. [45] to be 0.041 bar. The condenser temperature is set to 18 °C at which temperature, like in the reference paper, the best efficiency is achieved. Under design conditions 86% of the water content is condensed.

In the evolution of the simulation for this thesis a cycle modification in comparison to the reference cycle is carried out. It became apparent that for the part-load operation it is favourable and necessary to direct the water condensate stream of the condenser after the compressor C3 (cf. stream 22 in Figure 6.2) to the water stream 21 of the LPT condenser. In the original cycle a water sink was arranged. Without this modification at lower cycle load the sink 25 gave negative mass flows. The new cycle arrangement is shown in detail in Figure 6.2, where the mentioned stream 22 is indicated. Besides that, the option of an additional condenser before the CPU is considered, see Figure 6.2. The values including this optional condenser are marked with an asterisk (*). This cycle modification improves

Table 6.2: Key parameters of the Graz cycle power plant at design point conditions

Variable	Symbol	Typical value	
		ASME 05	Thesis
HTT inlet temperature	TIT	1400 °C	1400 °C
HTT exhaust gas temperature	TET	579 °C	569 °C
HTT inlet pressure	$p_{\text{HTT,in}}$	40 bar	40 bar
HTT outlet pressure or HRSG pressure hot-side	$p_{\text{HTT,out}}$ $p_{\text{HRSG,hot}}$	1.053 bar	1.053 bar
HPT inlet temperature	$T_{\text{HPT,in}}$	549 °C	549 °C
HPT inlet pressure	$p_{\text{HPT,in}}$	180 bar	180 bar
LPT inlet temperature	$T_{\text{LPT,in}}$	216 °C	203 °C
LPT inlet pressure	$p_{\text{LPT,in}}$	1.013 bar	1.013 bar
LPT outlet pressure or condenser pressure	$p_{\text{LPT,out}}$ $p_{\text{Condenser}}$	0.0413 bar	0.0413 bar
Natural gas mass flow	\dot{m}_{NG}	2.9 kg/s	2.45 kg/s
O ₂ mass flow	\dot{m}_{O_2}	11.5 kg/s	10.1 kg/s
CO ₂ mass flow to storage	\dot{m}_{CO_2}	8.9 kg/s	7.7 (7.3*) kg/s
C1/C2 mass flow	$\dot{m}_{\text{C1/C2}}$	45.3 kg/s	34.7 kg/s
C1/C2 pressure ratio	$\pi_{\text{C1/C2}}$	41.2	41.2
C1 inlet temperature	$T_{\text{C1,in}}$	97 °C	102 °C

the CO₂-purity at the CPU inlet (cf. stream 19* in Table 6.1), furthermore enhances the power output of the cycle (cf. Table 6.3) and as a result the cycle efficiency shown in Table 6.4. The reason is that with the added condenser more water is extracted from stream 19 and therefore the mass flow to the CO₂ compression unit is reduced and subsequently the power effort for the carbon dioxide compression from 1 to 100 bar diminishes.

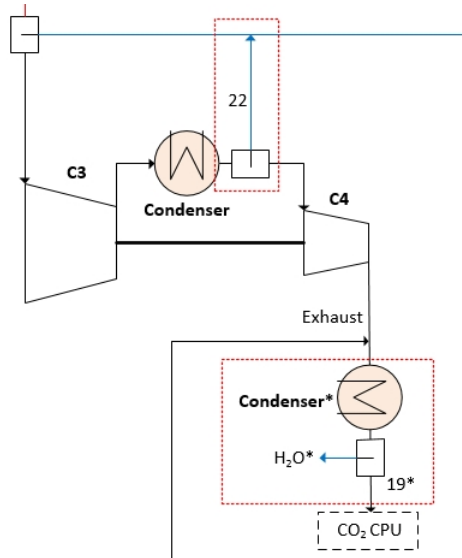


Figure 6.2: GC modifications for this study with the additional condenser marked with an asterisk (*)

In Table 6.3 the GC data of the power balance for the design point (full-load simulation) is given and compared between the two cycles. As already mentioned, the Graz cycle plant elaborated in this thesis has a lower net power output and net shaft power. Furthermore the Table 6.3 shows how great the HTT power fraction is, it accounts for 84% of the total turbine power. The specific values of the two cycles are used for a model validation and verification. Therefore the reference cycle can be compared to the actual cycle in Table 6.4 in terms of efficiencies.

Table 6.3: Graz cycle power balance at design point conditions

Variable	ASME 05	<i>spec.</i>	Thesis	<i>spec.</i>
HTT power [MW]	119.4	<i>0.83</i>	95.5	<i>0.84</i>
HPT power [MW]	8.4	<i>0.06</i>	6.6	<i>0.06</i>
LPT/LPST power [MW]	14.6	<i>0.10</i>	11.3	<i>0.10</i>
Total turbine power P_T [MW]	142.4	<i>0.99</i>	113.4	<i>1.00</i>
C1 power [MW]	26.0	<i>0.18</i>	20.7	<i>0.18</i>
C2 power [MW]	17.1	<i>0.12</i>	13.2	<i>0.12</i>
C3 power [MW]	2.2	<i>0.015</i>	2.2	<i>0.02</i>
C4 power [MW]	0.9	<i>0.01</i>	0.9	<i>0.01</i>
Pump power [MW]	0.9	<i>0.01</i>	0.6	<i>0.005</i>
Total compression power P_C+P_P [MW]	47.1	<i>0.33</i>	37.6	<i>0.33</i>
Net shaft power without losses [MW]	95.3	<i>0.66</i>	76.3	<i>0.67</i>
Electrical power output incl. losses [MW]	92.7	<i>0.65</i>	73.6	<i>0.65</i>
O ₂ generation and compression P_{O_2} [MW]	14.1	<i>0.10</i>	10.9	<i>0.10</i>
CO ₂ compression to 100 bar P_{CO_2} [MW]	3.1	<i>0.02</i>	2.3 (2.2*)	<i>0.02</i>
Net power output [MW]	75.5	<i>0.526</i>	60.4 (60.5*)	<i>0.532</i>
Total heat input Q_{in} [MW]	143.4	-	113.7	-

The efficiencies are defined in the equations in subsection 4.1.4. Albeit the mechanical losses between the two versions are kept the same, the difference in the thermal cycle efficiency and the net electrical cycle efficiency is 0.1%-point (compare Table 6.4). So that the thermal cycle efficiency of the cycle elaborated by Sanz et al. is 66.5% compared to 66.4% of the actual work. This is due to the different fuel composition input discussed earlier on.

If considering the energy expenditure for oxygen production and compression to combustion pressure level of 41.7 bar an efficiency of 55.0% compared to 54.8% is achieved. This is a relative difference of 0.36%. The reason of this gain in efficiency is, because the production of the new cycle oxidant (the oxygen of the actual work has a 95%-purity) is much less energy expensive. The detailed values of oxygen production and compression, respectively, the CO₂-compression at the end of the carbon capture chain is presented and compared in the general assumptions (see Subsection 5.3.1). If considering the effort of CO₂-compression for liquefaction to a pressure level of 100 bar, the net cycle efficiency is reduced to 52.9% and would be 53.0% if the cycle modification proposal of the additional

condenser ahead of the CPU is taken into account. As already mentioned earlier, this modification suggestion is indicated by an asterisk enclosed the value. The corresponding value of the cycle proposal of Sanz et al. [45] is 52.6%. This is 0.75% below the net efficiency of the thesis. The higher difference in net efficiency of the two cycles in comparison to the value without CO₂-compression is due to a lower assumption made for the CO₂-compression, cf. Table 5.2.

Table 6.4: Comparison of cycle efficiencies between ASME 05 and actual work

Variable	ASME 05 [%]	Thesis [%]	Rel. diff. [%]
Thermal cycle efficiency η_{th} (eq. 4.11)	66.5	66.4	-0.15
Net electrical cycle efficiency (eq. 4.12)	64.6	64.5	-0.15
Efficiency considering O ₂ -supply (eq. 4.13)	54.8	55.0	0.36
Net efficiency η_{net} (eq. 4.14)	52.6	52.9 (53.0*)	0.57 (0.75*)

Figure 6.3 shows the energy exchange between the water stream and the flue gas stream, which takes place in the HRSG. An idealized heat exchanger has a constant temperature profile along the energy transfer rate, which means that the product of mass flow ratio and specific heat capacity, or the energy transferred per unit temperature, must be the same in both streams for any given point in order to keep energy and exergy losses low [18]. If this temperature difference (pinch-point) between the water/steam and the flue gas stream tends towards zero, the surface of the heat exchanger tends towards infinity. Therefore the trade-off consists in creating a heat exchanger with optimal heat exchange (the lower the pinch-point the more steam is generated) and ensuring cost-effectiveness. Pinch-points for combined cycles are typically between 8 and 15 K [18]. This limits are met for the heat exchange in the superheater and ECO1 (cf. Figure 6.3). The temperature difference for the ECO2 water stream outlet amounts to 5 K at design point conditions. In this case the pinch-point is small and causes large heating surfaces and costs.

However, the component which sets the economic parameter of the plant is the low pressure condenser (where large dimensions are foreseen). No insuperable technological barrier is predicted for the heat exchanger hardware [35].

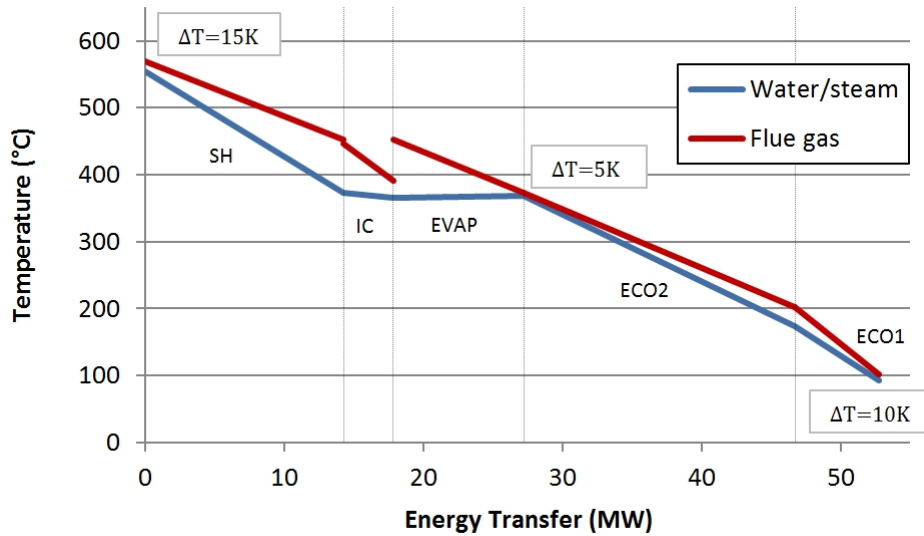


Figure 6.3: TQ-diagram for the HRSG operating at full-load

6.2 Control Strategy

The overall control objective is the operation of the Graz cycle as efficiently as possible at varying conditions, i.e. loads. For this thesis a plant load control system is developed to meet the requirements of the electrical grid.

In Figure 6.4 the diagram of the principle GC plant load control structure is illustrated. Depending on the data input of the electrical grid an operating point P_s (i.e. power set point) is given, which sets the value of the overall load control system KAR. The load controller KAR distributes the information first of all to the combustion controller CC and to the water valve controller WVC. The control unit CC is from fundamental importance because it regulates the fuel input valve (in Figure 6.4 it is signalised as V1) which directly determines the overall plant load. Indeed, for the part-load simulation the fuel input is used for the load regulation. The KAR receives a load/frequency-signal from the frequency transmitter LFT and checks how the measured values fit to the desired values. Accordingly eventual corrections are sent to the subjacent controllers. The fuel input subsequently determines the oxygen demand of the combustor (it is set by the air-to-fuel ratio λ_s), which is controlled by the well-tuned air-to-fuel ratio controller FFC, which regulates the oxygen valve V2 (cf. Figure 6.4), such that a constant O_2 excess ratio is maintained.

The fuel and O_2 streams enter separately in the combustor. It is assumed that both of these are controlled with flow controllers and the FFC regulates the oxygen inlet valve [70][75].

Another important aspect of the control structure is the turbine inlet temperature TIT. Since it is not possible to directly measure this temperature, values of the turbine pressure

ratio and the turbine outlet temperature TAT (measured by the transmitter TT) are used to calculate the TIT, which has a limit T_1 due to the strength of materials of the HTT-turbine. The TIT regulates the natural gas and oxygen valve through the combustion controller. The water valve controller regulates the excess water valve V4 by input of the overall load value and the measured flow rate at the water stream 23. The valve V3 regulates the mass flow rate of the lower temperature Rankine cycle and is controlled by the CC, which knows the respective load of the cycle and the related mass flow rate.

As already mentioned, the Figure 6.4 shows the main plant load control loop. The investigation about the control and automation of the Graz cycle led to three different strategies, presented in Table 6.6. The three strategies bring forth different results and efficiencies at the part-load simulation and are analysed in the next section. They differ from each other in the so-called secondary control loops, which maintain the important process parameters and assure the safety of the plant at all operating conditions. The closed-loop control structures of the operation modes are illustrated in Figure 6.5, 6.6 and 6.7.

Instead of the usage of VGV for the compressors C1/C2, a speed control system of compressor shafts is used in order to regulate their mass flow. As already mentioned in Chapter 5, for the VGV implementation in the model a parametrization of the compressor map along the VGV position would be necessary [76]. The disuse of VGVs is valid for all three control strategies listed in Table 6.6.

In this paragraph the controlled variables and manipulated variables of the Graz cycle process shall be briefly explained, before the different control strategies are discussed. This is proceeded by taking the control strategy S1 as an example, see Table 6.5.

By adding a part-load model to the steady-state model in the process simulation a control degree of freedom (DOF) is lost. The DOFs are the set points (i.e. manipulated variables) in the process simulation and have to be identified. All the active constraints in the simulation have to be controlled [58]. Table 6.5 defines the position (related to Figure 6.5), the manipulated variables and the controlled variables of the Graz power cycle. In this way pairings for the active constraints are resulting, so that for example the control of the condenser¹ pressure is done by activating the valve V7, which regulates the cooling water. The cooling water keeps the condenser pressure constant. The control of the condenser could also be designed that way, that the cooling mass flow is kept constant (which is common), which is applied with the second condenser following compressor C3. Here the pairing is: control of cooling mass flow with MV14. In this case the constant cooling mass flow leads to a decrease in condenser pressure due to a decrease in ΔT for the cooling flow at part load.

¹The condenser after the LPT is the only model of the part-load simulation which is kept for simplification in steady-state design. It is operated by keeping the condenser pressure constant. The product heat transfer coefficient times area ($k \cdot A$) is not set as an active constraint.

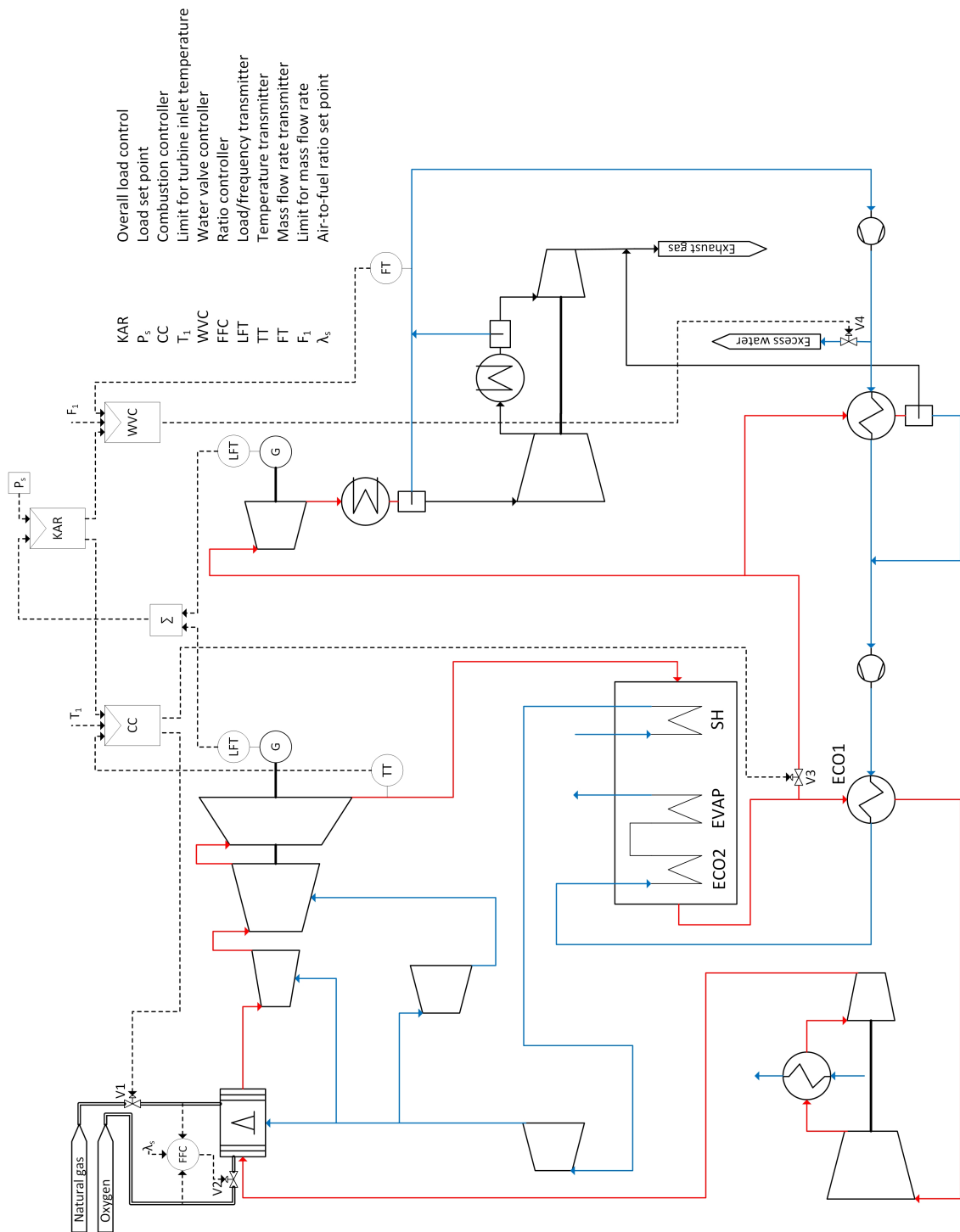


Figure 6.4: Structure of the load control system of the Graz power cycle

Due to the fact that start-ups and shutdowns are not considered in this work, the bypasses (like for example V8 for the LPT bypass) are closed and the mass flows are equal zero. The two orifices, as well as the two pumps are also part of the manipulated variables, since they are degrees of freedom. The orifices (cf. control strategy S1 in Figure 6.5) fix the split ratios between the main stream and the turbine cooling water stream.

Three different control strategies are compared. First of all the control strategy S1 shall be described.

As it is shown in Table 6.6, the key controlled variables are the power output, the HTT downstream pressure (equal to 1.053 bar) and the condenser pressure (equal to 0.041 bar). If a conventional HRSG is used for the Graz power cycle the $p_{\text{HTT,out}}$ is normally kept constant at atmospheric pressure range, due to wall thickness in the OTSG. However, it is not given beforehand that the steadiness of the pressure in the HRSG is beneficial in terms of efficiencies for this process. As it is shown in Table 6.6, the p_{HRSG} is one of the issues, which are investigated priorily in the next section.

The set point for \dot{W} must be set such that the power cycle output becomes as desired by using the fuel (heat) input to regulate the power, like also shown in Table 6.5. The remaining DOF should be used to keep the efficiencies as high as possible while respecting important process constraints [76]. The control strategy S1 uses two orifices to control the split ratios to HTT1 and HTT2, like illustrated in Figure 6.5. For the LPT and HPT throttle control is used. As illustrated in the priorily mentioned Figure, the live steam pressure for LPT and HPT is controlled with V6, respectively, V10. Both turbines are using one of the standard industrial control structures, in this case the turbine driven operation [58]. This operation strategy has the advantage that the response time to load changes is fast. However, it has to deal with valve throttling losses at the turbine inlet [58].

The LPST is operated in floating pressure operation (cf. in Figure 6.5). It means that the valve V12 is kept fully open in order to minimize throttling losses and therefore the live steam pressure is left uncontrolled. The Pump1 and Pump2 keep the pressure constant at a pressure level of 1 bar, respectively, 213 bar, like indicated by the set points P_s as input of the pressure controller in Figure 6.5. The valve V5 controls the here so-called pegging exhaust gas line (which in a combined cycle is named pegging steam line). It measures the temperature of the deaerator downstream water line. According to this temperature it sets the valve V5 position.

Table 6.5: Example of manipulated and controlled variables for the particular control strategy S1

Pos.	Manipulated variable	Controlled variable
V1	MV1: Fuel input	CV1: Power
V2	MV2: Oxygen input	CV2: (Constant) Air-to-fuel ratio
V3	MV3: LPT/condenser line	CV3: Exhaust gas recycle ratio
V4	MV4: Excess water valve	CV4: Water flow ratio
V5	MV5: Pegging exhaust gas line	CV5: Feedwater temperature
V6	MV6: LPT valve	CV6: Turbine inlet pressure
V7	MV7: Cooling water	CV7: (Constant) Condenser pressure
V8	MV8: LPT bypass	CV8: Turbine mass flow
V9	MV9: ECO1 bypass	CV9: Recycled exhaust gas temperature
V10	MV10: HPT valve	CV10: Live steam pressure
V11	MV11: HPT bypass	CV11: Turbine mass flow
V12	MV12: LPST valve	CV12: Live steam pressure
V13	MV13: LPST bypass	CV13: Turbine mass flow
V14	MV14: Cooling water	CV14: (Constant) Cooling mass flow
Orifice1	MV15: Orifice plate	CV15: (Constant) HTT1 steam mass ratio
Orifice2	MV16: Orifice plate	CV16: (Constant) HTT2 steam mass ratio
Pump1	MV17: Feedwater pump	CV17: (Constant) Feedwater pressure
Pump2	MV18: Feedwater pump	CV18: (Constant) Feedwater pressure

The control strategy S2 (cf. Figure 6.6) uses a throttle control instead of Orifice1. The released degree of freedom is used to set the TIT constant. The control strategy of maintain the turbine inlet temperature high as the mass flow is reduced, is commonly used in combined cycles. According to the Carnot cycle this strategy is paid off in terms of efficiency. The LPT uses throttle control by putting up throttling losses, as already strategy S1 did. Basically the method of cooling the section HTT1 is changed. In this case the operation mode of MV15 is replaced by a valve, which is turbine driven by setting the inlet cooling ratio by means of the turbine power output of HTT1.

Table 6.6: Control strategies of the Graz cycle

Str.	Key controlled variables	VGV	Orifice1	$p_{\text{HRSG}}=\text{const.}$	$p_{\text{HTT,out}}$	TIT
S1	$\dot{W}, p_{\text{HTT,out}}, p_{\text{Condenser}}$	no	yes	yes	1.053 bar	$t(\dot{W})$
S2	$\dot{W}, p_{\text{HTT,out}}, p_{\text{Condenser}}, \text{TIT}$	no	no	yes	1.053 bar	1400 °C
S3	$\dot{W}, p_{\text{Condenser}}, \text{TIT}$	no	no	no	$p(\dot{W})$	1400 °C

In operation mode S3 the pressure in the HRSG is allowed to vary, which can be critical in low pressure, but is constrained between 0.5 and 1.053 bar. As it is shown in Table 6.6 the downstream pressure of the HTT is depending on the power cycle output ($p(\dot{W})$). The LPT uses floating pressure operation and follows the gas turbine outlet pressure by generating power with whatever steam conditions are available from the OTSG, see Figure 6.7. If greater overall plant efficiencies are obtained by the variability of the

HRS_G pressure is investigated in Section 6.3. After a gas turbine load change the LPT load follows automatically with a few minutes delay depending on the response time of the heat recovery steam generator (for further information about the time-scale of response of heat exchangers, see Section 6.4) [18]. This is the disadvantage of floating pressure operation, that the response for load changes is slow [58]. However, this kind of automation technique is very common in industrial combined cycle plants. Like indicated in Table 6.6, the strategy S3 has no Orifice1, instead it is using a throttle operation mode for the HTT1 cooling stream, as described already for strategy S2.

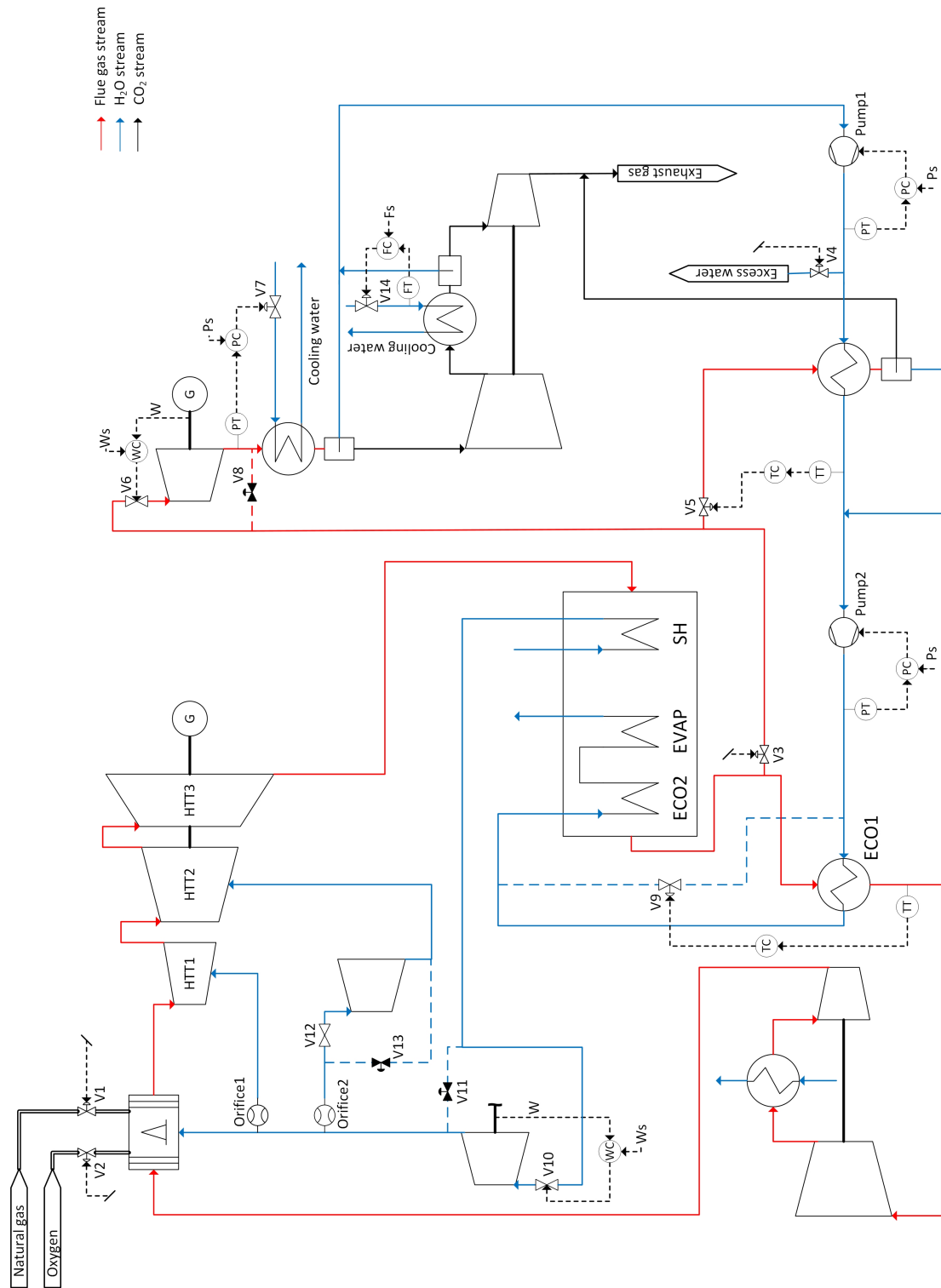


Figure 6.5: Closed control loops for the operation mode S1 of the Graz power cycle

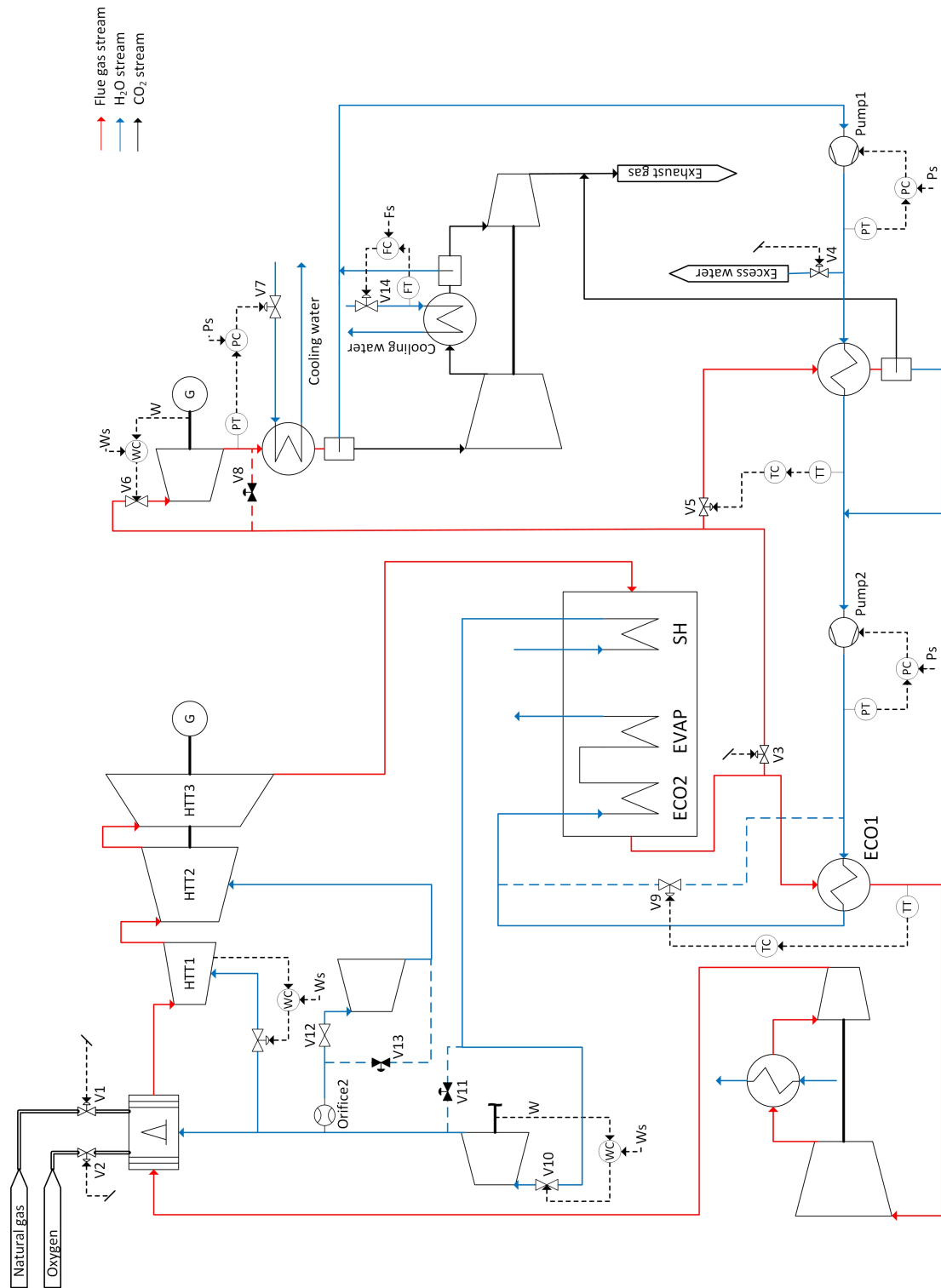


Figure 6.6: Closed control loops for the operation mode S2 of the Graz power cycle

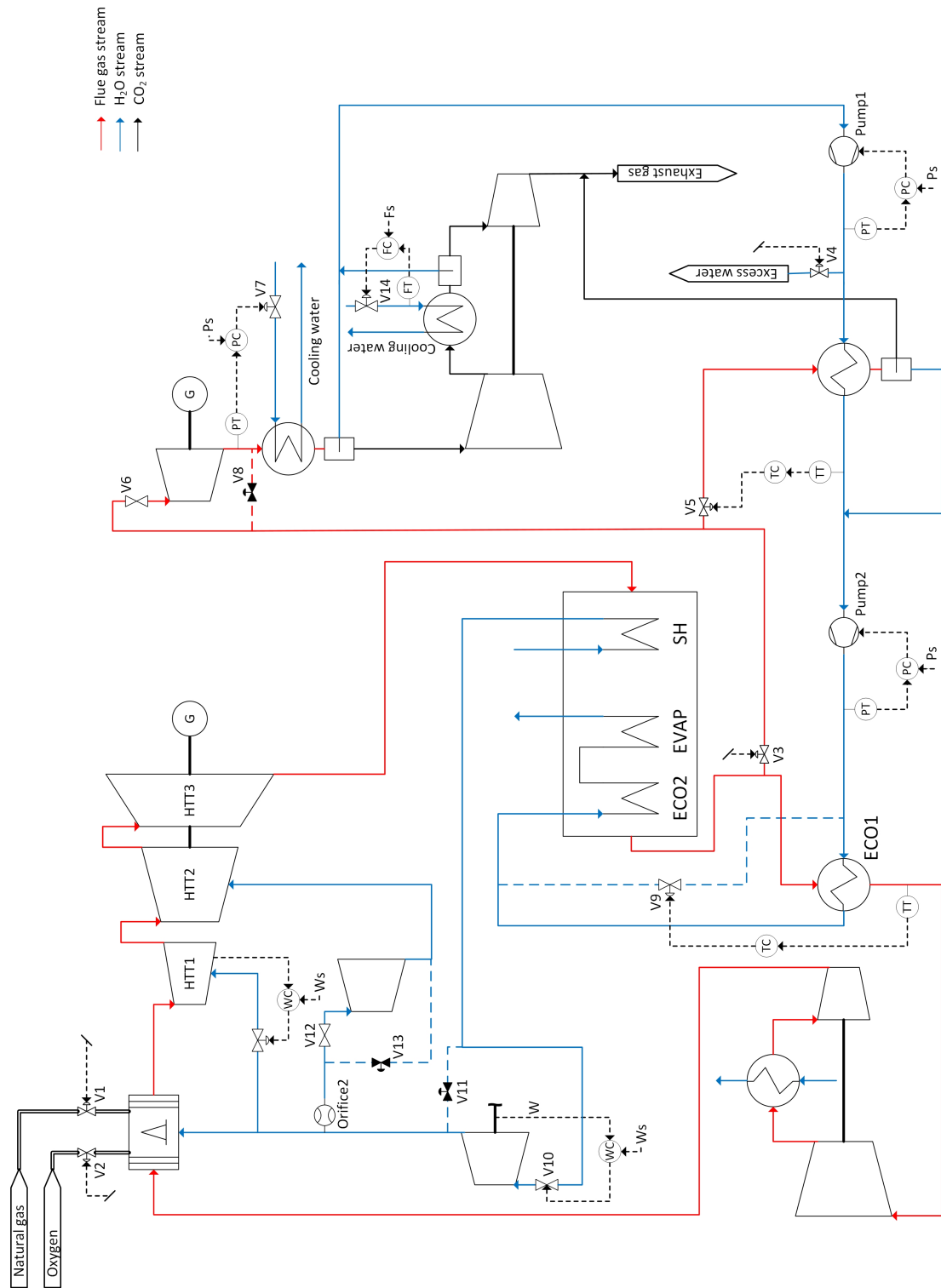


Figure 6.7: Closed control loops for the operation mode S3 of the Graz power cycle

6.3 Part-load performance

Here, as reported in Chapter 4.4, the part-load performance is presented, which is the steady-state off-design simulation and the background are the off-design models created earlier on. Up to now all simulated investigations are performed at full-load heat supply and turbines running at nominal conditions. Since the GC is different to common combined cycles and has a recycled mass flow ratio, it is not a priori self-evident how the cycle will react in part-load conditions and how far the cycle load can be reduced.

The three control strategies discussed previously are compared in terms of efficiency in Figure 6.8 operating at part-load conditions. The load is decreased down to 60% of the nominal load. Strategy 3 hereby achieves clearly the best results and gives an efficiency of 48.4% at 0.6 relative load, compared to 46.1% for strategy 1 and 45.4% for strategy 2, respectively.

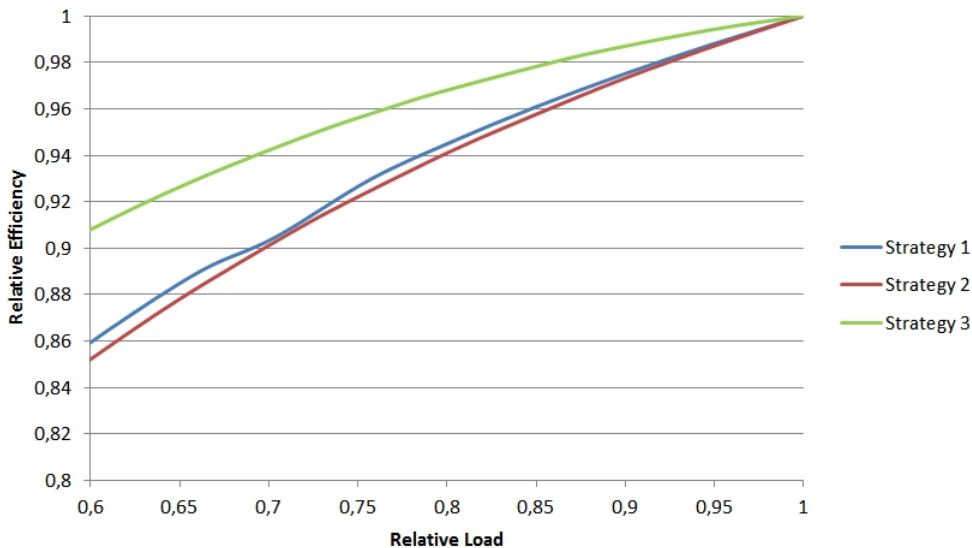


Figure 6.8: Optimal steady-state GC net efficiencies for the three different control strategies at part-load operation

This absolute values are visible in Figure 6.9, in which the net efficiencies (that means including oxygen production and compression and CO₂ compression) of strategy 1 (blue) and strategy 3 (green) are compared with S2 faded out. Later on only the strategy 3 will be pursued, because it is the control operation mode with the highest efficiency. The load could have been reduced even lower than the 40% indicated in Figure 6.9, however, at this point the water excess stream (cf. stream 25 in Figure 6.1) would become negative. By the author opinion this could be solved easily by a water input and a simple control valve regulated by the overall load controller.

Figure 6.10 and 6.11 analyze the cause of the differences between cycle control strategies S1 and S3 in terms of efficiency. To get a certain percentage of load for S1 more heat (fuel)

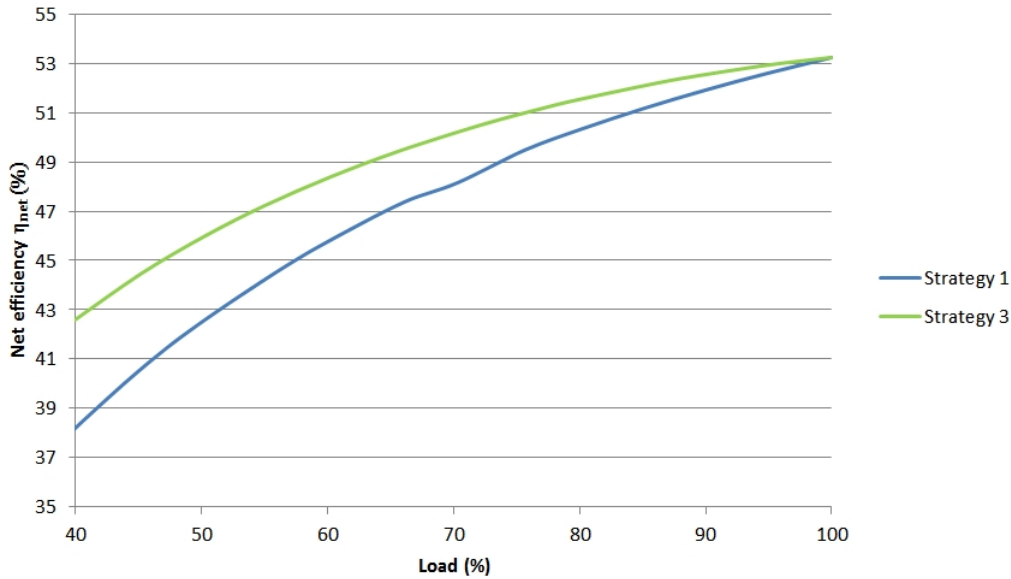


Figure 6.9: Comparison of the GC net efficiencies between S1 and S3 when operating at part load

input is necessary. In Figure 6.10 the discrepancy of the condenser heat release between strategies S1 and S3 is illustrated. In strategy S1 the heat release in the condenser at 40% load is amounted to 16.3 MW, whereas in strategy S3 the same value is equal to 11.8 MW. That is a difference of 4.5 MW. This difference in values is due to the higher mass flow rate through the condenser in S1 (at 40% load 10% more mass flow is running through the condenser), as shown in Figure 6.10. The thermal efficiency is linked to the heat release in the condenser (cf. equation 4.1). The lower the heat loss in the condenser, the higher is the thermal efficiency. As a consequence, the higher heat loss in strategy S1 leads to a lower net plant efficiency compared to strategy S3.

In Figure 6.11 another comparison between cycle operation mode S1 and S3 is shown, to wit the behaviour of turbine and compressor power at part-load operation. The recycled mass ratio is important for the compression power effort. In strategy S1 the recycled mass ratio is increasing rapidly at part loads. Therefore the compression power is almost constant at part-load conditions, whereas the compression power for S3 decreases significantly. The relation of compression power and the mass ratio, which is recycled to the combustion chamber, is shown in Figure 6.11. Both parameters are higher in strategy S1. But also the resulting turbine power for S1 is greater than for S3 at the same load conditions. Therefore no significant impact on the plant efficiency is expected, but the efficiency gain of strategy S3, as stated previously, is found in the condenser heat release.

Like already mentioned in the full-load investigation, the major part of the turbine power is caused by the HTT. The HTT power accounts for about 85% of the total generated turbine power. This power distribution is also valid in off-design conditions for each control

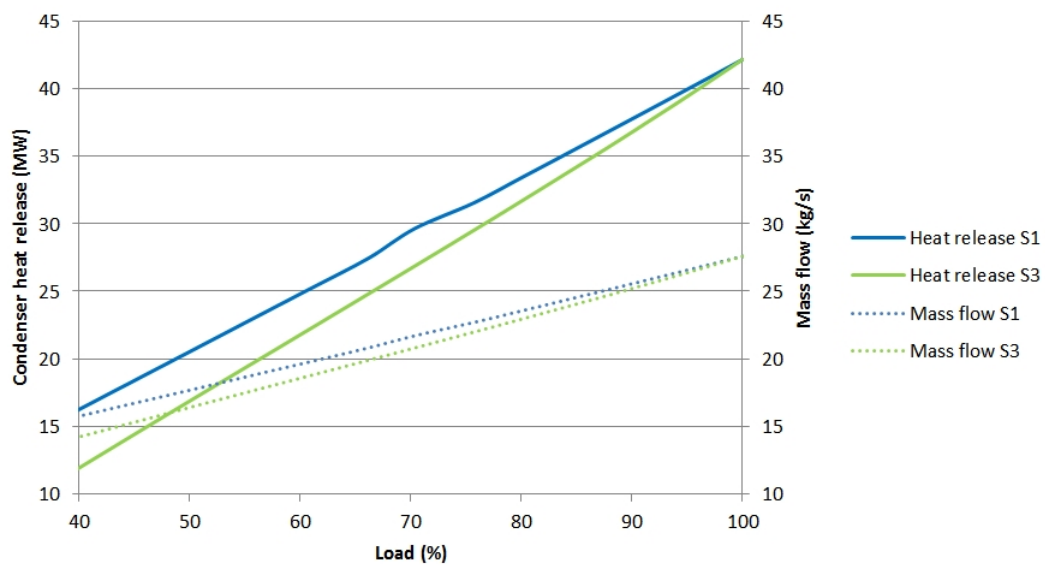


Figure 6.10: Heat release in the condenser for strategy S1 and S3

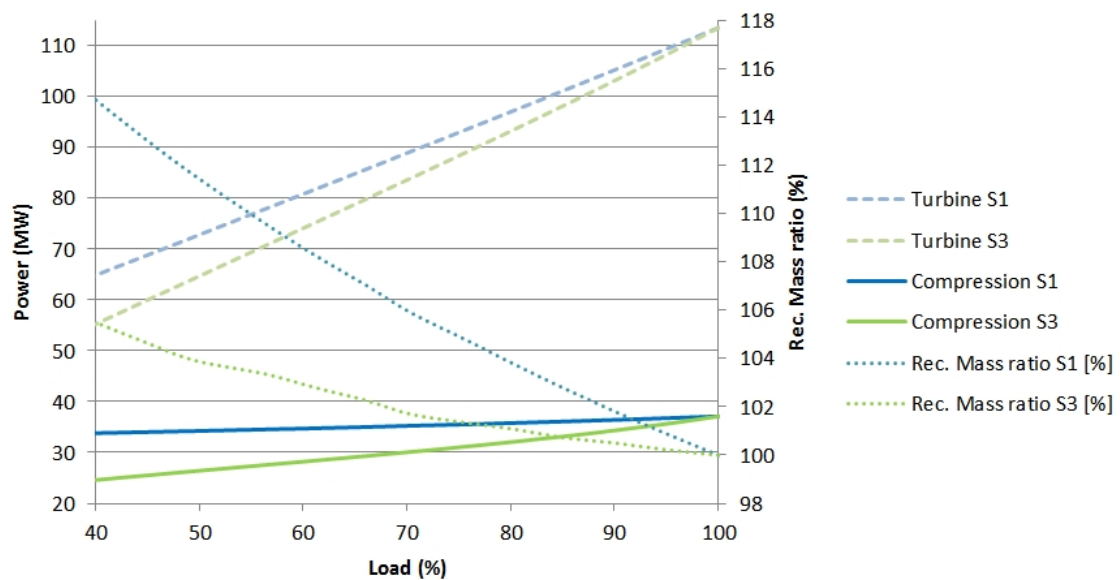


Figure 6.11: Compression and turbine power at part-load conditions for strategy S1 and S3

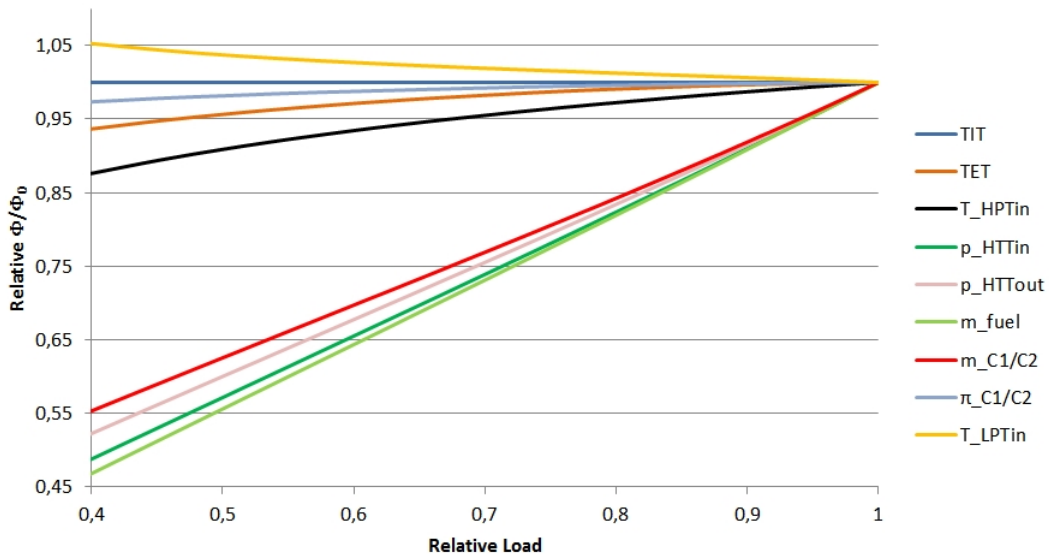


Figure 6.12: Important process parameters of the Graz Cycle at part-load operation of the control strategy S3

strategy. In common combined-cycle power plants the gas turbine efficiency accounts for two-thirds of the total power output.

In Figure 6.12 some of the GC process parameters when operating at part-load conditions are shown (for control strategy S3). Since the figure uses dimensionless numbers, it is referred to Table 6.2, where the design-point results are shown. Like already described in the previous section the TIT for the control strategy S3 is kept constant at 1400 °C. The HPT inlet temperature is restricted to 600 °C, which is not reached at any point in the load reduction. The LPT inlet temperature is the only value, which increases at part load in this overview. The outlet pressure of the HTT is at the same time the hot-side HRSG pressure. If this value is allowed to vary (like it is the case for strategy 3) a greater overall part-load cycle efficiency can be achieved due to the fact that the pressure on the low side of the compressors and turbines is allowed to change, so that the pressure ratio of the turbomachinery can be kept almost constant (cf. the pressure ratio of the compressors C1 and C2 in Figure 6.12), even when the mass flow is reduced.

Figure 6.13 investigates the critical component of the Graz power cycle, which is the OTSG. The temperature differences between cold and hot side of the heat exchangers at 40% load conditions are very low. The pinch-point at ECO2 outlet is reduced to 2 K. At the superheater outlet the temperature difference between the two mediums decreased from 15 K at full-load condition to 4 K. Since the OTSG is designed at design-point conditions, the low pinch-points are a good side effect. The HRSG efficiency in the economizer sections at part-load condition is very high, compare the streams of the hot and cold fluid in Figure 6.13. However, the small temperature differences in the HRSG simulation at full-load performance lead to large volumes for the OTSG equipment. No insuperable technological

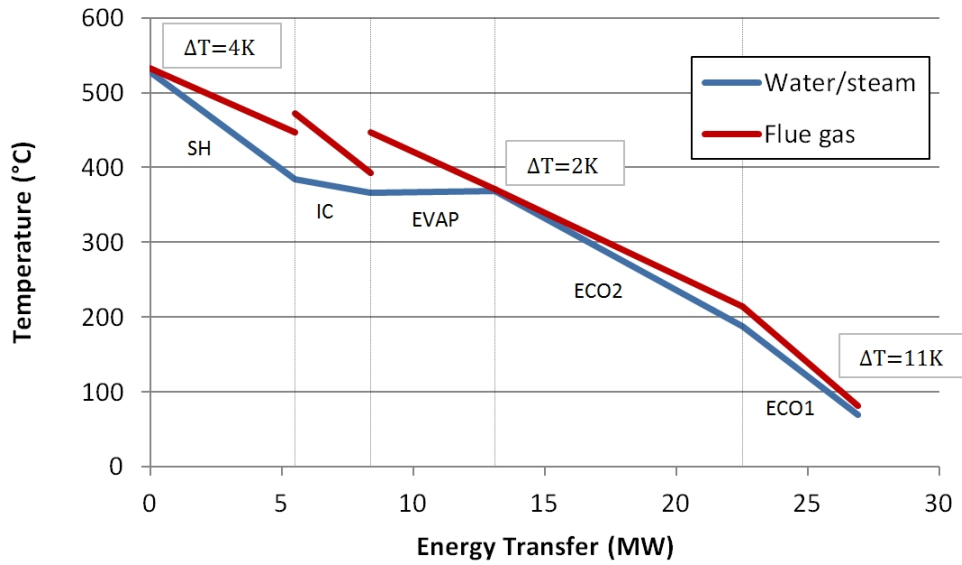


Figure 6.13: T-Q diagram for the OTSG for control strategy S3 when operating at 40% base load

barrier is foreseen for this component, but for the HRSG results large heat exchanger surfaces (like already mentioned in Section 6.1).

The CO₂-purity at the exhaust gas drain (cf. stream 19 in Figure 6.1) is shown in Table 6.7. Due to the low purity of the carbon dioxide, particularly at 40% load, where the purity amounts to 53.5%², it is suggested to complete the cycle with another water separator (like proposed in Section 6.1) in order to increase this value. In this case the CO₂-purity would rise to a value of 64.5%. By adding a second additional condenser this value amounts to 74.0% (cf. Table 6.7, value marked with two asterisk). However, at this particular point of the cycle by following the carbon capture chain, the exhaust gas stream would enter the CPU. The necessary extra power for strategy S3 for compressing the exhaust gas from 0.52 bar at 40% load to 1 bar is unaccounted in the process calculation.

Table 6.7: Gas purity at the exhaust gas drain of control strategy S3 when operating at part load

	100 % load	40% load
CO ₂ purity [%]	85.7 (90.1*)	53.5 (64.5*) (74.0**)

6.4 Dynamic simulation

In this subsection a first approach to simulate components of the Graz cycle in a dynamic (transient) way is performed. Since the once-through steam generator was found as a the

²This value is at 0.52 bar for strategy S3 due to pressure variation in the HRSG.

critical component in the case study in Subsection 4.5.1, the dynamic simulation is done for ECO1.

6.4.1 Design of the heat exchangers

In this subsection the design of the heat exchanger ECO1 is performed in order to find the geometry design data for the dynamic process simulation. This is necessary, because in equation 4.46 and 4.47 the volume of the tube and shell hardware is included.

At first, the Reynolds number for the cold side of ECO1 is calculated by eq. 6.1:

$$Re_{d_i} = \frac{c \cdot d_i}{\nu} = \frac{1 \cdot 32.8 \cdot 10^{-3}}{0.225 \cdot 10^{-6}} = 145519.08 > 10^4 \implies \textit{turbulent} \quad (6.1)$$

The Prandtl number for the cold side of the heat exchanger is calculated as follows:

$$Pr_c = \frac{\nu}{a} = \frac{c_p \eta}{\lambda} = \frac{4213.9 \cdot 212.45 \cdot 10^{-6}}{0.696} = 1.286 \quad (6.2)$$

By following the guidance and doing the iteration process of Subsection 4.5.3 the deriving data are listed in Table 6.8. Heat losses of the heat exchanger equipment are neglected. Correlations for the calculation of tube and shell geometry are found in Sinnott [70], whereas some more details about the specifications of the ECO1 are presented in Subsection 5.3.3.

Table 6.8: Calculation of heat exchanger parameter specifications

Parameter	Section OTSG ECO1
Re_{d_i}	145519.08
Pr_c	1.286
ξ	0.01646
$Nu_{d_i,turb}$	5.734
α_c	$121.51 \frac{W}{m^2K}$
Re_{d_e}	15023.59
Pr_h	0.926
Nu_{d_e}	73.217
α_h	$55.745 \frac{W}{m^2K}$
k	$36.317 \frac{W}{m^2K}$

The values in Table 6.8 are listed to assure replicability of the dynamic process simulation approach. Once the appropriate heat transfer coefficient k is found, the geometry data of the heat exchanger is calculated. The geometry of ECO1 is calculated using the design point (full-load performance) data. In order to find the appropriate dimension of the heat exchanger, the number of tubes are calculated by using following equations: [69]

$$\dot{Q}_{/tube} = \rho_w A v_i c_{p_w} (T_2 - T_1) \quad (6.3)$$

$$\dot{Q}_{/tube} = 942.5 \cdot \frac{(32.8 \cdot 10^{-3})^2 \pi}{4} \cdot 1 \cdot 4.2 \cdot (174.4 - 92.4) = 275.3 \text{ kW} \quad (6.4)$$

$$n_{tubes} = \frac{\dot{Q}_{trans}}{\dot{Q}_{/tube}} = \frac{6037.2}{275.3} \simeq 22 \text{ tubes} \quad (6.5)$$

The total length of a tube is calculated by means of equation 6.6. [69]

$$l_{tube} = \frac{\dot{Q}_{trans}}{n_{tubes} \cdot k \cdot d_o \cdot \pi \cdot \Delta\vartheta_m} \quad (6.6)$$

$$l_{tube} = \frac{6047.2 \cdot 10^3}{22 \cdot 36.3 \cdot 38 \cdot 10^{-3} \cdot \pi \cdot 17.7} = 3576 \text{ m} \quad (6.7)$$

The overall geometry data of the ECO1 as a section of the once-trough steam generator is covered in Table 6.9. These data are used for the dynamic modelling in the simulation tool. The dimensions used for the OTSG section (ECO1) are close to real dimensions of HRSGs in combined-cycle power plants.

Table 6.9: Geometry data employed for the dynamic model of the OTSG

Parameter	Symbol	Section OTSG ECO1
Number of tubes [-]	n_{tubes}	22
Total length of tube [m]	l_{tube}	3576
Vertical tube length [m]	h_{OTSG}	20
Longitudinal rows of tubes [-]	n_{rows}	179
Height of the OTSG [m]	h_{OTSG}	20
Depth of the OTSG [m]	d_{OTSG}	4
Length of the ECO1 [m]	l_{ECO1}	8.5
Volume of tubes [m ³]	V_{tube}	22.75
Volume of shell [m ³]	V_{shell}	3.88

6.4.2 Dynamic results

As described in the approach of the thesis (see Section 5.2) by Figure 5.3 the steady-state results are utilized to validate the dynamic models. Both design and off-design operating conditions in the dynamic simulation environment are validated in order to show accuracy and reliability of the results.

At first the economizer 1 is simulated under full-load (design point) conditions by using the equations of Subsection 4.5.2 and the assumptions made in Subsection 5.3.3 and Subsection 6.4.1. In Figure 6.14 the thermodynamical data and the extract of the ECO1 at design point conditions is presented. The thermodynamic data written in bold letters are the settings for the dynamic simulation, meanwhile the rest of the data are the expected results (which have origin from the steady-state simulation). In order to understand the context of Figure 6.14 it is helpful to take into account the whole process scheme shown in

Figure 6.1.

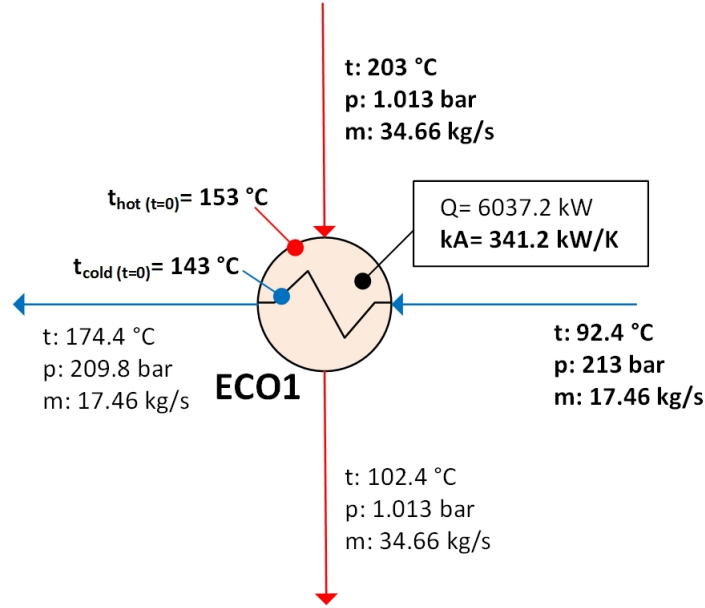


Figure 6.14: Process simulation of the ECO1 at design point conditions

The initial temperatures of the differential equations of the dynamic model (see eq. 4.46 and eq. 4.47) are calculated as follows.

The temperature of the hot-side (or shell-side) is calculated as the mean temperature of the flue gas inlet and outlet temperature:

$$t_{hot(t=0)} = \frac{t_{hot,in} + t_{hot,out}}{2} \quad (6.8)$$

$$t_{hot(t=0)} = \frac{203 \text{ °C} + 102,4 \text{ °C}}{2} = 153 \text{ °C} \quad (6.9)$$

Meanwhile the initial temperature of the cold-side (or tube-side) is calculated by taking into account all inlet and outlet temperatures of the heat exchanger, see eq. 6.10.

$$t_{cold(t=0)} = \frac{t_{cold,in} + t_{cold,out} + t_{hot,in} + t_{hot,out}}{4} \quad (6.10)$$

$$t_{cold(t=0)} = \frac{92,4 \text{ °C} + 174,4 \text{ °C} + 203 \text{ °C} + 102,4 \text{ °C}}{4} = 143 \text{ °C} \quad (6.11)$$

The results of the design point investigation are used for the validation of the dynamic model. Besides that, since the dynamic simulation is time-dependent it is interesting to see how long it takes to attain constant results along the time-scale, i.e. a straight line in a time-temperature diagram (see Figure 6.16). It is mentioned already in the case study of the dynamic modelling approach (see Subsection 4.5.1) that the heat exchange is an asymptotic solution. The dynamic investigations for the ECO1 during nominal operation

led to the results shown in Table 6.10.

Table 6.10: Validation results of the ECO1 at design point operation

Parameter	Steady-state	Dynamic	Error
$T_{\text{cold,out}} [^{\circ}\text{C}]$	174.4	174.9	0.29%
$T_{\text{hot,out}} [^{\circ}\text{C}]$	102.4	102.8	0.39%

The relative error between the steady-state full-load results and the results obtained by the dynamic model are very similar, to wit the error of the cold (water)-side is about 0.29%, meanwhile the error of the hot (flue gas)-side accounts for 0.39%. All obtained results are considered to be in an acceptable error range. In order to ensure replicability of the dynamic results, Table 6.11 shows the specific data of the heat exchanger hardware and the hot and cold fluid.

Since the dynamic simulation produces reliable results for the next case a load reduction from nominal load conditions to 80% relative load is simulated. Hereby the assumption is made that the hot gas stream, which is the flue gas coming from the HTT, as well as the cold stream, which is following the LPT/condenser line, are reacting very fast to load changes. In reality the LPT/condenser line reminds of a Rankine cycle, but in case of the Graz cycle the hot gas, coming from the combustor, instead of a pure water/steam flow circulates. After the condenser the flue gas gets extracted and pure water is sent forward, and after passing pumps and deaerator the water enters the economizer 1. Since there are heat exchange processes in between, especially the temperature and in second place the mass flow rate could be retarding in reality.

Table 6.11: Data of the dynamic investigation of ECO1

Case [-]	$c_{p_{\text{tube}}}$	$c_{p_{\text{shell}}}$	$c_{p_{\text{cold}}}$	$c_{p_{\text{hot}}}$
1: 100% load (ECO1) [kJ/kgK]	0.489	0.489	4.21	1.75
2: 100% to 80% load reduction (ECO1) [kJ/kgK]	0.489	0.489	4.25	1.73

The case of 100% to 80% load reduction is presented in Figure 6.15, where the thermodynamic data is shown. For the part-load results strategy 3 (which is presented in the previous sections) is selected. The initial temperatures of the heat exchanger hardware are the same as in the first study, where the full-load performance is simulated by application of the dynamic model. Besides that, the relation of heat transfer coefficient, described by eq. 4.42, is implemented in the dynamic model. As a result the product of heat transfer coefficient times area is not part of the settings anymore (therefore the parameter is not written in bold letters, see Figure 6.15).

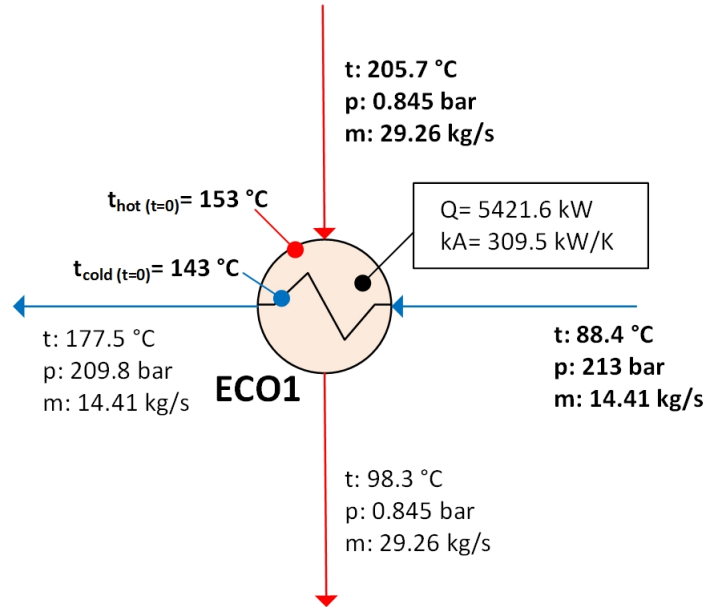


Figure 6.15: Process simulation of the ECO1 at design point conditions for the case study of load reduction from nominal load to 80% load

In Table 6.12 the results of the dynamic simulation is shown. The validation is carried out in order to identify eventual inaccuracies. The relative errors of the outlet temperatures are very small, i.e. 0.17% relative error for $T_{\text{cold,out}}$ and 0.10% for $T_{\text{hot,out}}$, which lead to the insight that the dynamic model is very reliable. As stated before the parameter $k \cdot A$ is not placed as setting and the arised relative error in comparison to the steady-state part-load simulation is 0.06%. Of utmost importance in this load reduction case study is the time, which the economizer takes to obtain the following results, therefore in Table 6.12 the time factor is implemented. The simulation time required for the heat exchange in ECO1 is 1000 s (or 16,6 min) in order to obtain the below-mentioned results.

Table 6.12: Off-design results of the ECO1 for load reduction from 100% to 80% of baseload

Parameter	Steady-state	Dynamic	Error	Time
$T_{\text{cold,out}} [^{\circ}\text{C}]$	177.5	177.2	0.17%	1000 s
$T_{\text{hot,out}} [^{\circ}\text{C}]$	98.3	98.2	0.10%	700 s
$kA [\text{kW}/\text{K}]$	309.5	309.3	0.06%	1000 s

In Figure 6.17 and 6.18 the time-temperature diagrams are shown, which indicate the outlet temperatures of the economizer 1 as well as the time, which takes to obtain those heat exchange results. Once more the asymptotic expansion is visible and the selection of the heat exchangers as a critical component in terms of heat storage and sluggishness of the heat exchange equipment is proved. Like shown in Figure 6.17, after 450 s (7.5 min) the outlet temperature of the cold-side amounts to 176 °C, which is a value close to steady-state result. The deviation from the steady-state condition at this point in time

accounts for 0.68%. At the hot side of the heat exchanger already after 700 s the outlet temperature is 98.2 °C (cf. Figure 6.18, where after 700 s a line results).

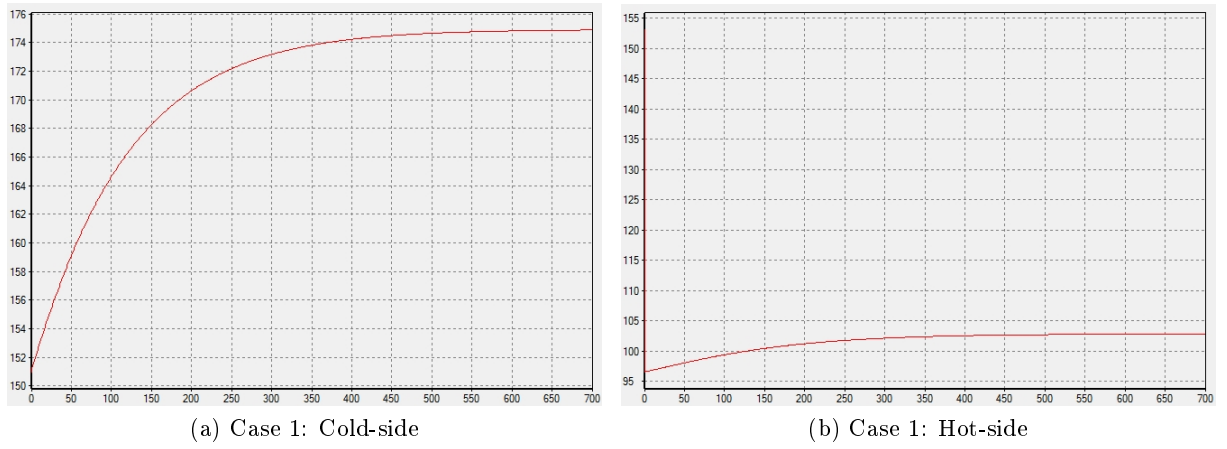


Figure 6.16: Time-temperature diagram of the dynamic simulation of ECO1 at full load operation

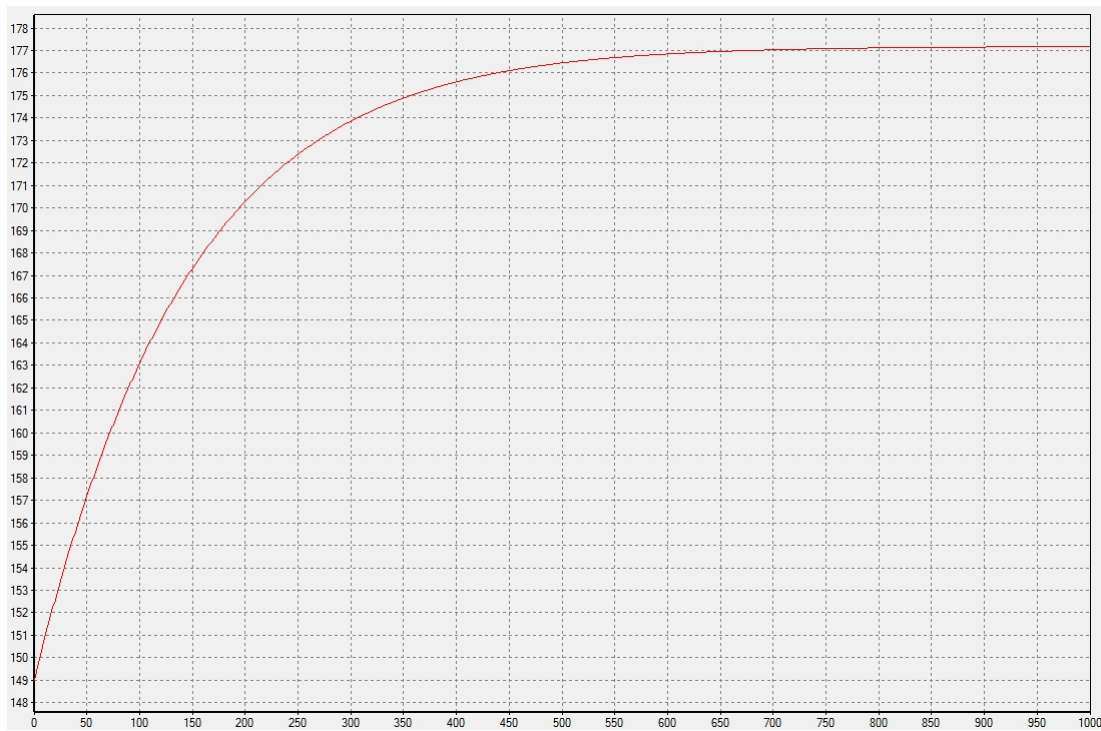


Figure 6.17: Time-temperature diagram of the cold-side of ECO1 for load reduction from 100% to 80% of baseload

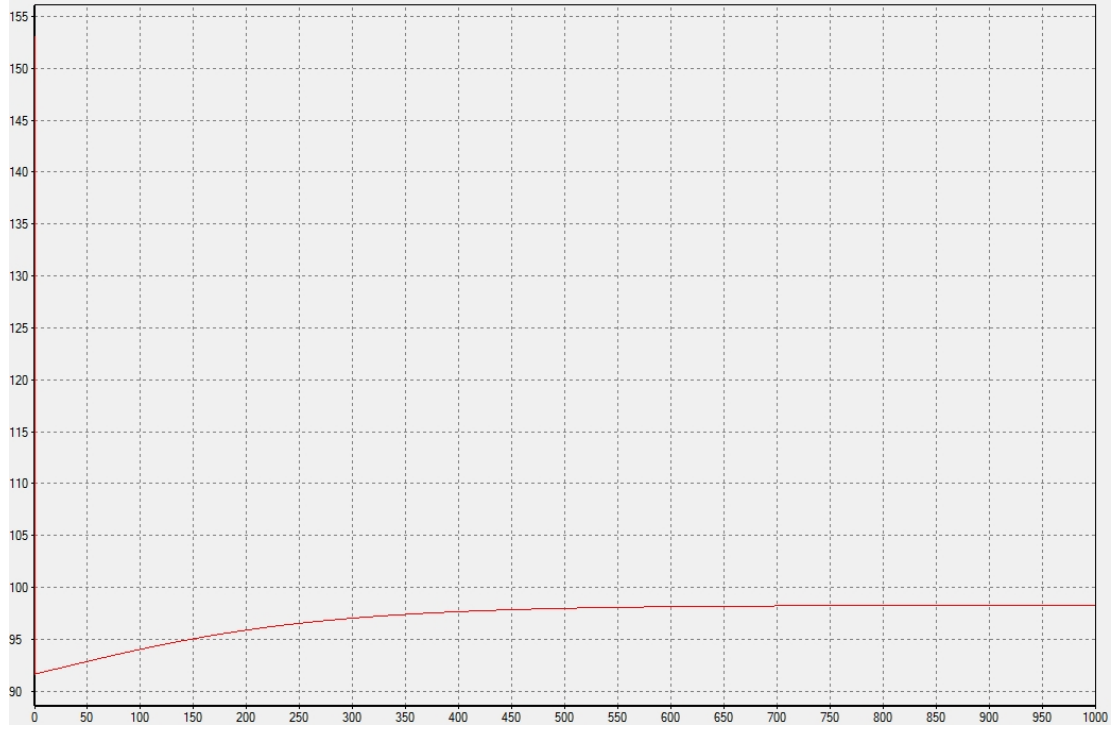


Figure 6.18: Time-temperature diagram of the hot-side of ECO1 for load reduction from 100% to 80% of baseload

Chapter 7

Conclusion

7.1 Final remarks

This Master thesis contributes to the discussion on the importance of Carbon Capture and Storage or Utilization. The focus thereby was set on the oxy-combustion fuel cycles and first and foremost on the simulation and assessment of the Graz cycle, one of the most promising CCS cycles so far invented. Emphasis were put on the thermodynamic modelling of the cycle, where intensive literary research and model development were conducted. The simulation tool IPSEpro was shown to be an ideal modeling language in order to perform these analysis also due to its capability to perform dynamic simulations. The guidelines for the development of the individual models, which are devised in this study, are detailed in order to assure replicability of the process simulation; not least the creation of an approach to build dynamic models were performed.

Different Graz power cycle configurations were studied and evaluated and the simulations were performed on the Basic Graz cycle for an electrical power output of 73.6 MW at design point (full-load) conditions and a net plant power output of 60.5 MW. The net efficiency at design point is 53.0%, including ASU oxygen production and compression as well as CO₂ compression in the CPU.

For the GC off-design simulation one change in the cycle configuration was done, which was necessary to run stable part-load operation. An important aspect of the work were the controllability of the GC. For this purpose different suitable control strategies were developed, studied and implemented in the simulation in order to meet the requirements of the power cycle in the most efficient way. The three control strategies are compared in terms of efficiency and overall performance in the part-load simulation. Consequently the best control strategy (S3) was chosen and further investigated. In this strategy the pressure in the HRSG - a once-through boiler was selected for the Graz cycle in this work - was allowed to vary and the load could have be reduced down to 40% with excellent results and performances (42.6% net plant efficiency). The OTSG was chosen as critical

component for the dynamic simulation because of its huge heat storage potential.

As a result of the prior investigations a first approach of a GC dynamic simulation was performed in the simulation of the Economizer, where transient heat curves were achieved and analyzed. Validation results proved that the dynamic models were able to generate reliable results.

7.2 Further work

Further work to complement the investigation of this study include:

- Development of models for each individual component of the Graz cycle, including turbines, compressors, pumps etc. So far only the most critical component, to wit the heat exchanger, with its large surfaces and therefore huge heat storage potential is investigated for the GC. The heat exchanger dynamic simulation should be extended on the entire OTSG system.
- Development of a closed-cycle model consisting of dynamic models that allows a detailed assessment of its simultaneous transient operation under different load points and variations in the fuel (heat) input
- Study and development of start-up and shut-down strategies for the Graz power cycle.
- Since climate change is threatening the globe, further work could be in the development of the Graz power cycle for bio-fuels, because CCS plus biomass is the only possibility to achieve negative emissions.

Bibliography

- [1] J. Walsh and D. Wuebbels. Our changing climate. Technical report, U.S. Global Change Research Program, 2014.
- [2] J. Walsh, D. Wuebbels. "Observed Change". Global Change. Retrieved from: <http://nca2014.globalchange.gov/report/our-changing-climate/observed-change>. 23.02.2015.
- [3] European Commission. Energy roadmap 2050, December 2011.
- [4] Zero Emissions Platform. CO2 Capture and Storage - Recommendations for transitional measures to drive deployment in Europe. Technical report, European Commission, 2013.
- [5] C. Littlecott, V. Scott, and S. Haszeldine. Carbon Capture and Storage in the EU's 2030 climate and energy framework. Technical report, SCCS Policy Briefing, 2014.
- [6] IEA. *Harnessing Variable Renewables - A Guide to the Balancing Challenge*, chapter Introduction, page 25. 2011.
- [7] F. Johnsson, M. Odenberger, and L. Göransson. Challenges to integrate CCS into low carbon electricity markets. *Elsevier*, 2013.
- [8] A. Miller, J. Lewandowski, K. Badyda, S. Kiryk, J. Milewski, J. Hama, and N. Iki. Off-design analysis of the graz cycle performance. In *Proceeding of the international gas turbine congress 2003, Tokyo, november 2-7, 2003*.
- [9] W. Sanz, M. Braun, H. Jericha, and M. F. Platzer. Adapting the zero-emission Graz Cycle for hydrogen combustion and investigation of its part load behavior. *International journal of hydrogen energy*, 43(11):5737–5746, 2018.
- [10] K. Wimmer. Thermodynamischer Vergleich des Graz Cycle mit dem NET Power Cycle in Voll- und Teillast. Master's thesis, Technische Universität Graz, 2018.
- [11] R.K. Pachauri and L.A. Meyer. Climate change 2014: Synthesis report. contribution of working groups i, ii and iii to the fifth assessment report of the intergovernmental panel on climate change. Technical report, IPCC, 2014.

- [12] Lesch, H. "Der Klimawandel (ZDF)". YouTube. Retrieved from: <https://www.youtube.com/watch?v=TG-Wu36-G7g>. 22.09.2019.
- [13] O. Bolland. Power Generation: CO2 Capture and Storage (Compendium). 2011.
- [14] "The Paris Agreement". United Nations Climate Change. Retrieved from: <https://unfccc.int/process-and-meetings/the-paris-agreement/the-paris-agreement>. 08.09.2019.
- [15] "EU Emissions Trading System (EU ETS)". European Commission. Retrieved from: <https://ec.europa.eu/clima/policies/ets>. 08.09.2019.
- [16] "European Emission Allowances Auction (EUA) Primary Market". EEX. Retrieved from: <https://www.eex.com/en/>. 09.09.2019.
- [17] European Commission. European smartgrids technology platform: Vision and strategy for europe's electricity network of the future. Brussels, 2006.
- [18] R. Kehlhofer, J. Warner, H. Nielsen, and R. Bachmann. *Combined-cycle Gas & Steam Turbine Power Plants*. PennWell, 1999.
- [19] F. Heitmeir. Thermische Turbomaschinen Grundlagen (Compendium). 2014.
- [20] E. M. Helsing. Adiabatic compressed air energy storage. Master's thesis, Norwegian University of Science and Technology, 2015.
- [21] Schwarzer, Ch. M. "Brennstoffzelle: Die große Unbekannte". Zeitonline. Retrieved from: <https://www.zeit.de/mobilitaet/2017-12/brennstoffzelle-elektroautos-batterie-produktion-ersatz>. 11.10.2019.
- [22] European Technology Platform for Zero Emission Fossil Fuel Power Plants (ZEP). Carbon Capture and Storage (CCS): an essential technology to reconcile EU energy security with climate objectives. Retrieved from: <https://www.zeroemissionsplatform.eu/library/publication/247-ccsenergysecurity.html>, 2014.
- [23] "Energy Units and Calculators". Environment and Ecology. Retrieved from: <http://environment-ecology.com/what-is-energy/90-energy-units-and-calculators.html>. 12.10.2019.
- [24] "Natural gas". eia: U.S. Energy Information Administration. Retrieved from: <https://www.eia.gov/dnav/ng/hist/rngwhhdD.htm>. 12.10.2019.
- [25] Rose, K. Industrial Energy Management (Lecture notes). 2016.

- [26] K. Riahi. Energy System Analysis (Lecture Notes). 2017.
- [27] "Global Energy & CO₂ Status Report 2019". iea. Retrieved from: <https://www.iea.org/geco/>. 13.10.2019.
- [28] R. Soundararajan. *Oxy-combustion coal based power plants with CO₂ capture: Process integration approach to reduce capture penalty*. PhD thesis, Norwegian University of Science and Technology, 2015.
- [29] Edenhofer, O. et al. IPCC, 2014: Climate Change 2014: Mitigation of Climate Change. Contribution of Working Group III to the Fifth Assessment Report of the Intergovernmental Panel on Climate Change. Technical report, Cambridge University Press, 2014.
- [30] T. F. Wall. Combustion processes for carbon capture. *Proceedings of the Combustion Institute*, 31(1):31 – 47, 2007.
- [31] B. Metz, O. Davidson, H. De Coninck, M. Loos, and L. Meyer. *Carbon dioxide capture and storage*. IPCC Geneva, Switzerland, 2005.
- [32] Mann, D., Cole, A. "Breakthrough Carbon Capture: Exploiting Trade-offs". Triz Journal. Retrieved from: <http://www.triz-journal.com/breakthrough-carbon-capture-exploiting-trade-offs>. 24.02.2015.
- [33] J. Gibbins and H. Chalmers. Carbon capture and storage. *Energy Policy*, 36(12):4317 – 4322, 2008. Foresight Sustainable Energy Management and the Built Environment Project.
- [34] A. Darde, R. Prabhakar, J. P. Tranier, and N. Perrin. Air separation and flue gas compression and purification units for oxy-coal combustion systems. *Energy Procedia*, 1(1):527 – 534, 2009. Greenhouse Gas Control Technologies 9 Proceedings of the 9th International Conference on Greenhouse Gas Control Technologies (GHGT-9), 20 November 2008, Washington DC, USA.
- [35] N. Ferrari. Oxy-turbine power plants. Technical report, IEAGHG, 2014.
- [36] Hangx, S. "New study of natural CO₂ reservoirs". EGU Blogs. Retrieved from: <https://blogs.egu.eu/geolog/2016/07/28/>. 13.10.2019.
- [37] H. M. Kvamsdal, K. Jordal, and O. Bolland. A quantitative comparison of gas turbine cycles with capture. *Energy*, 32(1):10 – 24, 2007.
- [38] Ph. Mathieu and R. Nihart. Sensitivity analysis of the MATIANT cycle. *Energy Conversion and Management*, 40:1687 – 1700, 1999.

- [39] Allam, R.J. et al. High efficiency and low cost of electricity generation from fossil fuels while eliminating atmospheric emissions, including carbon dioxide. *Energy Procedia*, 37(0):1135 – 1149, 2013. GHGT-11.
- [40] R.E. Anderson, S. MacAdam, F. Viteri, D.O. Davies, J.P. Downs, and A. Paliszewski. Adapting gas turbines to zero emission oxy-fuel power plants. *Proceedings of ASME Turbo Expo 2008*, 2008.
- [41] R. Anantharaman, O. Bolland, and K. I. Åsen. Novel cycles for power generation with CO₂ capture using OMCM technology. *Energy Procedia*, 1(1):335 – 342, 2009. Greenhouse Gas Control Technologies 9 Proceedings of the 9th International Conference on Greenhouse Gas Control Technologies (GHGT-9), 16-20 November 2008, Washington DC, USA.
- [42] E. Yantovski, J. Gorski, B. Smyth, and J. ten Elshof. Zero-emission fuel-fired power plants with ion transport membrane. *Energy*, 29(12-15):2077 – 2088, 2004. Efficiency, Costs, Optimization, Simulation and Environmental Impact of Energy Systems.
- [43] Sanz, W. "Graz Cycle - A Zero Emission Power Plant for CCS (Carbon Capture and Storage)". Retrieved from: <http://www.graz-cycle.tugraz.at/>. 01.05.2015.
- [44] H. Jericha, W. Sanz, and E. Göttlich. Design concept for large output graz cycle gas turbines. In *ASME Paper GT2006-90032*, 2006.
- [45] W. Sanz, H. Jericha, F. Luckel, E. Göttlich, and F. Heitmeir. A Further Step Towards a Graz Cycle Power Plant for CO₂ Capture. In *ASME Paper GT2005-68456*, 2005.
- [46] W. Sanz, C.-W. Hustad, and H. Jericha. First Generation Graz Cycle Power Plant for near-term deployment. In *ASME Paper GT2011-45135*, 2011.
- [47] W. Sanz, H. Jericha, M. Moser, and F. Heitmeir. Thermodynamic And Economic Investigation Of An Improved Graz Cycle Power Plant For CO₂ Capture. In *ASME Paper GT2004-53722*, 2004.
- [48] B.T. Chorpening, G.A. Richards, K.H. Casleton, M. Woike, B. Willis, and L. Hoffman. Demonstration of a Reheat Combustor for Power Production With CO₂ Sequestration. In *ASME Paper 2003-GT-38511*, 2003.
- [49] H. Jericha and W. Sanz. Wärmekraftanlagen mit Verbrennung von Kohlenwasserstoffen mit reinem Sauerstoff zur Stromerzeugung bei Rückhaltung von Kohlendioxid, 2001.
- [50] P. Breeze. *Power Generation Technologies*. Elsevier Science, 2nd edition, 2014.

- [51] Chr. Lechner and J. Seume. *Stationäre Gasturbinen*. Springer, 2nd edition, 2010.
- [52] K. Menny. *Strömungsmaschinen: Hydraulische und thermische Kraft- und Arbeitsmaschinen*. Teubner Wiesbaden, 5th edition, 2006.
- [53] J. M. Moran and H. N. Shapiro. *Fundamentals of Engineering Thermodynamics*. John Wiley & Sons, Inc., sixth edition, 2010.
- [54] H. Eichlseder. *Thermodynamik (compendium)*. 2009.
- [55] "Feedback control system or closed loop control system". *Instrumentation and Control Engineering* [Blog post]. Retrieved from: <http://instrumentationandcontrollers.blogspot.com/2011/05/feedback-control-system-or-closed-loop.html>. 25.09.2019.
- [56] M. P. Boyce. *Handbook for Cogeneration and Combined Cycle Power Plants*. ASME Press, 2002.
- [57] R. Dolezal. *Durchlaufkessel*. Vulkan-Verlag Classen, 1962.
- [58] C. Zotica, L. O. Nord, J. Kovacs, and S. Skogestad. Optimal operation and control of heat-to-power cycles: a new perspective using a systematic plantwide control approach. In *Computer Aided Chemical Engineering*, volume 46, pages 1429–1434. Elsevier, 2019.
- [59] H. Sigloch. *Strömungsmaschinen: Grundlagen und Anwendungen*. Hanser, 5th edition, 2013.
- [60] R. Kehlhofer, F. Hannemann, B. Rukes, and F. Stirnimann. *Combined-cycle gas & steam turbine power plants*. Pennwell Books, 2009.
- [61] A. S. Morris and R. Langari. *Measurement and instrumentation: theory and application*. Academic Press, 2012.
- [62] B. S. Wallentinsen. Concentrated Solar Power Gas Turbine Hybrid with Thermal Storage. Master's thesis, Norwegian University of Science and Technology, 2016.
- [63] K. Jordal, O. Bolland, and A. Klang. Effects of Cooled Gas Turbine Modelling for the Semi-Closed O₂/CO₂ Cycle with CO₂ Capture. *ASME Paper 2003-GT-38067, ASME Turbo Expo 2003, Atlanta, USA*, 2003.
- [64] F. Luckel. Weiterentwicklung des graz cycle und der vergleich mit anderen co₂-rückhaltekonzepten. Master's thesis, Technische Universität Graz, 2004.
- [65] L. Pierobon. *Novel design methods and control strategies for oil and gas offshore power systems*. PhD thesis, Technical University of Denmark, 2014.

- [66] A. Stodala. *Die Dampfturbinen*. 1903.
- [67] B. J. Halvorsen. Power Plant with CO₂ Capture based on Absorption - Part-load Performance. Master's thesis, Norwegian University of Science and Technology, 2012.
- [68] L.O. Nord. Pre-combustion CO₂ capture: Analysis of integrated reforming combined cycle. Norwegian University of Science and Technology, 2010.
- [69] C. Hochenauer. *Wärmetechnik 1 (Compendium)*. 2013.
- [70] R.K. Sinnott. *Chemical Engineering Design*, volume 6 of *Coulson and Richardsons Chemical Engineering Series*. Elsevier Butterworth-Heinemann, 4th edition, 2005.
- [71] Chr. Hochenauer. *Numerische Verfahren in der Energietechnik (Compendium)*. 2013.
- [72] D. E. Seborg, D. A. Mellichamp, T. F. Edgar, and F. J. Doyle III. *Process dynamics and control*. John Wiley & Sons, 2010.
- [73] H. Jericha, W. Sanz, and E. Göttlich. Design concept for large output gas cycle gas turbines. *Journal of engineering for gas turbines and power*, 130(1), 2008.
- [74] F. Richter. Die physikalischen Eigenschaften der Stähle "Das 100-Stähle-Programm". Technical report, Technische Universität Graz.
- [75] L. Imsland, D. Snarheim, R. Ulfsnes, O. Bolland, and B. A. Foss. Modeling and control of a o₂/co₂ gas turbine cycle for co₂ capture. *IFAC Proceedings Volumes*, 37(9):727–732, 2004.
- [76] D. Snarheim, L. Imsland, B. A. Foss, R. Ulfsnes, and O. Bolland. Control design for a gas turbine cycle with CO₂ capture capabilities. *IFAC Proceedings Volumes*, 38(1):109–114, 2005.
- [77] M. Klell and R. Almbauer. *Höhere Thermodynamik (Compendium)*. 2014.
- [78] F. C. Andrews. *Thermodynamic: Principles and Applications*. John Wiley & Sons, Inc., 1971.

Appendix A

Basic Thermodynamics

For the understanding of this thesis it is fundamental to know the basic thermodynamics laws and principles. For further study of these concepts it is referred to [54, 77, 53].

Not all changes of the properties of matter are accounted by the classical physics of mechanics, electricity and magnetism, optics, etc.; that is the point where thermodynamics is needed. In the case that you insert a burner to a system, it changes the properties of the system radically. Thermodynamics call the burner system a heat interaction rather than a work interaction; and there is no treatment of heat, thermal energy or friction in general in the classical disciplines. Thermodynamics as it aims to relate and predict the different properties of the macroscopic matter, particularly, if there is temperature as a variable of heat involved [78].

Thermodynamics is a phenomenological discipline; in a sense that it treats phenomena and not their ultimate causes. It does not seek an explanation on a molecular level and therefore it does not feed a mechanistic world conception of the nature but it sees only the observable properties. The method of thermodynamics is based on the belief that accurately controlled physical experiments and observations give the same results tomorrow as they do today [78].

A.1 The conservation law of mass

The conservation law of mass is valid for mass (in kg) and for the quantity of atoms, but not for the amount of particles in mol. The amount of particles can change during chemical reactions depending on the complexity of the reaction itself. The principal difference between open and closed systems is that in an open system mass can be transferred across the system boundaries. If there are no sources in between the system boundaries, then the conservation law of mass is applied with following rule of sign [77]:

$$\dot{m} = \frac{dm_i}{dt} = \sum_{in} \dot{m}_{in} - \sum_{out} \dot{m}_{out} \quad (\text{A.1})$$

Equation A.1 states that the change in the open system mass must be equal the rate of change in mass in and out of the control volume [20]. It takes also into account the index i which is related to the transported elements of mass dm_i across the system boundaries.

A.2 The first law of Thermodynamics

A fundamental law in nature, called the first law of thermodynamics or conservation of energy, states that energy in an isolated system can neither be destroyed nor produced, but only be converted. The total energy in a closed system remains constant and the only way to change it is through energy transferred across the system boundaries in form of work or heat [62].

In equation A.2 the first law of Thermodynamics is applied on an unsteady open system, where the mass dm_i is transported across the system boundaries during the time period dt . Also energy gets transferred into the control volume meaning technical work δW_t and external heat δQ_{ex} . The energy transport increases the inner and outer energy of the system in terms of dU and dE_{ex} [77]:

$$\delta W_t + \delta Q_{ex} + \sum_i dm_i (h_i + e_{ex_i}) = dU + dE_{ex} \quad (\text{A.2})$$

$$h = u + pv \quad (\text{A.3})$$

Equation A.3 already takes into account the equation for enthalpy, denoted h . The use of enthalpy in the first law of thermodynamics is generally for convenience since it simplifies the algebraic balance and in fact the enthalpy is given in most tables along other specific properties [20].

If we complement the equation A.2 by the conservation law of mass A.1 and the expression for the transported external energies e_{ex_i} by the mass dm_i , we get following energy balance:

$$\delta W_t + \delta Q_{ex} + \sum_{in} \dot{m}_{in} \left(h_{in} + \frac{c_{in}^2}{2} + gz_{in} \right) - \sum_{out} \dot{m}_{out} \left(h_{out} + \frac{c_{out}^2}{2} + gz_{out} \right) = dU + dE_{ex} \quad (\text{A.4})$$

The amount of transferred work δW_t and heat δQ_{ex} are imperfect differentials which are used in thermodynamics to express the path dependence of a particular differential. In contrast the expressions dU and dE_{ex} are exact differentials, which can be expressed as the

gradient of another function and is thus path independent. They can be seen as variables of state; whereas the work δW_t and the heat δQ_{ex} as variables of process [77].

A.3 The second law of thermodynamics

The second law of thermodynamic expresses - following the Clausius statement - that it is impossible that a system itself operates in such a way that energy flows from a cooler to a hotter body. Spontaneous heat flow between two reservoirs can occur as long as they reach the same state [53, 62].

A process is called reversible when the system can be brought to its initial state without inflicting changes to its surroundings. Change to its surroundings means that it is necessary to apply work to restore the system to initial conditions. If this condition is not fulfilled the process is irreversible. Reversible processes are theoretical. Our experience and various experiments show us that natural processes are irreversible as for example equilibration processes and friction processes [53, 77].

For a better understanding of the second law of thermodynamics the property entropy S is introduced. Thus the mathematical formulation for a closed adiabatic system is following [77]:

$$dS_{irr} \geq 0 \quad (\text{A.5})$$

It means that all natural systems produce irreversible entropy and for any system undergoing a process there is an increase in entropy, which by itself strives to a maximum in the universe. Reversible processes are only idealised borderline cases of irreversible processes, the process is then called isentropic ($dS = 0$). The definition of entropy change is denoted in Equation A.6 [77].

$$dS = \frac{\delta Q_{ex} + \delta Q_F}{T} \quad (\text{A.6})$$

The term δQ_{ex} stays for the heat transfer across the system boundaries. δQ_F is the differential of heat derived from friction in the system. The change of entropy can never be negative in an adiabatic system ($\int \delta Q_{ex} = 0$), because it would be contradictive to the Clausius statement quoted above and thus to the second law of thermodynamics [20, 77].

The entropy of a system is changed by heat transfer and mass flow across the system boundaries and by generation of entropy through irreversible processes within the system. Entropy is a variable of state and an indicator of irreversibility. Equation A.7 states the entropy rate balance for a control volume [77]:

$$\dot{S} = \frac{dS}{dt} = \sum_j \frac{\dot{Q}_j}{T_j} + \sum_i \dot{m}_i s_i + \dot{S}_{irr} \quad (\text{A.7})$$

The sum of this equation is zero for a system operating in steady state. During time interval dt entropy gets transported across the system boundaries in form of the heat rate \dot{Q}_j/T_j and the mass flow $\dot{m}_i s_i$. The term \dot{S}_{irr} is the rate of entropy due to irreversibilities. The impact of work on the system has no influence on the entropy balance.

A.4 Ideal gas and polytropic process

A.4.1 Ideal gas model

The ideal gas is an imaginary conception of a fluid without any molecular interactions. Even though the ideal gas theorem is theoretical, it is fulfilled by most of the real gases (e.g. air, superheated steam). The equation of state of ideal gases is shown in equation A.8, where v is the specific volume: [54]

$$pv = RT \quad (\text{A.8})$$

The gas constant R has a different value for each gas. The ideal gas equation is valid for gases, when the temperature is relatively high compared to the critical temperature (T_c), or when the pressure is relatively small compared to the critical pressure (p_c). It can be multiplied by the mass m : [54, 20]

$$pV = mRT \quad (\text{A.9})$$

The Avogadro's law states that the same volume of different ideal gases with the same pressure and temperature, has the same amount of particles (moles). A given amount of substance with the same equation of state has therefore always the same volume V_m (molar volume):

$$pV_m = R_m T \quad (\text{A.10})$$

R_m is the general gas constant and a natural constant with the value, $R_m = 8314, 47 \frac{\text{J}}{\text{kmolK}}$. The gas constant is related to the molecular mass in following way: $R = \frac{R_m}{M}$, whereby $n = \frac{m}{M}$. The equation A.10 for a molar amount n of substance can be written as:

$$pV = nR_m T \quad (\text{A.11})$$

A.4.2 Mixture of ideal gases

In mixtures of ideal gases each single component obeys the gas laws. The components do not influence each other because there are no interactions on an atomic level. The specific volume v_i is different for each component and is larger than the overall specific volume v

of the mixture. Hence the partial pressure p_i of the individual component is different from the pressure p of the composition. The law of Dalton states that the sum of the partial pressures of the components has to be the pressure of the mixture: [54]

$$p = \sum_{i=1}^n p_i \quad (\text{A.12})$$

For the calculation of the equation of state three different approaches are possible. First of all the composition of mass fractions:

$$\mu_i = \frac{m_i}{m} \quad (\text{A.13})$$

$$\sum_{i=1}^n \mu_i = 1 \quad (\text{A.14})$$

Second the composition is given in mole fractions:

$$\nu_i = \frac{n_i}{n} = \frac{p_i}{p} \quad (\text{A.15})$$

$$\sum_{i=1}^n \nu_i = 1 \quad (\text{A.16})$$

The third option is the composition given in volume fractions:

$$\varphi_i = \frac{V_i}{V} = \nu_i \quad (\text{A.17})$$

$$\sum_{i=1}^n \varphi_i = 1 \quad (\text{A.18})$$

To calculate the gas constant and the molar mass of the composition, following two equations are valid:

$$R = \sum_{i=1}^n \mu_i R_i \quad (\text{A.19})$$

$$M = \sum_{i=1}^n \mu_i M_i \quad (\text{A.20})$$

A.4.3 Enthalpy and specific heats

The specific heat is a value which states how much heat is needed to raise the temperature by one degree Celsius for a given mass m . The internal energy and enthalpy of an ideal gas depends only on the temperature with c_v as the specific heat capacity for heat added at constant volume, and c_p the specific heat capacity for heat added at constant pressure

is: [54]

$$du = c_v(T) dT \quad (\text{A.21})$$

$$dh = c_p(T) dT \quad (\text{A.22})$$

By taking into account the equation $h = u + RT$, the following equation results:

$$c_p - c_v = R \quad (\text{A.23})$$

$$\kappa = \frac{c_p}{c_v} \quad (\text{A.24})$$

The ratio of the the two specific heat capacities, shown in equation A.24, results in the isentropic exponent κ . For an isentropic process following equation describes the process, presupposed $dq_{rev} = 0$:

$$pv^\kappa = \text{const.} \quad (\text{A.25})$$

A.4.4 Polytropic process

A polytropic process often gets approximated by a hyperbola written in the equation A.26, whereby the polytropic exponent n is a constant defined for the specific process. The polytropic exponent n is not a state variable like the isentropic exponent κ and the process is often referred as quasi-stationary meaning that the small process steps all reach an equilibrium: [54]

$$pv^n = \text{const.} \quad (\text{A.26})$$

For a polytropic process between two states equation A.27 is valid:

$$p_1 v_1^n = p_2 v_2^n \quad (\text{A.27})$$

Consequently following equations are resulting:

$$\frac{T_2}{T_1} = \left(\frac{p_2}{p_1}\right)^{\frac{n-1}{n}} = \left(\frac{v_1}{v_2}\right)^{n-1} \quad (\text{A.28})$$

$$q_{rev} = c_v \frac{n - \kappa}{n - 1} (T_2 - T_1) \quad (\text{A.29})$$

$$c = \frac{dq_{rev}}{dT} = c_v \frac{n - \kappa}{n - 1} \quad (\text{A.30})$$

The different changes in state, which are fundamental in the field of thermodynamics, can be considered as special cases of the polytropic process. Table A.1 summarizes the different cases: [54]

Table A.1: Different changes of state of polytropic processes [54]

State	Variable	Polytropic exp.	Equation of state	Heat cap.
isochoric	$v = const.$	$n = \pm\infty$	$pv^\infty = const.$ oder $p^{\frac{1}{\infty}}v = const.$	$c = c_v$
isobaric	$p = const.$	$n = 0$	$pv^0 = const.$	$c = c_p$
isothermic	$T = const.$	$n = 1$	$pv^1 = const.$	$c = \infty$
isentropic	$s = const.$	$n = \kappa$	$pv^\kappa = const.$	$c = 0$

A.4.5 Real gas model

As described in Chapter A.4.1, the ideal gas shows negligible interactions between molecules. That is the case with high specific volumina, that means high temperature und small pressure. The real gas behaviour can be different, i.e. that the equation $pv = RT$ is not valid anymore, because there are molecular interactions. The inner energy u and the enthalpy h is not independent of the pressure and the specific volume as it was the case in the ideal gas model. In Figure A.1 the Ts-diagram is presented, in which it can be seen that the enthalpy curves in the real gas region are not horizontal in contrast to the ideal gas. [54]

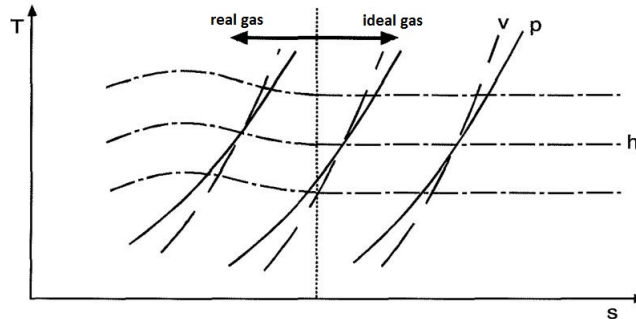


Figure A.1: Difference between real gas and ideal gas [54]

A discretionaly exact method to describe real gas behaviour is the so called compressibility factor Z . This factor Z is dimensionless and its deviation from 1 is a measure of the real gas condition. The real gas equation is following: [77]

$$Z = \frac{pv}{RT} = \frac{pV_m}{R_m T} \quad (\text{A.31})$$

Figure A.2 shows the compressibility factor of the medium air as a function of pressure p and temperature T . If the pressure is very high and temperatures are of a medium high level (around 350 °C), then air is the farthest away from the ideal factor 1. That means,

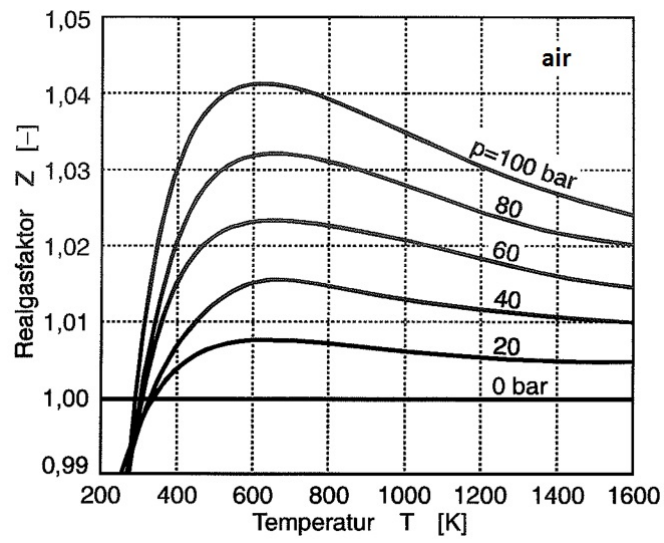


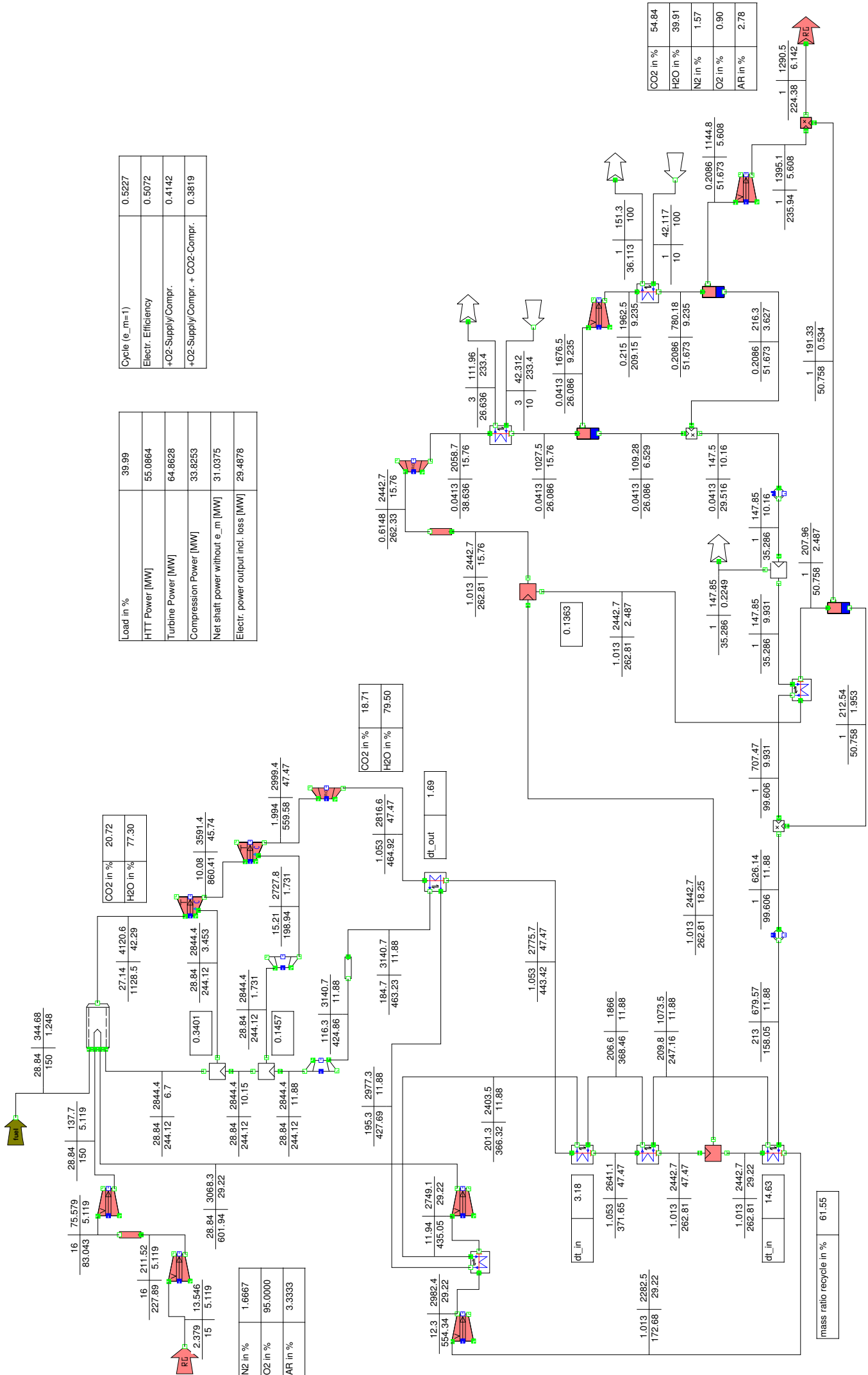
Figure A.2: The compressibility factor of air [54]

that only under particular conditions, the ideal gas model is applicable. [54]

Appendix B

Process stream data

Basic Graz power cycle Master Thesis S1



Load in %	39.99
HTT Power [MW]	55.0864
Turbine Power [MW]	64.8628
Compression Power [MW]	33.8263
Net shaft power without e_m [MW]	31.0375
Electr. power output incl. loss [MW]	29.4878
Cycle (e_m=1)	0.5227
Electr. Efficiency	0.5072
+O2-Supply/Compr.	0.4142
+O2-Supply/Compr. + CO2-Compr.	0.3819

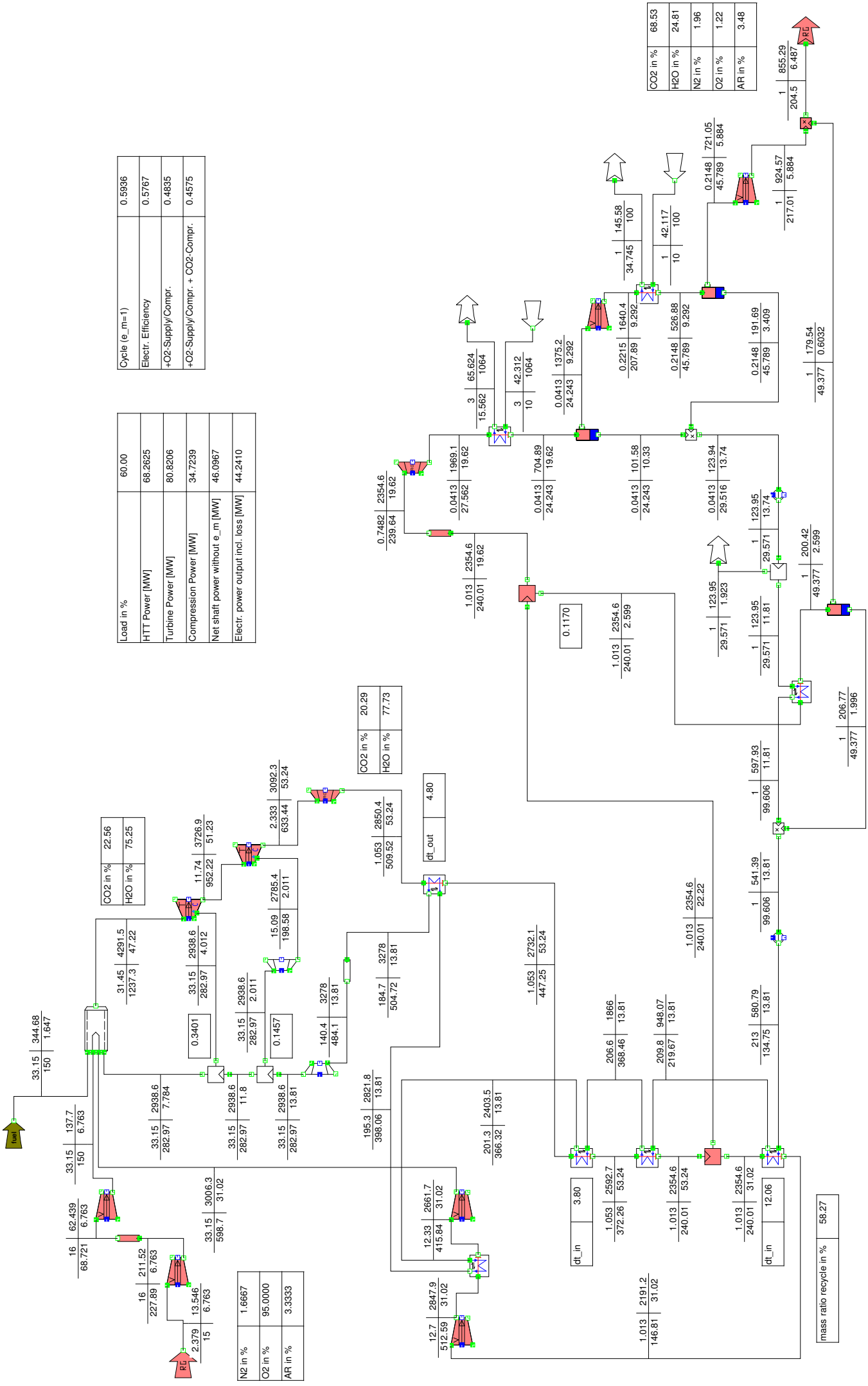
CO2 in %	20.72
H2O in %	77.30
dt_out	1.69
CO2 in %	18.71
H2O in %	79.50
dt_in	3.18
mass ratio recycle in %	61.55

N2 in %	1.6667
O2 in %	95.0000
AR in %	3.3333

CO2 in %	54.84
H2O in %	39.91
N2 in %	1.57
O2 in %	0.90
AR in %	2.78

p[bar] | h[kJ/kg]
T[°C] | mass[kg/s]

Basic Graz power cycle Master Thesis S1



Cycle (e_m=1)	0.5936
Electr. Efficiency	0.5767
+O2-Supply/Compr.	0.4835
+O2-Supply/Compr. + CO2-Compr.	0.4575

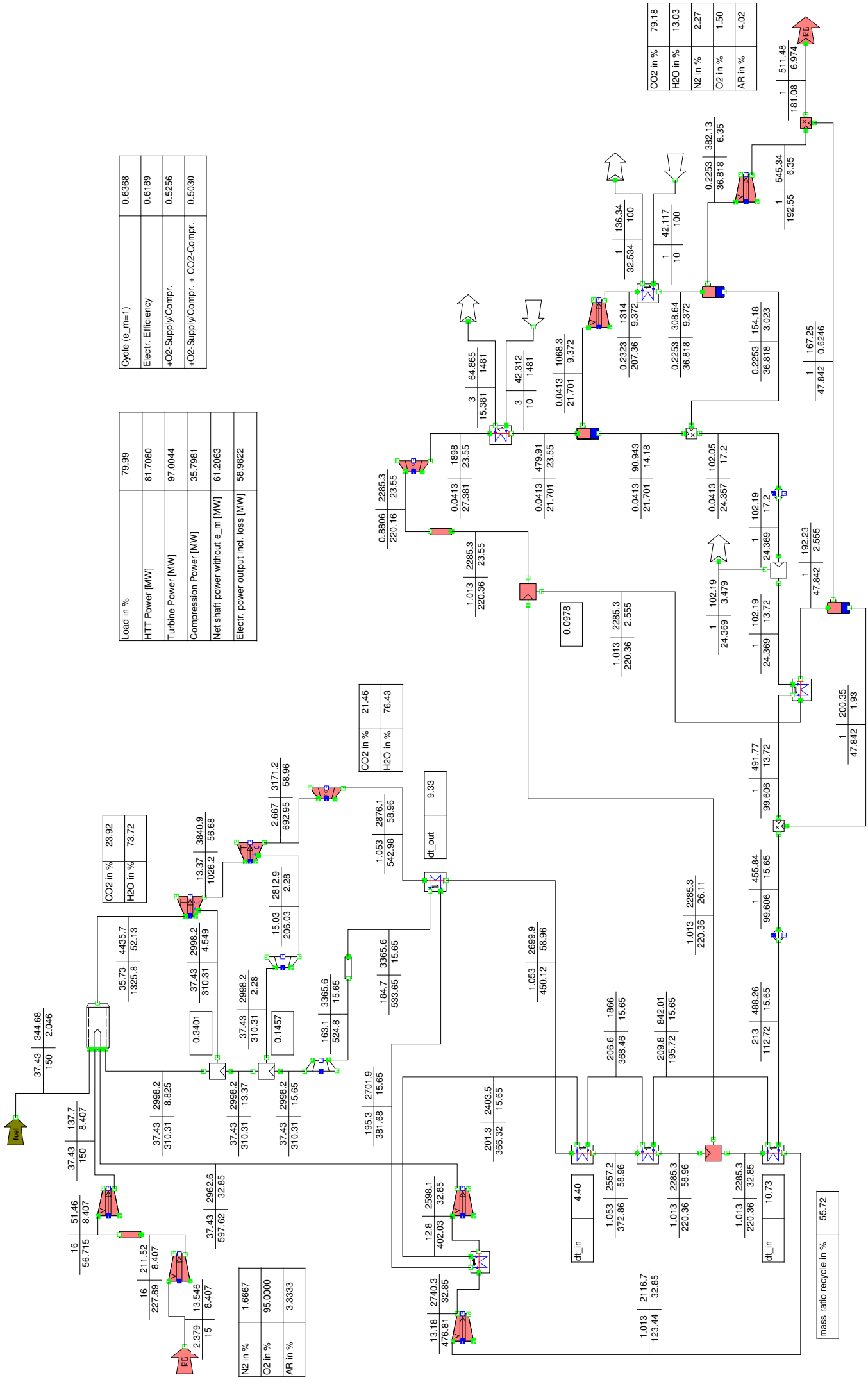
Load in %	60.00
HTT Power [MW]	68.2625
Turbine Power [MW]	80.8206
Compression Power [MW]	34.7239
Net shaft power without e_m [MW]	46.0967
Electr. power output incl. loss [MW]	44.2410

N2 in %	1.6667
O2 in %	95.0000
AR in %	3.3333

CO2 in %	68.53
H2O in %	24.81
N2 in %	1.96
O2 in %	1.22
AR in %	3.48

p[bar] | h[kJ/kg] | T[°C] | mass[kg/s]

Basic Graz power cycle Master Thesis S1



Cycle (e_m=1)	0.6368
Electr. Efficiency	0.6189
+O2-Supply/Compr.	0.5256
+O2-Supply/Compr. + CO2-Compr.	0.5030

Load in %	79.99
HTT Power [MW]	81.7080
Turbine Power [MW]	97.0044
Compression Power [MW]	35.7981
Net shaft power without e_m [MW]	61.2063
Electr. power output incl. loss [MW]	58.9822

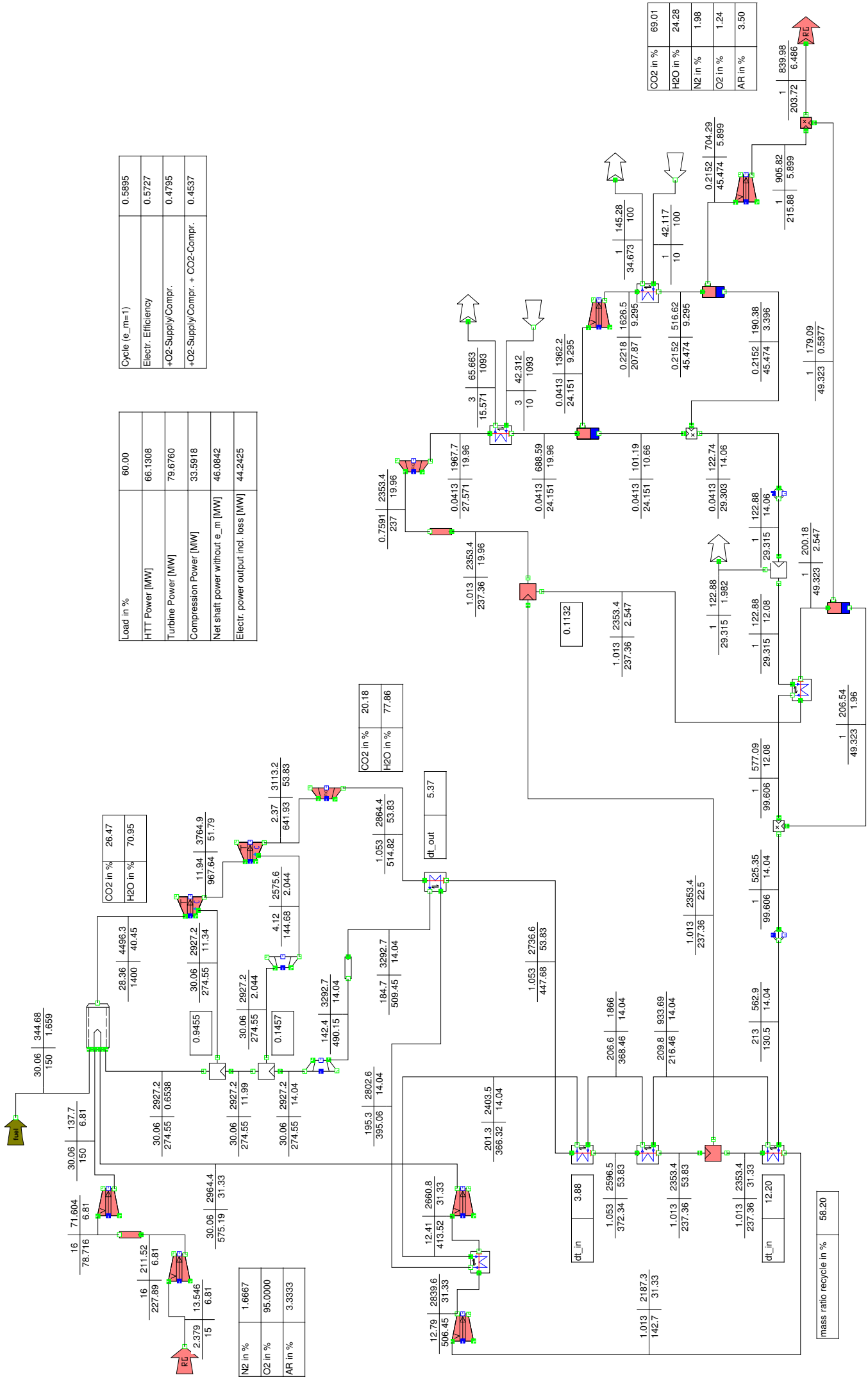
N2 in %	1.6667
O2 in %	95.0000
AR in %	3.3333

CO2 in %	79.18
H2O in %	13.03
N2 in %	2.27
O2 in %	1.50
AR in %	4.02

mass ratio recycle in % 55.72

p[bar] | h[kJ/kg] | T[°C] | mass[kg/s]

Basic Graz power cycle Master Thesis S2



Cycle (e_m=1)	0.5895
Electr. Efficiency	0.5727
+O2-Supply/Compr.	0.4795
+O2-Supply/Compr. + CO2-Compr.	0.4637

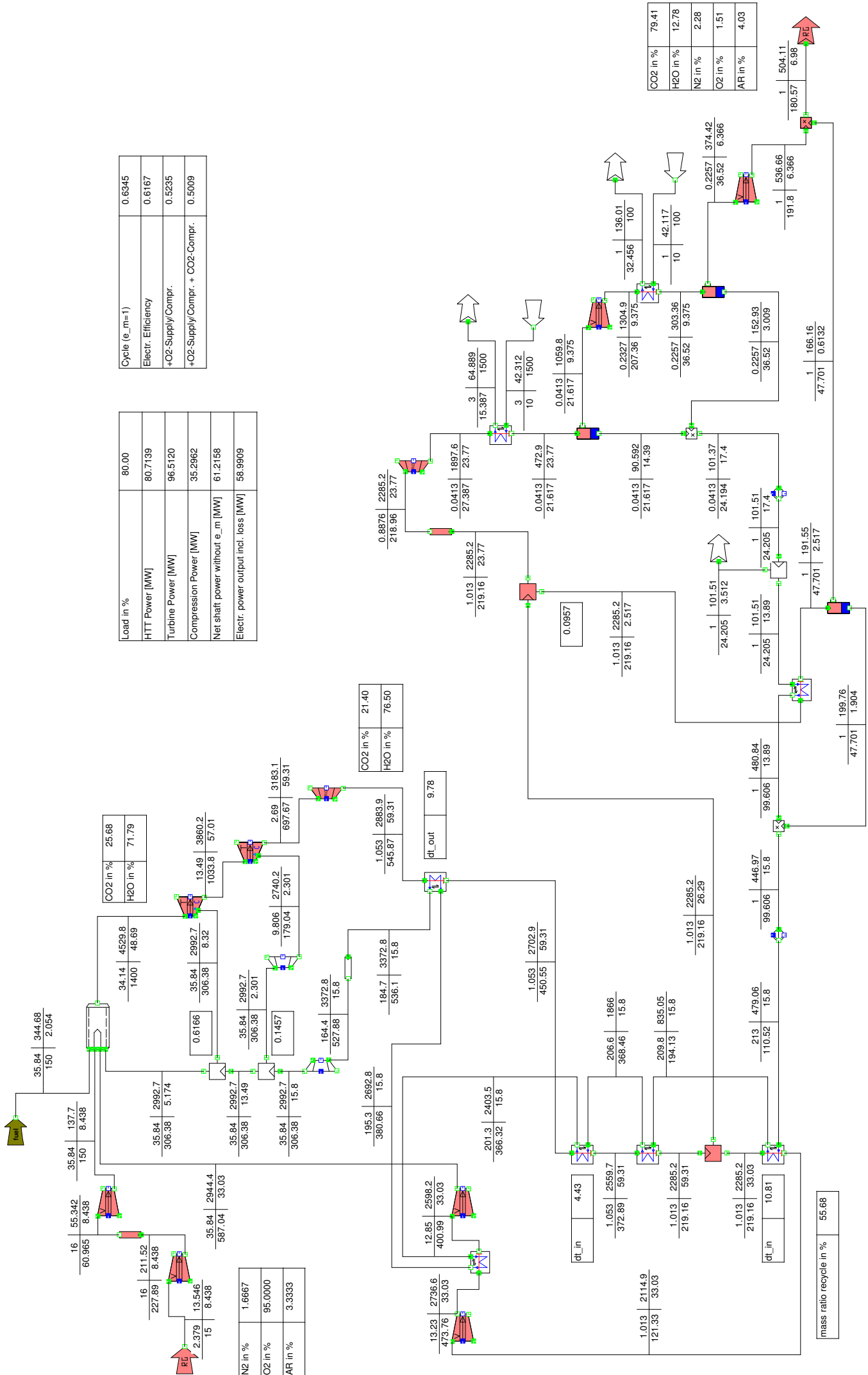
Load in %	60.00
HTT Power [MW]	66.1308
Turbine Power [MW]	79.6760
Compression Power [MW]	33.5918
Net shaft power without e_m [MW]	46.0842
Electr. power output incl. loss [MW]	44.2425

N2 in %	1.6667
O2 in %	95.0000
AR in %	3.3333

CO2 in %	69.01
H2O in %	24.28
N2 in %	1.98
O2 in %	1.24
AR in %	3.50

p[bar] | h[kJ/kg] | mass[kg/s]

Basic Graz power cycle Master Thesis S2



Cycle (e_m=1)	0.6345
Electr. Efficiency	0.6167
+O2-Supply/Compr.	0.5235
+O2-Supply/Compr. + CO2-Compr.	0.5009

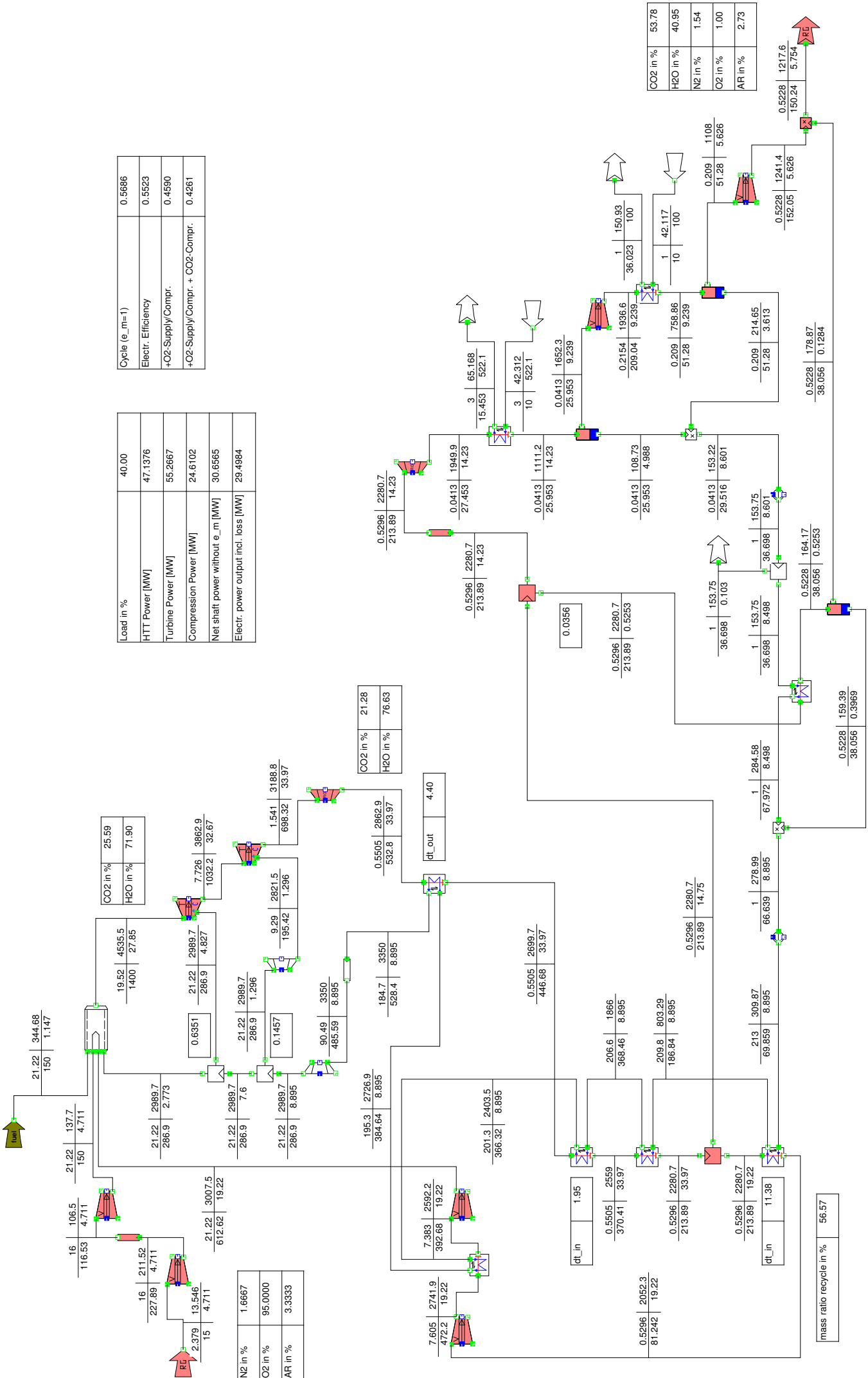
Load in %	80.00
HTT Power [MW]	80.7139
Turbine Power [MW]	96.5120
Compression Power [MW]	35.2962
Net shaft power without e_m [MW]	61.2156
Electr. power output incl. loss [MW]	58.9909

N2 in %	1.6667
O2 in %	95.0000
AR in %	3.3333

CO2 in %	79.41
H2O in %	12.78
N2 in %	2.28
O2 in %	1.51
AR in %	4.03

p[bar] | h[kJ/kg]
T[°C] | mass[kg/s]

Basic Graz power cycle Master Thesis S3



Cycle (e_m=1)	0.5886
Electr. Efficiency	0.5523
+O2-Supply/Compr.	0.4590
+O2-Supply/Compr. + CO2-Compr.	0.4261

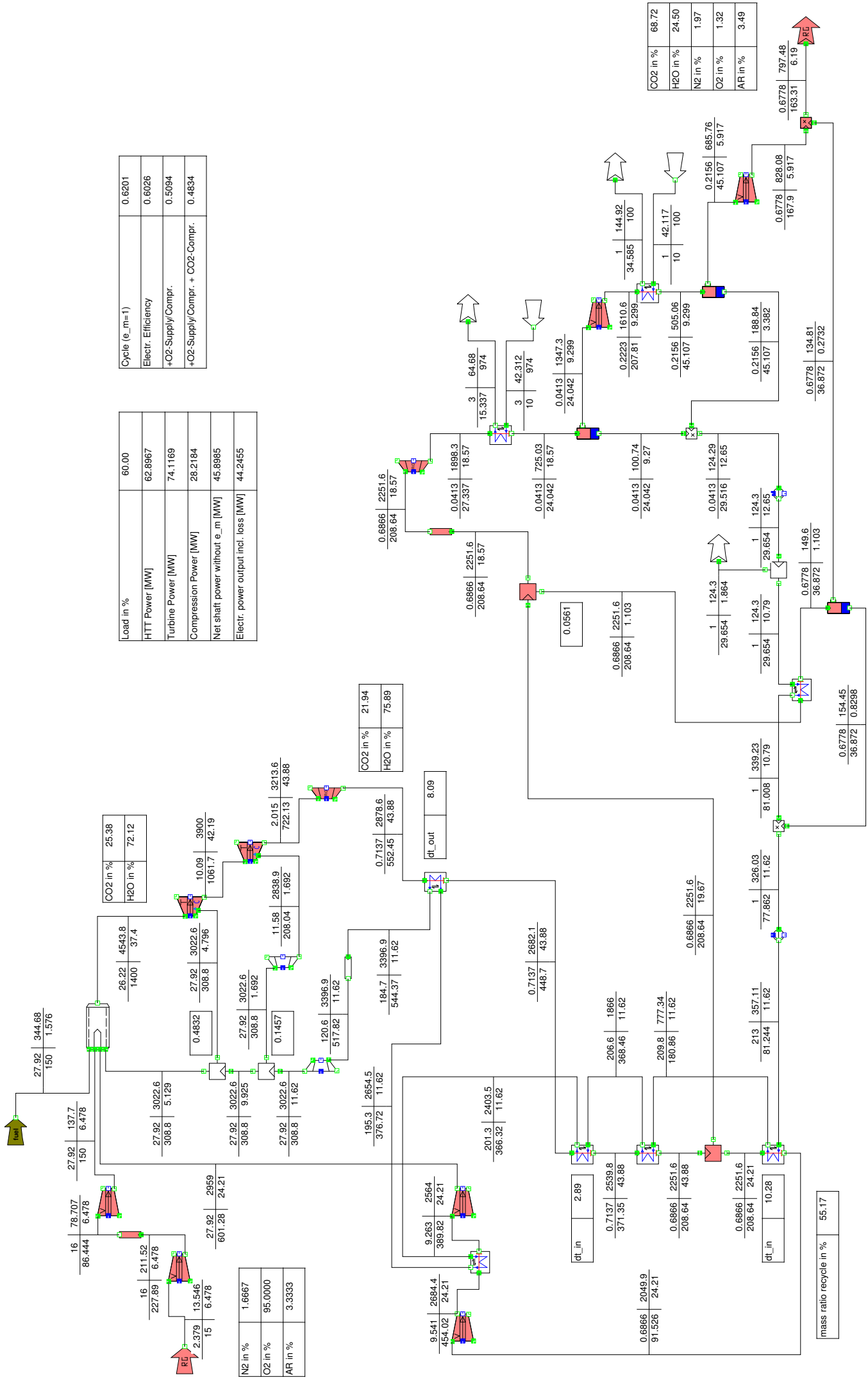
Load in %	40.00
HTT Power [MW]	47.1376
Turbine Power [MW]	55.2667
Compression Power [MW]	24.6102
Net shaft power without e_m [MW]	30.6565
Electr. power output incl. loss [MW]	29.4984

N2 in %	1.6667
O2 in %	95.0000
AR in %	3.3333

CO2 in %	53.78
H2O in %	40.95
N2 in %	1.54
O2 in %	1.00
AR in %	2.73

p[bar] | h[kJ/kg]
T[°C] | mass[kg/s]

Basic Graz power cycle Master Thesis S3



Cycle ($e_{m=1}$)	0.6201
Electr. Efficiency	0.6026
+O2-Supply/Compr.	0.5094
+O2-Supply/Compr. + CO2-Compr.	0.4834

Load in %	60.00
HTT Power [MW]	62.8967
Turbine Power [MW]	74.1169
Compression Power [MW]	28.2164
Net shaft power without e_m [MW]	45.8985
Electr. power output incl. loss [MW]	44.2455

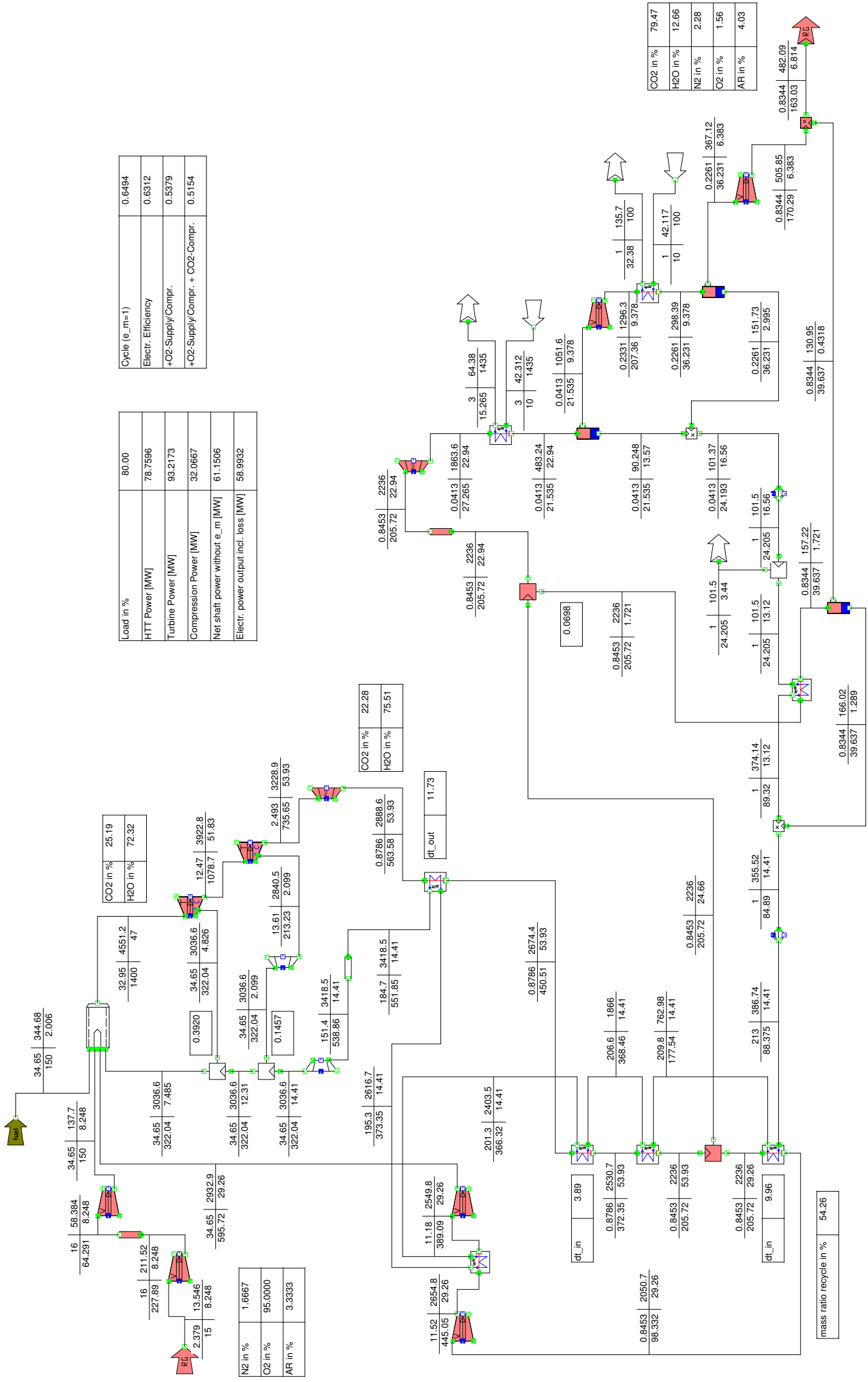
N2 in %	1.6667
O2 in %	95.0000
AR in %	3.3333

CO2 in %	68.72
H2O in %	24.50
N2 in %	1.97
O2 in %	1.32
AR in %	3.49

mass ratio recycle in % 55.17

p[bar] | h[kJ/kg] | mass[kg/s]

Basic Graz power cycle Master Thesis S3



Cycle (e_m=1)	0.6494
Electr. Efficiency	0.6312
+O2-Supply/Compr.	0.5379
+O2-Supply/Compr. + CO2-Compr.	0.5154

Load in %	80.00
HTT Power [MW]	78.7596
Turbine Power [MW]	93.2173
Compression Power [MW]	32.0667
Net shaft power without e_m [MW]	61.1506
Electr. power output incl. loss [MW]	58.9932

N2 in %	1.6667
O2 in %	95.0000
AR in %	3.3333

CO2 in %	22.28
H2O in %	75.51

CO2 in %	79.47
H2O in %	12.86
N2 in %	2.28
O2 in %	1.56
AR in %	4.03

mass ratio recycle in % 54.26

p[bar] | h[kJ/kg] | mass[kg/s]